Aalto-University
School of Engineering

Hassan Ali Hassan Ahmed

Use of Electrical Impedance Spectroscopy for Online Monitoring of Concrete Compaction

Master's thesis for the degree of Master of Science in Engineering submitted for inspection

Espoo 30.04.2020
Supervisor: Professor of Practice Jouni Punkki
Advisor: MSc. Teemu Ojala

Aalto University
School of Engineering

Aalto University, P.O. BOX 11000,
00076 AALTO www.aalto.fi

Abstract of master's thesis

Author Hassan Ali Hassan Ahmed

Title of thesis Use of Electrical Impedance Spectroscopy for Online Monitoring of Concrete Compaction

Master programme Building Technology **Code** ENG27

Thesis supervisor Prof. Jouni Punkki

Thesis advisor(s) MSc. Teemu Ojala

Date 30.04.2020 **Number of pages** 75+4 **Language** English

Abstract

Compaction of concrete is a crucial on-site step that enables concrete to reach design strength and density. This process is generally carried out using vibrators that pack the aggregates together and expel the entrapped air from the concrete element. Proper compaction ensures that all the entrapped air escapes the concrete without causing segregation. Based on the duration of vibration concrete can be under-vibrated, well-vibrated, or over-vibrated. Under-vibrated concrete causes many durability problems, such as: honeycombing, cold joints, and subsidence cracking. On the other hand, over-vibration of concrete leads to segregation and probable failure of the concrete element. Typically, compaction is subjectively monitored by personnel on site, which is insufficient to obtain a well-vibrated concrete.

This thesis investigates the use of Electrical Impedance Spectroscopy (EIS) to monitor concrete compaction during vibration. Concrete can be divided into a resistive part and a conductive part, where the first is the cement paste and water-filled voids, while the latter is the air voids as well as the aggregates. An electrode panel was designed to investigate top, middle, and bottom layers of tested concretes. This panel was fitted inside a plexiglass mould where seven samples of the same concrete mix were tested. Three vibration durations were chosen to obtain under-, over-, and well-vibrated concretes. Alternating current was sent at different frequencies using an impedance analyzer, and the resistance of each layer was obtained through analyzing the measured reactance and resistance of concrete. Followingly, three cores were drilled form each hardened concrete sample and the densities of these cores were statically analyzed to check for segregation. Additionally, vertical sections were cut to visually inspect the distribution of aggregates and air voids inside the concrete.

Analysis of the data showed that segregation could be detected by studying the variance of the resistance values for different layers during compaction. The top and middle layer showed a significant resistance decrease, whereas an increase was noted in the bottom layer. This change was linked to the observed segregation in the cut vertical segments, where the bottom layer had a higher amount of accumulated aggregates compared with the other two layers. Additionally, statistical analysis was carried out on the drilled cores densities, which showed a large variance in values denoting segregation. Further analysis was carried out comparing the difference between the resistance of top and bottom layers over the vibration duration. It was found that all segregated samples passed a limit of difference in those EIS obtained resistances compared with the unsegregated sample.

Keywords Concrete, vibration, compaction, EIS, segregation, monitoring

Preface

This master's thesis was conducted as a part of the Master Degree Programme in Building Technology at Aalto University School of Engineering. The topic of this master's thesis was proposed and supervised by Professor of Practice Jouni Punkki. Although compaction of concrete has direct effects on the durability and strength of concrete structures, the topic remains under-studied. Due to this lack of investigation there is no defined method for monitoring the quality of compaction, which is the focus of this thesis.

I would like to express my deepest gratitude for the support, guidance and valuable advice received from my supervisor Professor of Practice Jouni Punkki. I would also like to extend my deepest appreciation to MSc. Teemu Ojala for all his efforts throughout the different phases of planning, experimenting, and writing the thesis. My sincere thanks are also extended to the cooperative members of the University of Eastern Finland: Associate Professor Aku Seppänen and MSc. Petri Kuusela, who contributed to the electrical analysis and investigation part of the thesis. In addition, I would like to offer many thanks to D.Sc. (Tech.) Fahim Al-Neshawy for his unwavering support during the planning and the writing phase. I am also grateful to the professionally skilled concrete laboratory staff of Aalto University: Janne Hostikka and Pertti Alho, who made the experimenting phase go as smooth as possible.

Espoo, April 2020

Hassan Ali Hassan Ahmed

Table of Contents

Abbreviations

AEA	Air Entraining Agent
CA	Coarse Aggregates
CCP	Continuously Conducting Path
CE	Counter Electrode
CV	Coefficient of Variation
DCP	Discontinuously Conducting Path
EIS	Electrical Impedance Spectroscopy
FA	Fly Ash
GE	Grounding Electrode
GGBS	Ground-Granulated Blast-Furnace Slag
GNSS	Global Navigation Satellite System
GPS	Global Positioning Satellite
ICAR	International Centre of Aggregate Research
ICP	Insulator Conducting Path
IEM	Impact Echo Method
LOI	Loss of Ignition
ME	Measuring Electrode
OPC	Ordinary Portland Cement
PVC	Polyvinyl Chloride
RTK	Real-Time Kinematics
RE	Reference Electrode
SP	Superplasticizer
SR	Sulphate-Resistant
SRPC	Sulphate-Resistant Portland Cement
SW	Salt Water
UWB	Ultra-Wide-Band
WE	Working Electrode

1 Introduction

In the past few years, monitoring of concrete compaction has received increasing attention due to the significant effect of compaction quality on the strength and durability of concrete structures (Burlingame, 2004; Tian & Bian, 2014; Gong, et al., 2015; Tian, et al., 2019). According to ACI 309.1R-08 (2008) compaction of concrete was only introduced around the 1930s. Prior to that, concrete was drily cast with minimal reinforcement and strongly tampered into place. As the years went by, the use of reinforced concrete became more common, leading to thinner structural elements. This change required an increase in the water to cement ratio and the use of wetter mixtures. However, the wetter mixtures were lower in strength, less durable due to drying shrinkage, and susceptible to cracking. This led to the development of tools to introduce vibration into concrete. The first developed vibrators in 1936 had a design limitation, thus restricting the frequency range to 50-80 Hz. Nevertheless, after enough research, the producers managed to raise that frequency range, thereby providing better consolidation of the fresh concrete.

As shown in Cement Concrete & Aggregate Australia (2009) during the process of compaction, concrete is liquified and unwanted entrapped air is expelled from the mixture. This process is crucial for enabling concrete elements to reach their design strength and density, as well as to increase their durability. Compaction using vibrators is the most commonly used method for compaction on site. Despite the importance of vibration, it is generally monitored visually and subjectively by personnel responsible for the procedure. The subjective view on when to stop vibration is insufficient to provide the highest compaction quality. Since it might leave the concrete under- or over-vibrated, this can result in various durability complications, and even the failure of the concrete element.

1.1 Problem Statement

Monitoring compaction on site requires real-time recording of the location and duration of vibration in certain areas within the element. During this process, there is a need for assessing the sufficiency of vibration time in order to ensure the best possible quality of compaction (Tian & Bian, 2014).

A number of methods have recently been described to monitor concrete vibration, including the use of thermal imaging to locate the vibrated areas on site (Burlingame, 2004). However, this method had several drawbacks, including the inability to track compaction of multiple layers and the lack of recorded vibration time, thus leaving the quality of compaction unassessed. These problems have been overcome by constructing a real-time tracking method consisting of a Global Positioning System (GPS) paired with a Real-Time Kinematics (RTK) measuring mode to track vibrated point locations, along with a devised electrode panel to record vibration duration (Tian & Bian, 2014). However, this system was unable to analyse the depth of vibration, the quality assessment was based solely on statistical data acquired from previous vibration of different mixes, and the cost of constructing the system was high.

Most of these challenges were overcome by Gong et al. (2015), who used an Ultrawide-Band (UWB) technique to wirelessly track the motion of vibrators on site, along with a tool developed to monitor the duration of the vibration. Although the UWB system provided the ability for real-time 3D visualization of the vibration procedure at a low cost, the system could only be used on lab-scale experiments and also relied on predetermined statistical data of adequate vibration times. More recently, Tian et al. (2019) developed a newer system that utilised a Global Navigation Satellite System (GNSS) to track the vibrator location and the change in motor voltage for specifying vibration duration. While this method proved successful for use in actual construction projects, the assessment of vibration quality still depended on predetermined limits based on statistical calculations. Although numerous studies have devised methods for compaction monitoring, these have mainly focused on developing an efficient tracking system for recording the location and duration of vibration, with less effort directed at the assessment method used for determining the vibration quality.

The aforementioned methods have used statistical data to classify the measured vibration areas into three groups: under-vibrated, well-vibrated and over-vibrated. Although the vibration duration was acquired in real-time, the method used to estimate the adequacy of these times was based on comparison with already existing reference data, instead of utilizing a technique for real-time assessment of the vibration quality. Hence, this thesis addresses the use of an online monitoring technique for evaluating the quality of compaction.

1.2 Thesis Objectives and Methods

The aim of this thesis is to design and develop a measurement device for evaluating in real-time the degree of compaction of fresh concrete using Electrical Impedance Spectroscopy (EIS). To achieve this goal, a special electrode panel fitted inside a plexiglass mould is tested to evaluate the degree of concrete compaction for different vibration durations.

Each set of concrete mixes is characterized by its own vibration duration, which can be categorized into three levels of compaction: under-vibrated, well-vibrated, and over-vibrated. The evaluation process is accomplished by dividing the vibration time into smaller time steps and sending an alternating current at different frequencies through the panel after each time step while recording various electrical parameters. Additionally, the electrode setup allows the recording of these parameters for three different layers representing the top, middle, and bottom levels of a tested specimen. Analysis of the measured parameters enables identifying the resistance of each fresh concrete layer.

To ensure the feasibility of the suggested design, the resistance values obtained for each layer are compared with the observed segregation in the hardened concrete. Segregation is identified by drilling cores from the different layers and comparing the densities of these cores, along with visual inspection of vertically cut segments in the hardened concrete. Finally, between the difference in resistance between layers, vibration time and segregation are compared to determine the relationship between these three variables.

1.3 Thesis Scope

This thesis is limited to investigating one concrete mixture, given that EIS measurements are highly sensitive to changes in mix design, such as the water-cement ratio, the type of cement, and the use of mineral admixtures (McCarter, et al., 2004). The chosen mixture has a fixed W/C ratio of 0.45, and the type of cement used is Sulphate Resistant (SR) Portland cement without any mineral admixture replacement. Additionally, the study of normal slump and low slump concrete is excluded from the scope, since a highly flowable concrete provides much better contact with the electrodes leading to more accurate measurements, and highly flowable concretes are more prone to segregate compared with concretes of less workability, hence the choice of a slump class S5 concrete for EIS investigation.

1.4 Thesis Outline

The remainder of this thesis is divided into five chapters. Chapter 2 reviews the literature on compaction of concrete, the previous techniques used for monitoring compaction, and the concept as well as the applications of EIS investigation. Chapter 3 describes the development and calibration of the measuring device along with the experimental methodology. Chapter 4 presents the results obtained from the EIS investigation of fresh concrete, and the observations of the segregation from the drilled cores as well as the cut sections from the hardened concrete. Chapter 5 discusses the relationship found between the acquired resistance from EIS and the vibration quality based on the observed segregation. Additionally, Chapter 5 introduces suggestions for future research to improve and further test the device. Chapter 6 concludes the thesis by summarizing the findings presenting the drawn conclusions from using EIS investigation to monitor vibration.

2 Literature Review

In order to develop a technique for monitoring compaction in fresh concrete using EIS, it is first necessary to review the literature on the concrete compaction process, along with the concept and applications of EIS. This chapter has been divided into three sections: Section 2.1, Section 2.2, and Section 2.3.

Section 2.1 is organized as follows. The first subsection discusses the mechanism of the compaction process in general. The compaction effect on different concrete rheological properties as well as segregation is presented in the second and third subsections, respectively. The fourth subsection investigates the various compaction methods classified into 2 types: mechanical and manual. The importance of compaction for hardened concrete is highlighted in the fifth subsection. Section 2.2 presents a review of past studies tracking the changes in fresh concrete during vibration. Finally, Section 2.3 is divided into three subsections: the first one introduces the general concept of EIS, while the second one presents the different electrical properties of fresh concrete, and the last subsection provides a summary of previous approaches using EIS in the field of concrete.

2.1 Compaction of Concrete

Walker et al. (2006) showed that each concrete element has a system of air-voids that is formed during the process of mixing, placing and vibration. Since vibration is the last step before leaving the concrete to harden, it plays a major role in the formation of its final air-voids system. They have shown that air in hardened concrete is classified into three different categories: entrained air, entrapped air, and water voids. The entrained air voids are spherical in shape and are formed by adding air-entraining admixtures into the mix. Whereas the entrapped air and water voids are quite similar in size, the first are spherically shaped and are mainly caused by improper mixing, placement or vibration, while the latter are irregularly shaped, and are formed by bled water under aggregates that could not escape to the surface.

Hover (2001) pointed out that entrained air causes the concrete to be more workable by reducing the internal friction within the mixture. Moreover, in countries where the temperature drops below zero, it provides the concrete element with resistance to the damage caused by cycles of freeze and thaw. This is accomplished by these voids providing enough space for water inside the concrete to freeze and expand, which prevents rupture in the concrete due to the ice expansion pressure.

2.1.1 Mechanism of Concrete Compaction

Cement Concrete & Aggregates Australia (2006) defined compaction as the procedure through which entrapped air is released from the concrete mix while packing the aggregates to increase the density of the concrete. Additionally, they stated that compaction helps relieve the internal friction between the aggregates, hence filling the formwork with concrete, instead of the particles arching against each other. As shown in Figure 1, the vibration process could be illustrated in two stages. The first represents the slumping of aggregates as they start to be packed and the concrete mix starts to fully fill the formwork. The second stage is when the entrapped air starts to be expelled preventing the formation of honeycombs or air pockets in the hardened concrete.

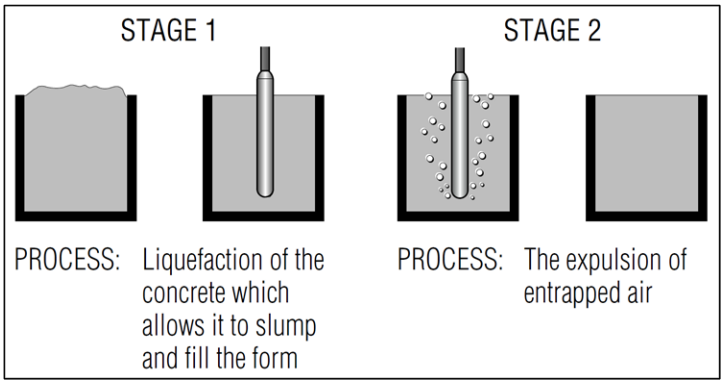

Figure 1. Representation of the process of vibration as two main stages; liquefaction of the mix and the expulsion of entrapped air (Cement Concrete & Aggregates Australia, 2006).

Ghadban (2016) stated that during the process of vibration, fresh concrete is exposed to high energy oscillations under certain frequencies, resulting in subjecting it to two types of waves: compression and shear waves. As illustrated in Figure 2, compression waves occur when masses are excited in the same direction of the wave propagation. On the other hand, shear waves are a result of the particles moving perpendicular to the propagation direction. These two types of waves can travel through fresh concrete depending on its compression and shear properties as a fluid. However, it is of great difficulty to be able to obtain the compressive properties for fluids of such a level of complexity as concrete. Since these fluids are normally studied with the assumption of being incompressible.

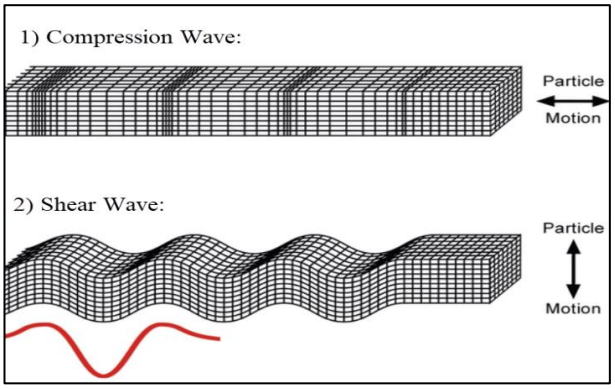

Figure 2. Illustration of the two types of oscillation waves; compression and shear, during the process of vibration (Shoushtari, 2016).

ACI 309.1R-08 (2008) showed that generally the vibrators used depend on the rotation of an eccentric weight to produce a harmonic motion, which can be studied as a sinusoidal wave. These waves are described using the definition of wave frequency and amplitude; where frequency (f) is the number of oscillations per a unit of time, and amplitude (s) is the maximum difference between the current position and the position of rest.

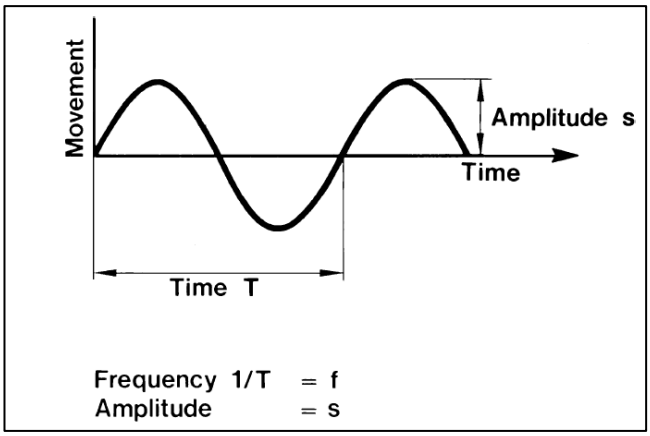

Figure 3. Sinusoidal vibratory motion (ACI 309.1R-08, 2008).

When time during which the wave is propagating is defined by (t) in seconds, this wave (Figure 3) is represented by the following equations:

$$y = s \cdot \sin(2 \cdot \pi \cdot f \cdot t) \tag{1}$$

Where y is the wave movement, (m)
s is the wave amplitude, (m)
f is the wave frequency, (1/s)
t is the propagating time, (s)

$$v = 2\pi \cdot f \cdot s \cdot \cos(\pi \cdot f \cdot t) \tag{2}$$

Where v is the wave velocity, (m/s)

$$a = 4 \cdot \pi^2 \cdot f^2 \cdot \sin(2 \cdot \pi \cdot f \cdot t) \tag{3}$$

Where a is the wave acceleration, (m/s^2)

Additionally, it is shown in ACI 309.1R-08 (2008) that compaction of fresh concrete starts occurring when the acceleration reaches 4.9 m/s², as shown in Figure 4. Comparing the applied acceleration with the final compression strength value of the hardened concrete, it was shown that the consolidation effect rises linearly with accelerations ranging between 9.8 and 39.2 m/s², based on the concrete consistency, as long as the minimum value of amplitude was exceeded. This amplitude value is the second parameter required for compaction. It was proposed by Kolek as cited in ACI 309.1R-08 (2008) to be 0.04 mm. However, the compaction does not improve by increasing the acceleration beyond 39.2 m/s². It can also be seen from the frequency values provided in Figure 4 that the same consolidation results can be acquired over a wide frequency range, given that the minimum amplitude was surpassed, thus showing that the final compaction result is independent of the frequency or the amplitude.

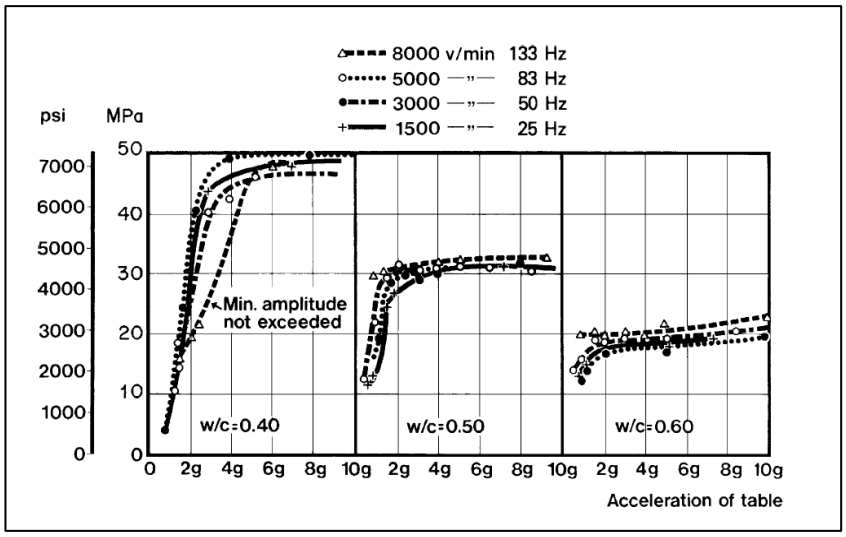

Figure 4. Relation between compressive strength of hardened concrete and vibration acceleration on a vibrating table for different W/C ratios (ACI 309.1R-08, 2008).

Consolidation of concrete is also dependent on the movement of the particles within the mix during vibration, as vibrations help these particles to overcome the internal frictional forces. L'Hermite and Tournon, as cited in ACI 309.1R-08 (2008), showed that stationary fresh concrete internal friction is 0.02 MPa, whilst during vibration it drops down to 0.001 MPa. This shows the large difference between both cases as vibration rids the mix of 95% of its original internal friction.

As Popovics (1973) stated, one other important parameter controlling the mechanism of compaction is the vibratory energy. There is a certain amount of energy needed for concrete to be compacted through vibration, and this energy is acquired from the vibrator converting the electrical and mechanical energies into mechanical oscillating energy. This energy was estimated by Kirkham and White, as cited in ACI 309.1R-08 (2008), using the following equation:

$$W = c_1 \cdot m \cdot s^2 \cdot f^3 \cdot t \tag{4}$$

Where W is the energy, (J)
c_1 is a constant depending on the stiffness and damping in concrete
m is the concrete mass, (kg/9.81 m/s^2)
s is the wave amplitude, (m)
f is the wave frequency, (Hz)
t is the time, (s)

In conclusion, when the minimum value of amplitude is achieved, the efficiency of compaction is controlled by two parameters: the acceleration of the propagating wave and the energy resulted from the vibration and transmitted to the fresh concrete, which are both dependent on the vibration time.

2.1.2 Effects of Vibration on Rheological Properties and Air Movement

Rheology is defined as the science of deformation and flow of matter (Hackley & Chiara, 2001). As stated by De Larrard & Roussel (2011) when the flow of fresh concrete in a steady state was studied, it was represented by an approximated yield stress model, known as Bingham model (Figure 5), which is of the following form:

$$\dot{\gamma} = 0 \; for \; \tau < \tau_0 \tag{5}$$

$$\dot{\gamma} \neq 0 \;\; for \; \tau = \tau_0 + \mu_p \dot{\gamma} \tag{6}$$

Where τ_0 is the yield stress, (Pa)
$\dot{\gamma}$ is the shear rate, (s^{-1})
μ_p is the plastic viscosity, (kg/9.81 m/s^2)

ACI 309.1R-08 (2008) explained that a Bingham material behaves as an elastic solid at yield stress values less than τ_0, and as a Newtonian fluid for higher values of stress. Stability of concrete is one important property that is understood through the rheological behaviour of concrete. They defined the stability as the ability concrete to keep its contents homogenously distributed during flow and setting. Additionally, they explained two types of stability: dynamic and static. Dynamic stability describes concrete's resistance to separation of its components as it is being cast and spread into the formwork. However, static stability represents the resistance of concrete to bleeding, segregation and settlement of surface after it has been cast and during the plastic phase.

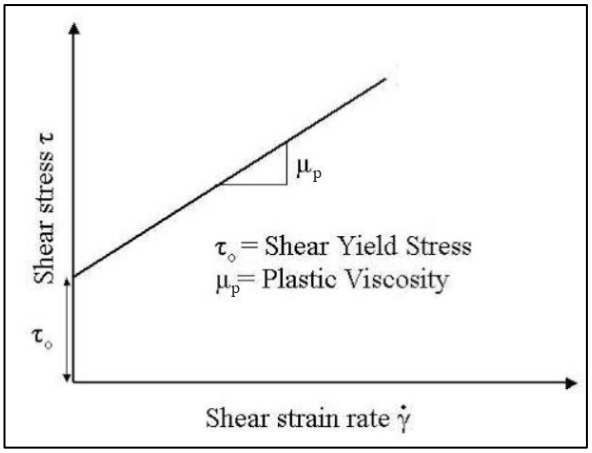

Figure 5. Bingham model describing fresh concrete rheological behaviour.

Having explained the static stability and its relation to the rheological properties of concrete, it can be defined that segregation of concrete is the instability of the mixture resulting from a low yield and low-viscosity matrix, which causes different aggregates to have an inhomogeneous dispersion (ACI 309.1R-08, 2008). It has also been shown by Banfill et al. (1999) that vibration of concrete causes the matrix to lose its yield value, and at a certain value concrete will flow under its own weight.

However, Koch et al. (2019) proved that modelling fresh concrete during vibration using a simple yield-stress fluid was not enough, and it should be modelled as a granular material. The main approach of their research was to test under vibration two translucent surrogate materials; Carbopol 980 representing yield-stress fluid; and a mixture of millimetric glass beads in silicone oil representing the granular model. Given that it is possible to see through these two materials, the motion of air bubbles during vibration was reported, and the more accurate model of fresh concrete was selected.

Koch et al. (2019) vibrated a concrete mixture using a probe with a 1 mm amplitude and 14,000 rpm oscillation speed, and it was found that the maximum distance from the probe and the air bubbles rising to the surface was of around 50 cm. In contrast, when the Carbopol fluid was vibrated using a similar oscillation speed, they found that the bubbles were not disturbed at all, not even in the vicinity of 1 cm around the probe and after vibration for several mins – unless they were in direct contact with the probe (Figure 6a). But when using the granular glass beads, they observed that as it was being vibrated bubbles of diameter around 1 mm started to rise to the surface (Figure 6b). Owing to the measured yield stress of both materials being almost similar, they concluded that concrete during vibration should be modelled as a granular material.

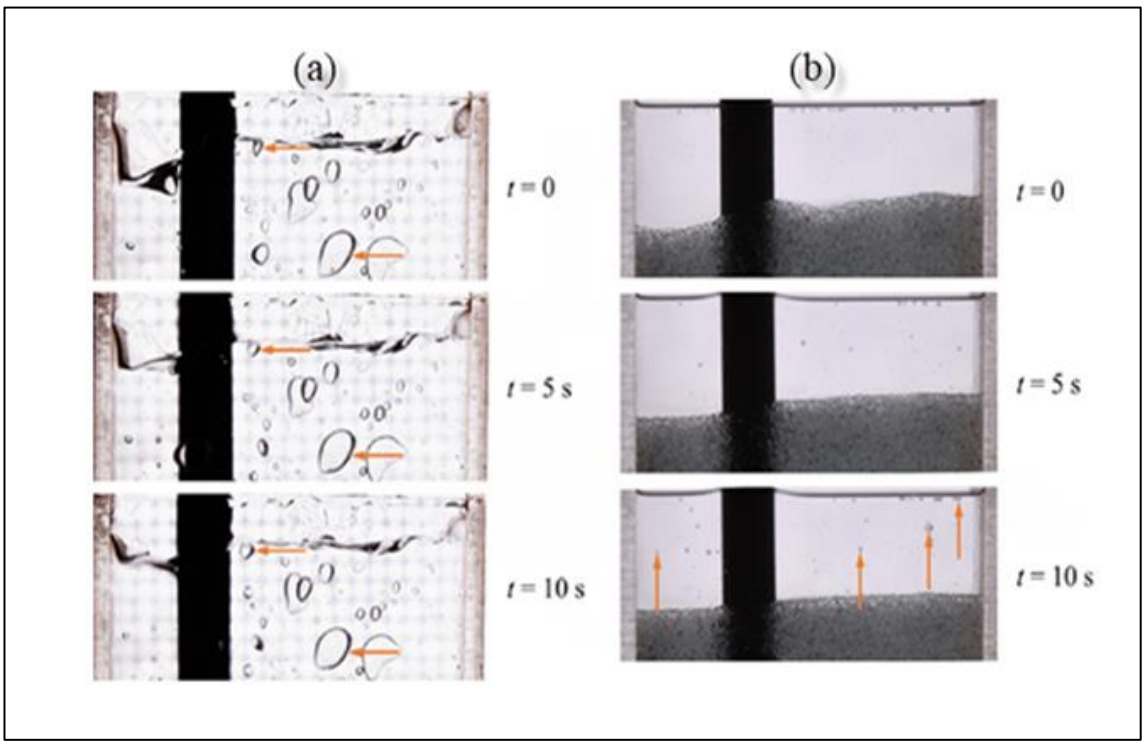

Figure 6. a) Undisturbed bubbles during vibrating Carbopol in water recorded every 5 s. b) Bubbles of diameter 1 mm rising during the vibration of glass beads in silicone oil recorded every 5 s. (Koch, et al., 2019).

Concrete's rheology was also measured by Koch et al. (2019) for conventional and high-flow concrete mixes; before and during vibration, and the graphs of the relationship between the shear stress and shear rate were drawn (Figure 7). The charts demonstrate that the high shear-rate is unaffected by vibration, but there is a significant decrease in different flow stresses, including yield stress for both concrete mixes at lower shear rates. This behaviour was confirmed to be constant after carrying out multiple experiments on different concrete specimens.

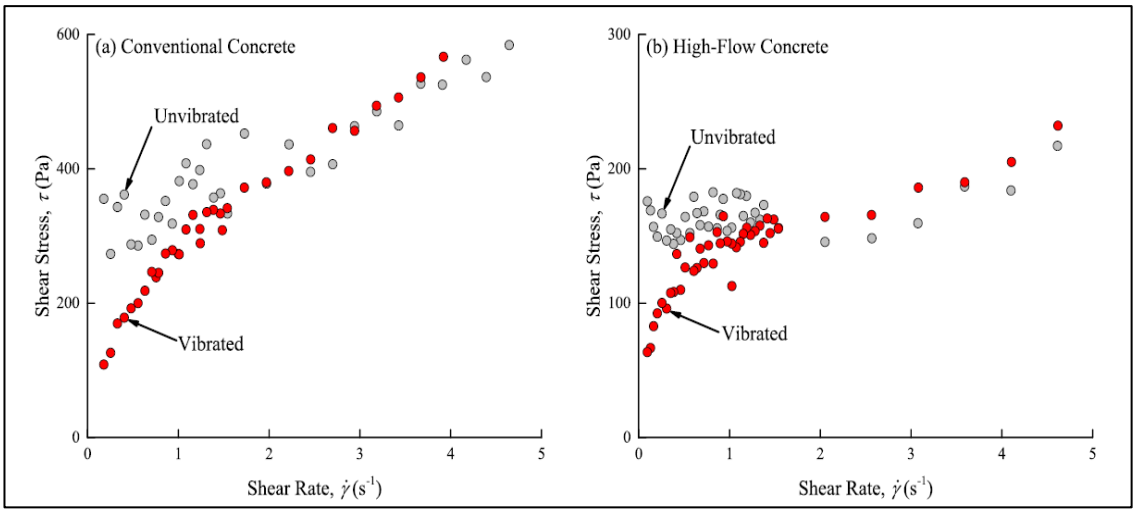

Figure 7. Rheology of (a) conventional concrete and (b) high-flow concrete measured by International Centre of Aggregate Research (ICAR) rheometer, showing a similar behaviour for both mixes (Koch, et al., 2019).

The same measurements were carried out by Koch et al. (2019) for the Carbopol fluid and the glass beads in silicone oil. Consequently, they found that the behaviour of the granular material replicates that of fresh concrete before and during vibration, unlike the simple yield-stress fluid, as can be seen in (Figure 8). This proves that the granular model provides a better representation of concrete during vibration.

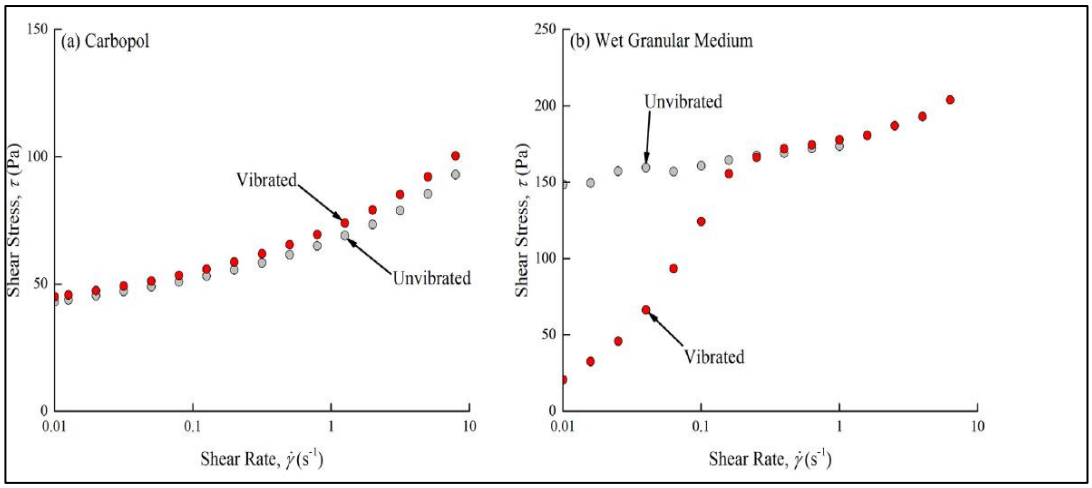

Figure 8. Rheology of (a) Carbopol in water and (b) glass beads in silicone oil measured by ICAR Rheometer, indicating difference in behaviour for vibrated concrete (Koch, et al., 2019).

As stated by Koch et al. (2019) understanding the behaviour of concrete during vibration through the granular model, presents the idea that vibration is not directly concrete overcoming its yield-stress, however it changes the whole character of the fluid adopting new constitutive laws, displaying a Newtonian behaviour. Moreover, they showed that it introduces the concept of force chains, which composes the skeleton of concrete. This concept suggests that when vibration starts, the force chains are disrupted, leading to the loss of yield-stress and liquefaction of concrete. Therefore, they found that it allows air bubbles to rise to the surface with buoyancy.

Findings by Banfill et al. (2011) shows that the radius of action of a vibrator increases proportionally to the plastic viscosity, while decreasing as the value of yield stress rises. In fact, using the granular model approach, as suggested by Koch et al. (2019), implies a depth-dependency of the yield stress, where the deeper it is in the concrete, the more yield stress there is. Consequently, it was proposed that the radius of action decreases with depth, meaning that the effective vibrated area can no longer be viewed as a cylinder, and the adoption of an inverted cone of action is more likely.

This suggestion was tested by monitoring the vibration of the translucent granular medium after introducing some stainless-steel particles inside, and it was found that there exists an inclined fluidization line (Figure 9), under which the stainless-steel particles almost remained stationary even after vibration for 4 minutes. Thus, based on the rheological understanding of concrete, the inverted cone model is a more accurate representation of the effectively vibrated area.

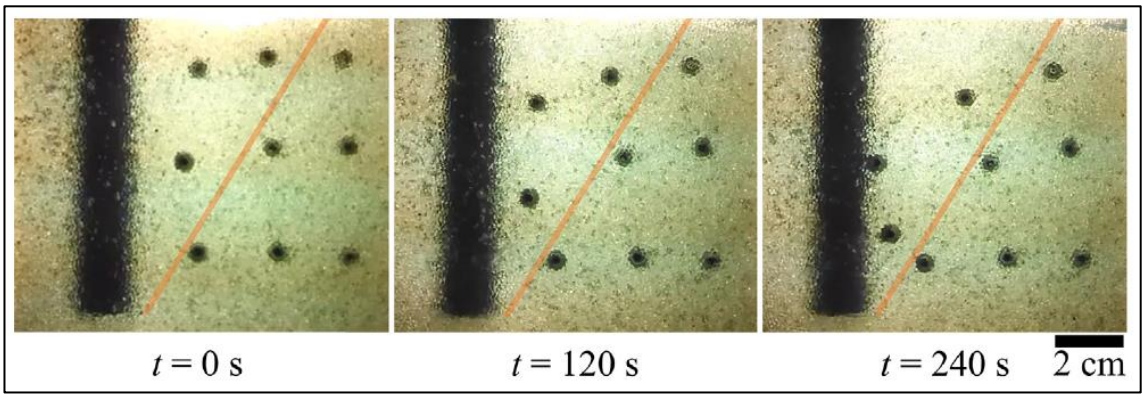

Figure 9. Vibration of glass beads in silicone oil with intruding stainless-steel particles with the fluidization line drawn suggesting an inverted cone like effective vibration area (Koch, et al., 2019).

Focusing on air bubbles inside the concrete mixture, Lange et al. (2016) showed that the use of Bingham model to study the behaviour of concrete at rest shows its ability to entrap small air bubbles inside. However, when concrete starts to lose its yield stress due to vibration as explained previously, those bubbles start rising under buoyant forces. As shown in Figure 10, the rise of bubbles takes place when the buoyant force is equal to Stoke's drag force, which can be represented by the following equation:

$$F_{buoy} = F_{drag}$$
$$\frac{1}{6}\,\pi \cdot \Delta\rho \cdot\ g \cdot D^3 = 3\ \cdot \pi \cdot\ \mu \cdot\ U \cdot\ D \qquad (7)$$

Where $\Delta\rho$ is the density difference, (kg/m³])
μ_1 is the fluid viscosity, (Pa.s)
g is the gravitational acceleration, (9.81 m/s^2)
D is the air bubble diameter, (mm)
U is creep-flow velocity of a particle in a Newtonian fluid, (m/s)

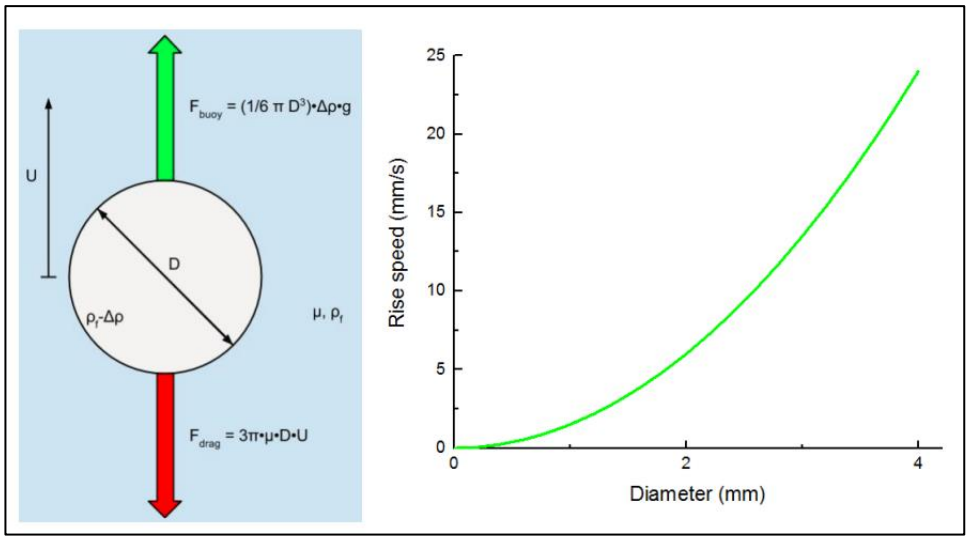

Figure 10. Representation of the forces affecting a bubble inside fluid losing its yield stress, and on the right a chart illustrating the simulation of the relationship between the rise speed of air bubbles and their diameters (Lange, et al., 2016).

A simulation of the speed with which the bubbles rise during the vibration of a yield stress fluid was carried out by Lange et al. (2016), and the result was that the larger bubbles had a higher rise speed than smaller ones (Figure 10). This model shows that vibration rids the concrete of larger diameter bubbles quicker than smaller ones. Consequently, it supports the understanding of how air bubbles move inside the concrete mix as it is being vibrated, and that for well-vibrated concrete, the element should be rid of larger air bubbles while maintaining the entrained air bubbles for freeze-thaw resistance.

2.1.3 Effects of Vibration on Segregation

Segregation is generally defined as the process during which a bulk solid consisting of different components turns into a spatially non-uniform solid due to the relative movement of its constituents (Rosato, et al., 2002).

According to Ojala et al. (2019) segregation of concrete was linked to its over-vibration, and was categorized into 3 different types:

- Coarse aggregate separated from or settled down in the mix,
- Paste separating away from coarse aggregate,
- Water separating out of the mixture – due to its low specific gravity.

The physical factors influencing segregation during vibration were reported by Belkhman I. et al. (2014) as five different factors:

1. Fluidization of the mixture.

2. Resistance variance of particle movement in different possible directions. Firstly, towards the lower medium's boundary (F_-), where the particle is forced to thrust against any underlying particle to make its way. Secondly, away from the boundary (F_+), in which case the particle will have to uplift other particles in the way. Lastly, parallel to the surface (F_h), where resistance is at its highest. (Figure 11)

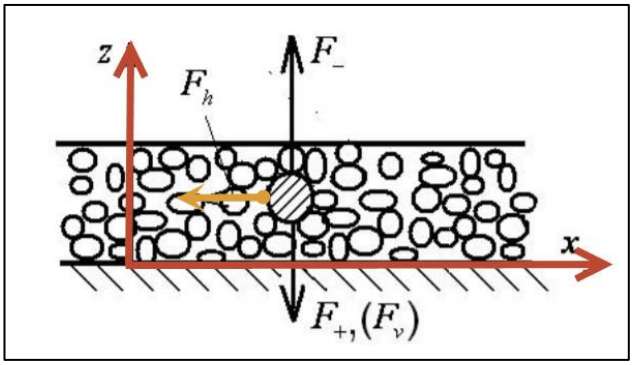

Figure 11. Schematic representation of resistance force particles in a granular medium during vibration (Blekhman I., et al., 2014).

3. Oscillations of particles with a relatively different density than that of the medium, including particles of fairly larger size inside a medium of smaller sized granules.

4. The Wedge Effect, shown in (Figure 12) takes place when mediums with some relatively larger particles are vibrated. These particles move upwards whilst its adjacent medium layers from both sides accumulate below that particle. This effect occurs in both cases of vertical and horizontal vibration, but in the latter the finer granules end up on the right or the left of the larger particles.

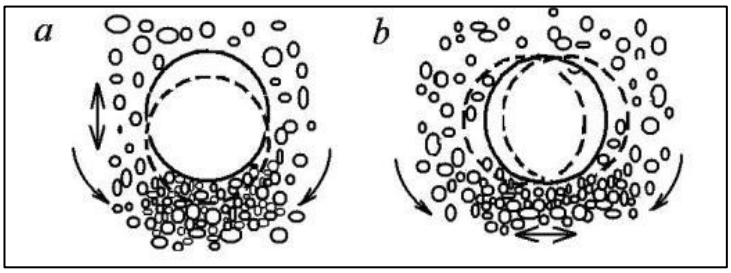

Figure 12. Wedge Effect: a) under vertical medium vibration and b) under horizontal medium vibration (Blekhman I., et al., 2014).

5. Fine particles are packing larger particles together, while smaller granules move towards the walls of the vibrated vessel. This can be seen at distances closer to the wall of the vessel, as the packing of coarser particles decreases, and more fine particles are found accumulated on the side and bottom walls of the vessel.

The settlement of spherical particles inside a fluid was reported by Beris et al. (1985) to occur when the yield stress parameter (Y_g) drops below 0.143. This parameter is defined by the following equation:

$$Y_g = \frac{3 \cdot \tau_0}{2 \cdot R \cdot |\Delta_\rho| \cdot g} \tag{8}$$

Where Y_g is the yield stress parameter
τ_0 is the yield stress, (Pa)
R is the radius of the particle, (mm)
Δ_ρ is the density difference between the particle and fluid, (gm/mm^3)
g is the gravitational acceleration = 9.81 m/s^2.

The velocity of these settling particles inside a Bingham plastic was defined by Petrou et al. (2000) through the following equation:

$$U = \frac{2 \cdot R^2 \cdot |\Delta_\rho| \cdot g}{9 \cdot \mu_p \cdot C_s} \quad (9)$$

Where U is the velocity of a sphere moving inside a fluid (mm/s)
μ_p is the plastic viscosity, (kg/9.81 m/s^2)
C_s is the Stokes drag coefficient

In case of concrete, Lopez & Navarrete (2016) stated that these particles are considered the Coarse Aggregates (CA), while the fluid is the mortar. Equation (8) shows that CA start moving depending on the yield stress (τ_0) of the mortar, the density difference between CA and the mortar, as well as the CA size. Additionally, Equation (9) provides that the speed at which CA move within concrete is inversely proportional to the plastic viscosity (μ_p), and directly proportional to the CA radius and density difference. They have pointed out that when concrete is vibrated, the values of (τ_0) decrease, whereas those of (μ_p) increase. This shows that as concrete is vibrated, segregation tendency highly increases.

Additionally, Ojala et al. (2019) inspected the effect of vibration effort on segregation tendency in concrete for both air-entrained and concrete without air entrainment. 19 concrete mixtures were tested, 17 of which had air-entrainment, while the remaining two were without entrained air. The measured slump was recorded for each mix. Different vibration efforts were realized for the mixes by varying the vibration duration between 15 and 60 seconds. After the concrete had hardened, six cores were drilled, and their densities measured in order to study the variation in density between cores using the standard deviation of these values.

The relationship between the measured standard deviation and the vibration effort for the different mixes is shown in Figure 13. It is apparent that air entrainment plays a major role in causing concrete to segregate. This is shown in the significant difference in values between the air-entrained S3 concrete and the other S3 without air entrainment, even though both concrete are in the same slump class. In addition, Figure 13 that concretes with higher workability showed a significantly higher rise in standard deviation compared with others of lower workability. This denotes that workable concretes are more prone to segregation due to vibration than less workable ones. Lastly, the behaviour of concretes without air entrainment shows that these concretes are highly resistant to segregation, even at a relatively higher slump class of S3.

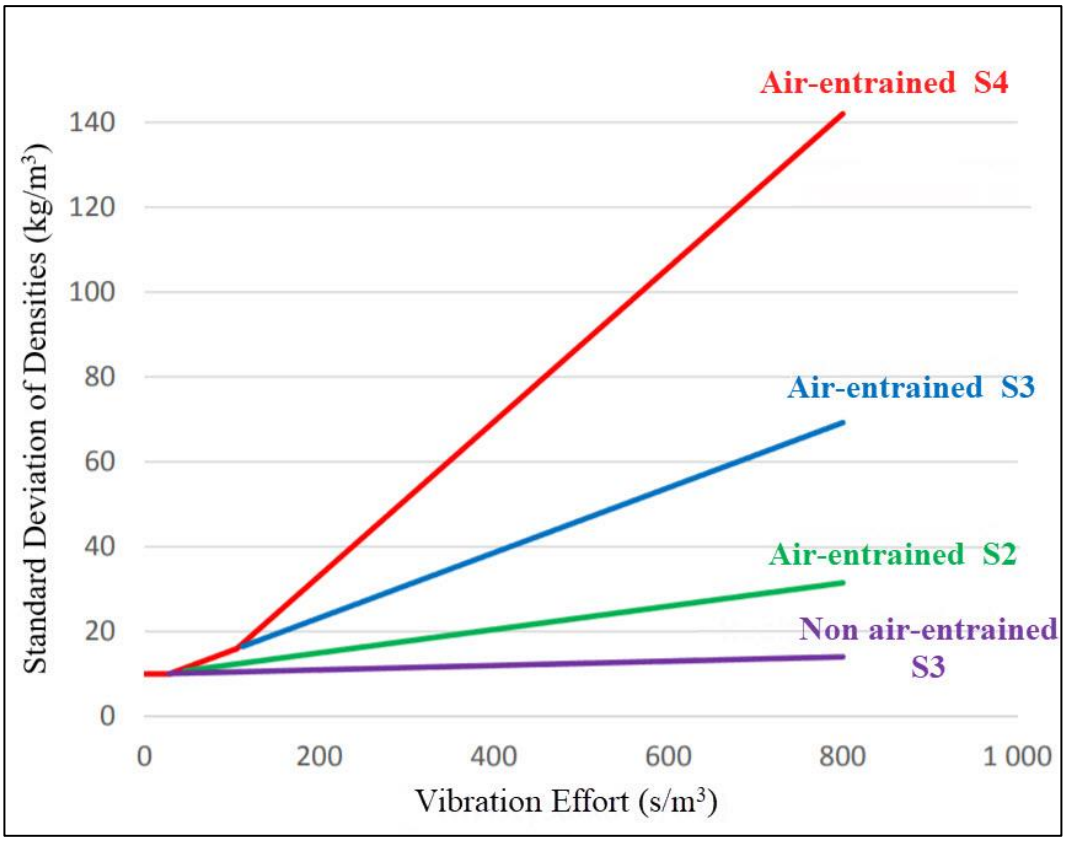

Figure 13. Relationship between vibration effort and standard deviation of densities for drilled cores from the concrete mixtures with different slump values (Ojala, et al., 2019).

2.1.4 Different Methods of Concrete Compaction

Compaction of concrete can be achieved by different methods. These techniques categorized by Suryakanta (2014) into two main approaches: hand compaction and mechanical compaction. The use of hand compaction is limited to ordinary and unimportant structures and some laboratory tests, whilst mechanical compaction is used broadly in the process of construction of concrete structural elements. In Patel (2019) hand compaction was divided into 3 different types:

a) **Rodding:** the process of poking the concrete using a steel rod, where the tamped layers reported by Suryakanta (2014) should be 15 to 20 cm high. This method is used to compact corners and edges of concrete cubes, and compact precast concrete blocks. (Figure 14a)

b) **Ramming:** concrete is rammed or puddled to release the entrapped air. It is only used in plain concrete elements, such as unreinforced foundations, and ground floor works. (Figure 14b)

c) **Tamping:** it is carried out by using a wooden beam of a typical cross section dimensions of 10 cm x 10 cm, where the surface is hit using this beam. It is mostly used in the compaction of roof slabs or Roller Compacted Concrete pavements, where the thickness of concrete is relatively low, and the surface finish is required to be smooth. (Figure 14c)

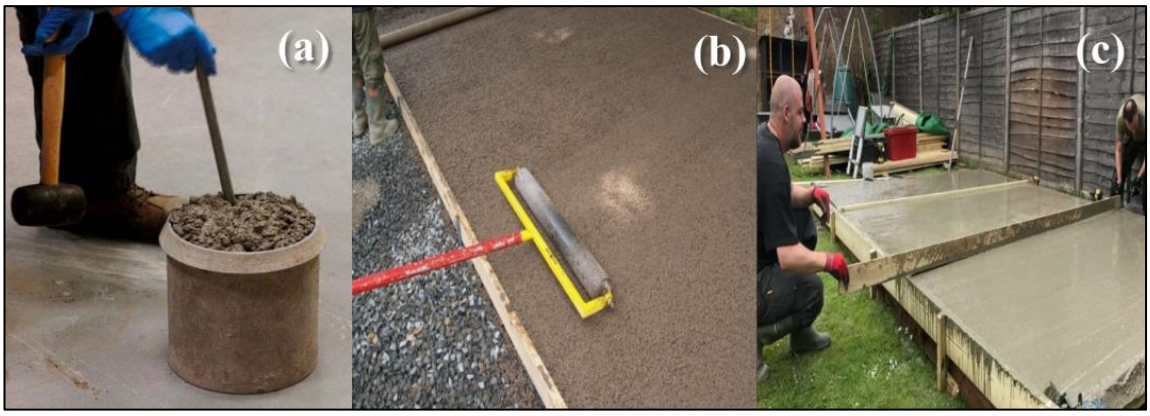

Figure 14. Different hand compaction methods: a) Rodding, b) Ramming and c) Tamping (Patel, 2019).

On the other hand, mechanical compaction was classified by Mata et al. (2014) into the following types (Figure 15):

1. **Immersion vibration:** the device used in this method is commonly referred to as a 'poker' or a 'needle' vibrator. These vibrators consist of a tubular housing with an eccentric rotating weight inside. Upon immersing the tube into the concrete, it transfers the vibration to the fresh mixture, leading to its compaction. The radius of action of these vibrators varies based on the amplitude and frequency provided by each vibrator, as shown in Table 1.

Table 1. Relation between the radius of action of vibrators based on their frequency and amplitude for different rate of concreting (Mata, Pitroda, & Bhavsar, 2014).

Head Diameter (mm)	Recommended Frequency (Hz)	Average Amplitude (mm)	Radius of Action (mm)	Rate of Concreting (cm/hr)
20-40	150-250	0.4-0.8	75-150	1-4
30-65	140-210	0.5-1.0	125-250	2-8
50-90	130-200	0.6-1.3	175-350	6-20
75-150	120-180	0.8-1.5	300-500	11-31
125-175	90-140	1.0-2.0	400-600	19-38

2. **Beam Screed Vibration:** in this method the vibrator is made up of one or two beams, made from steel, timber, or aluminium, with a vibrating unit attached to those beams to provide sufficient surface vibration. The width of the beams varies from 6 m up to 20 m in case of trussed units. Given that the compaction achieved from the surface depends on the thickness of the concrete element, only slabs with thickness of 10 cm to 20 cm will be vibrated efficiently. Additionally, the degree of compaction rises with higher beam weights, and larger amplitude and frequencies of the vibrating unit.

3. **Roller Screed Vibration:** the device used is quite similar to the beam screed vibrator, except for the beam being replaced by a lengthy cylindrical roller. Inside the roller exists a rotating imbalanced weight providing almost the same quality of compaction for the whole vibrated surface.

4. **Formwork Vibration:** this method involves attaching an external mechanical vibrating device to the formwork, where those devices first transfer the vibration energy to the form and in turn it is transmitted to the concrete, causing it to require much more power than other vibration methods. It is mostly used members with complicated geometry or highly dense reinforcements, and it requires a special design of the moulds.

5. **Table Vibration:** Patel (2019) stated that vibrating tables usually consist of a steel platform mounted on flexible springs, with the vibration generated by an eccentric mass strongly rotating resulting in a circular vibration motion. Moreover, some table vibrators generate vibrations using an electromagnetic field with a varying current. Normally, the range of frequencies of vibrating tables is 50 to 150 Hz.

Figure 15. Mechanical compaction methods: a) poker vibrator, b) beam screed vibrator, c) roller screed vibrator, d) formwork vibrating system, e) table vibrator (Patel, 2019).

According to Gopi (2010) there also exists two compaction methods that are application-specific: compaction by pressure and jolting and compaction by spinning. The first is used during the process of manufacturing concrete hollow blocks, solid blocks, and cavity blocks. The process includes pressing, vibrating, and giving jolts to the stiff concrete with very low water-cement ratio to compact it into dense blocks with high strength. Differently, the spinning compaction is used for fabricating concrete pipes. This procedure comprises of spinning the fresh concrete at exceedingly high speeds, while the centrifugal force plays the role of compacting the concrete pipe.

Mechanical vibration methods are the most commonly used on site – especially, immersion vibrators (Gong, et al., 2015), we will present the suggested insertion patterns and times in the following. Firstly, the insertion and withdrawing speed should always be low, in order to provide the opportunity for fresh concrete to regularly flow into the hole created by the vibrator. As reported by Bhattacharjee (2007) the withdrawal speed should be in the range of 3-7.5 cm/s to provide proper compaction.

Secondly, the spacing and number of insertion points was detailed by Cement Concrete & Aggregates Australia (2006) as shown in Figure 16. Insertion patterns should be followed, since otherwise parts of concrete might be left uncompacted. Moreover, vibrators should be inserted with a clearance of about 50 mm from the formwork's face, in order to avoid 'burning' marks that reflect on the final surface finish after demoulding.

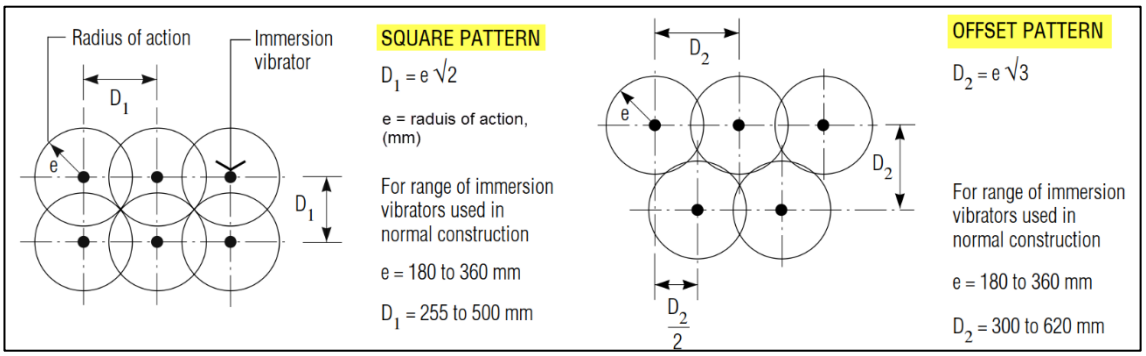

Figure 16. Illustration of the two different patterns of insertion points using immersion vibrators (Cement Concrete & Aggregates Australia, 2006).

Thirdly, the thicknesses of casting layers as recommended by Punkki et al. (2019) are as follows. In case of concrete without air entrainment, the layer thickness should not exceed 40 cm, whereas for air-entrained concretes, the layer thickness should be 30 cm.

Lastly, the duration of vibration; it is only monitored subjectively by the construction inspectors, where vibration is stopped when air bubbles stop rising to the surface of concrete (Tattersall, 2003). However, in theory the required time for vibration can be calculated using the following formulas reported by Bhattacharjee (2007):

$$t = \frac{25}{\phi} \cdot \left[\frac{100}{S+5} + A\right] \cdot F \cdot \sqrt{V}, \qquad \text{for V} < 25\ \text{dm}^3 \tag{10}$$

$$t = \frac{25}{\phi} \cdot \left[\frac{100}{S+5} + A\right] \cdot F \cdot (0.1V + 2.5), \qquad for\ \text{V} > 25\ \text{dm}^3 \tag{11}$$

Where t is the time required for vibrating V litres of concrete, (s)
ϕ is the diameter of the poker, (mm)
S is the concrete mass, (cm)
A is a coefficient representing the shape of aggregates; *A= 1.0* or *5.0* for rounded and crushed aggregates respectively
F is a Coefficient representing the denseness of steel; F=1.5 for very dense and *F=1* for no reinforcement.

Shraddhu (2017) has also stated that compaction time varies from one mix to another based on the different workability, with the variance range generally being from 5 s to 30 s, while in some cases, it might rise to 120 s. However, he pointed out that compaction is normally visually judged from the observed surface, as it should neither have excess mortar nor appear honey combed, with the first representing over-vibration and the latter indicating under-vibration.

2.1.5 Effects of Compaction on Concrete Strength and Durability

During the explanation of the mechanism of compaction, it was made clear that one important aspect of vibrating concrete is to release the unwanted entrapped air, since it dramatically affects the final strength of the concrete element. It was reported by Cement Concrete & Aggregates Australia (2006) that concrete samples with 10% extra entrapped air have strengths of about 50% less than those properly compacted .

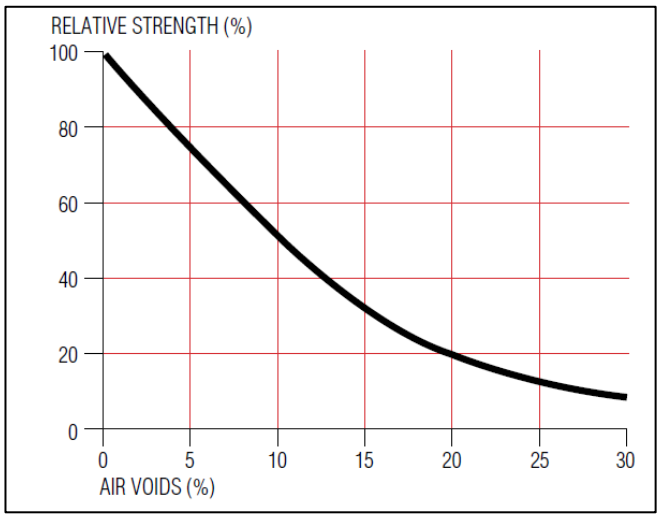

Figure 17. Loss of concrete strength due to the increase of air voids (Cement Concrete & Aggregates Australia, 2006).

Additionally, Tuncan et al. (2007) carried out an experiment where they divided a concrete mix into 3 different batches, each batch was treated differently in terms of compaction. The first batch was not compacted at all, while the second one was compacted by rodding and the third was mechanically consolidated by a poker vibrator. Afterwards they drilled cores from the specimens and tested under compression. The results are presented in Figure 18, and as they have shown the non-vibrated concrete was the weakest, while the rod-compacted was of a strength a bit higher, and the vibrated concrete provided the highest strength values, since the poker vibrator was able to rid the concrete specimens off of more entrapped air than rodding.

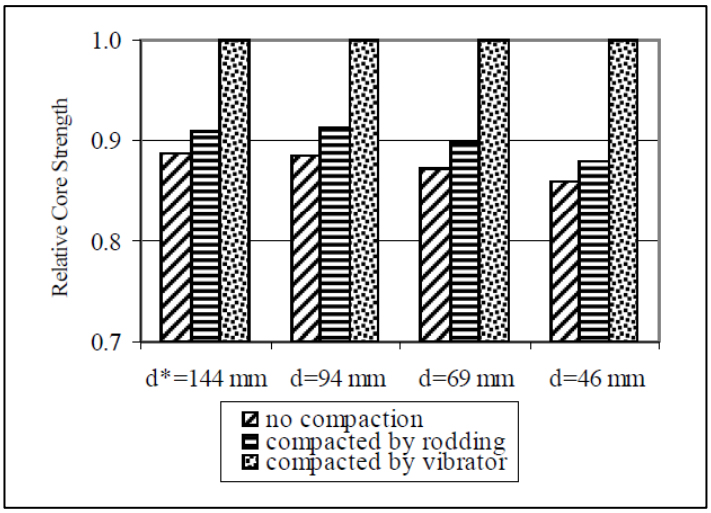

Figure 18. Relative drilled cores compressive strength for non-compacted, rod-compacted and poker compacted concretes (Tuncan, et al., 2007).

The effect of vibration time on strength of hardened concrete has also been studied by Arslan et al. (2011). They have tested the compressive strength of both high-performance and ordinary concrete samples with different water-cement ratios, which were vibrated for different times varying from 10 s to 240 s. The results are presented in Figure 19, and they show that after an optimum vibration time, the concrete's strength starts to plummet as the vibration time increases. Thus, it is of great importance not to over- or under-vibrate concrete since in both cases the optimum strength will not be met.

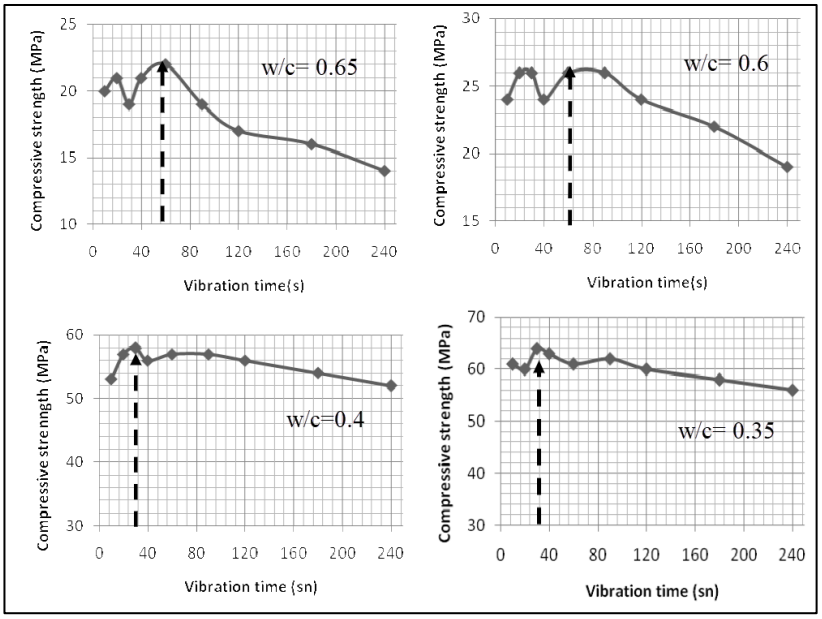

Figure 19. Compressive strength-vibration time relation for ordinary and high-performance concrete with different W/C ratios (Arslan, et al., 2011).

Cement Concrete & Aggregates Australia (2009) stated that compaction also leads to a more durable concrete, given that during the process of compaction the pores inside the concrete become discontinuously distributed, decreasing its permeability, and leading to better durability. Moreover, they reported that proper consolidation of concrete leads to a surface that is more resistant to abrasion. On the other hand, they showed that over-vibrating concrete results in the rise of a layer of mortar on the surface, leading to a much weaker finish that is more prone to abrasion.

Suprenant (1988) indicated that under-vibration is a more regular occurrence than over-vibration, and it causes more durability problems. He listed honeycombing, sand streaks, cold joints, and subsidence cracking, under durability issues by under-vibrated concrete. In addition, the ones caused by over-vibration usually include segregation and sand streaks. However, over-vibration puts the formwork at the risk of deflection or damage, and in some cases total failure.

2.2 Techniques Used for Compaction Monitoring

Given the fact that many different factors influence the quality of compaction, monitoring of compaction is of very high importance to ensure that concrete structures reach their design strength and be durable through their service period. Some methods were developed to keep track of the process, as listed below.

2.2.1 Infrared Thermal Imaging of Vibrated Areas

One of these methods was devised by Burlingame (2004), where the infrared thermal imaging was used to determine the location of vibrated areas and to what extent they were vibrated. They based the method on measuring the difference in temperature between vibrated and non-vibrated areas, since vibrated parts have a higher temperature, they could be traced, and their location recorded. The infrared cameras used by the researchers could observe the heat signature for a time up to 20 min after vibration. However, this method does not monitor either the time or depth of vibration. Moreover, it proved inapplicable for locating compaction of layered concrete, since new layers cover the old ones quickly, resulting in a change in the thermal difference.

2.2.2 Global Positioning System and Real-Time Kinematics Modes

Tian & Bian (2014) constructed a real-time visual monitoring system, which combines GPS, a GLONASS satellite receiver, and Real-Time Kinematics measuring mode, to track the location of immersion vibrators on site. They stated that the accuracy with which the system measures the location of the vibrators was within less than 5 cm. Moreover, an assembly of electrodes was devised by the researchers to record the time between the insertion and pull-out of the vibrator. They analysed the results acquired by that system and provided a map that tells whether the area has been vibrated or not. Additionally, it reports the quality of compaction (see Figure 20) based on statistical data obtained from different fresh concrete tests as shown in Table 2.

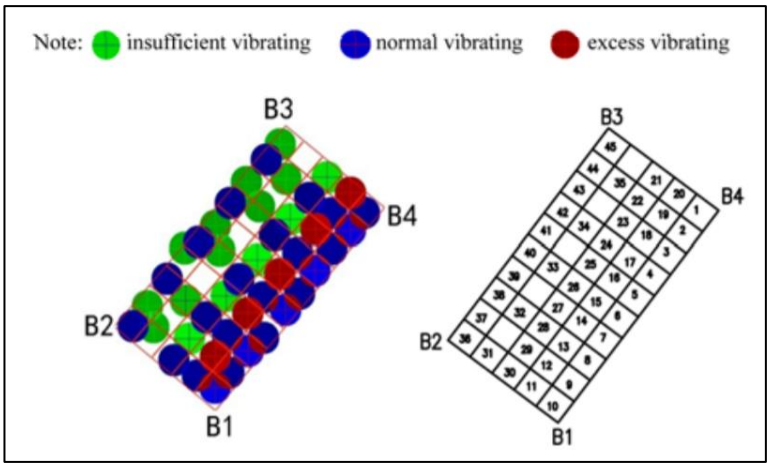

Figure 20. Analysed results from the monitoring system showing the different levels of vibration (Tian & Bian, 2014).

This method can provide a schematic representation of the normally, excessively, and insufficiently vibrated areas, however the statistical data used in identifying the quality of compaction is only mix specific and not location specific. Given that for the same concrete mix there are many different parameters that influence the degree of compaction, there still is a need for the development of a device that monitors the quality of compaction, rather than the time and location only. In addition, the system used was limited to two-dimensional space tracking since developing a system that visualizes in 3D the effects of vibrations proved to be challenging on a computational level.

Table 2. Statistical data of different vibration parameters and their corresponding vibration duration range (Tian & Bian, 2014). Note: "d" is vibrator head diameter in centimetres.

Series No.	Slump (cm)	Coarse Aggregate Size (cm)	Vibrating Duration (s)	Effective Vibration Radius
1	5-7	5-20	30-50	5-6d
2	5-7	5-40	40-60	4-5d
3	5-7	5-80	55-75	4-5d
4	7-9	5-20	20-40	5-7d
5	7-9	5-40	30-50	4-5d
6	7-9	5-80	40-60	4-5d
7	9-11	5-20	20-40	7-8d
8	9-11	5-40	20-40	6-7d
9	9-11	5-80	25-45	5-6d

2.2.3 Ultra-Wide-Band Quantification of Concrete Vibration

Another method was developed by Gong et al. (2015), which uses Ultra-Wide-Band (UWB) to quantitively assess the vibration of concrete. The UWB technology wirelessly senses and localizes moving objects over radio waves, and its use enabled the development of a tool that provides real-time 3D visualization of the location and duration of vibration with a 10 cm accuracy, even with reinforcement steel present (Gong, et al., 2015). Additionally, they stated that this technology is preferred over the use of GPS, since UWB tags are a lot smaller and cost much less money compared to GPS receivers and antennas.

In this method, they attached UWB tags to the vibrators, and signals are received from these tags throughout the compaction process. Consequently, they found that this system can track the location of the vibrator tip with a high accuracy, while recording and displaying the vibration duration in the form of colour maps. These maps acquired by the researchers (Figure 21) clearly display the trajectory of the vibrator inside the concrete, and also capture the un-vibrated effort represented by the colour scheme; where hotter areas mean more vibration effort and vice versa, whilst plain areas represent parts that were left unvibrated (Gong, et al., 2015).

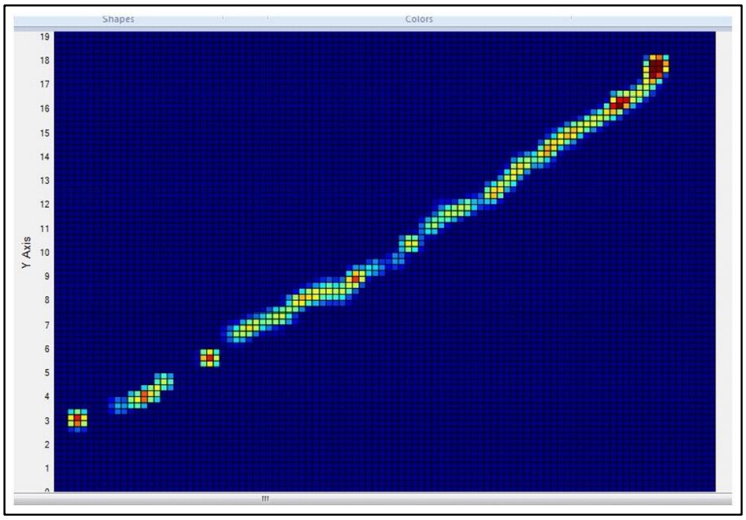

Figure 21. Visual plot of tip position for a mounted UWB tag 30 cm from the tip of the vibrator (Gong, et al., 2015).

As stated by Gong et al. (2015) the limitations of this method include the inability to track vibration effort within slabs of a thickness less than 15 cm, and there's another problem with the time of the setup, since it takes up to 90 min to arrange the measuring system. Moreover, it does not give precise data of when to stop vibrating to achieve the best quality possible. In addition, they identified that this method can only be applied in laboratory or very small-scale applications, since the creation of a 3D realistic model with real-time feedback of the vibration process is needed in order to apply a visual monitoring system to a real construction site, which requires the simultaneous transferring, analysis and storing of huge amounts of data. Hence, the requirement of producing a more efficient model of the system to be able to keep up with demand of an actual construction site (Tian, et al., 2019).

2.2.4 Global Navigation Satellite System for Compaction Monitoring

In order to overcome the limitations of the UWB method, Tian et al (2019) composed a new system, in which the trajectory of the vibrator is traced by the Global Navigation Satellite System (GNSS), and the insertion of the vibrator inside the fresh concrete is monitored on the basis of the difference in the motor's voltage, from which the vibration time can be calculated – on the basis of the switch from one state to another. Afterwards, they had the collected data sent to the cloud database using General Packet Radio Service (GPRS) for the radius of action and the effective vibrated zone to be computed. The collective set of data is displayed all together at a remote-control site using a 3D visualization system, while the shortcomings of the vibration process are sent to the inspector's mobile phone in a graphical form.

In order to check the accuracy of trajectory tracking, Tian et al. (2019) performed a test on a 3D area of the dimensions 6 m x 4 m x 0.5 m, at which some points where preassigned and then the tip of the vibrator was moved to the position of those points. Consequently, the results obtained (Figure 22) provided a location specification accuracy of 20 cm, which proves to be of practical use in construction sites.

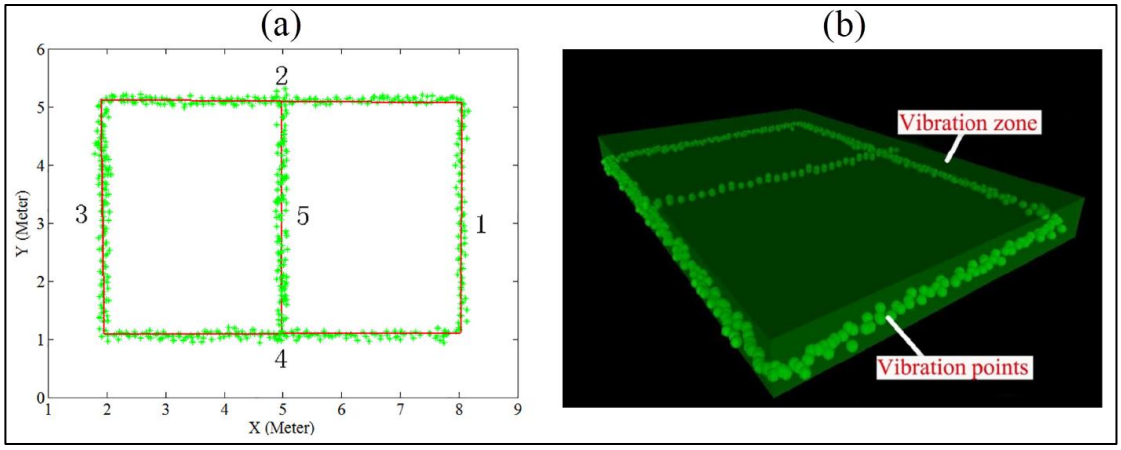

Figure 22. Plot of the tracked vibration points in: a) 2D, and b) 3D (Tian, et al., 2019).

In addition, Tian et al. (2019) carried out an on-site case study, where slabs and beams were monitored during vibration using their proposed system. The results of the monitoring are as presented in (Figure 23a), where the blue and green areas designate the well-vibrated concrete, and the yellow parts represent the under-vibrated regions. Additionally, (Figure 23b) shows the graphical representation of the status of vibration sent via the mobile application to the inspector's phone.

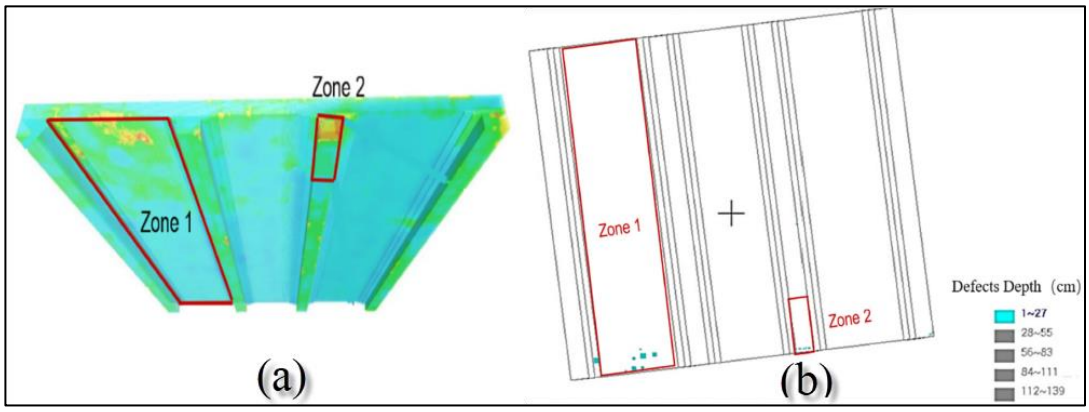

Figure 23. (a) 3D visualization of the compaction quality of the slabs and beams; (b) 2D visualization of compaction quality in the mobile App (Tian, et al., 2019).

As means of validation, the obtained results by Tian et al. (2019) were compared with those acquired from the investigation of the hardened concrete using the non-destructive Impact Echo Method (IEM), which is a technology that measures the impact-generated sound waves reflected by internal flaws in hardened concrete, such as large voids, cracks, delamination and honeycombing. The located defects using IEM were in correspondence with the ones specified in the 3D visualization model reported by the monitoring system. Thus, this system proved to be efficient in locating under-vibrated areas in real-time through the mobile application, and revibrating under-vibrated regions was possible (Tian, et al., 2019).

However, according to Tian et al. (2019) this system includes some limitations, such as the determination of the radius of action being based on experiments on a certain group of concrete mixtures, meaning this system cannot be universally used for random concrete mixes. Moreover, the effective vibration zone was considered as a perfect cylinder, and the diminishing in vibration energy as the waves propagate through concrete was not taken into account. Finally, some improvements could be implemented to better the accuracy of locating the vibrator's tip (Tian, et al., 2019).

2.3 Electrical Impedance Spectroscopy (EIS) Measurement Technique

The use of EIS is reported to have started around the year 1894 as cited in Grossi & Riccò (2017), when Nernst used it to measure the dielectric constant of aqueous electrolytes along with other organic fluids. Nevertheless, the use of EIS became more prominent in the 1980s, since computer technology prospered, and it was possible to take measurements much quicker and process them on higher levels of complexity. Grossi (2017) stated the applications of EIS in different scientific fields, which included: the analysis of corrosion of metal surfaces, the characterization of the hardening process of cement paste, the analysis of human body composition, and the determination of State of Charge and State of Health of a battery. Additionally, EIS tests for hardened concrete included locating of cracks and corroded reinforcement (Polder, 2001).

2.3.1 Concept of EIS Investigation

Electrical impedance is defined by Mahajan (2008) as the overall opposition displayed by a whole circuit or part of it to an electric current. He showed that it consists of resistance and reactance, where resistance is caused by the collision of particles carrying the current with the conductor, while reactance is the extra opposition to the motion of electrical charges, resulted from the varying magnetic and electric field in circuits with alternating current. Consequently, in case of steady direct current, impedance of a circuit scales down to resistance only.

As reported by Grossi & Riccò (2017), there are two types of EIS investigations: first the Potentiostat EIS, where a sine-wave voltage is applied to the tested specimen and the current induced is measured, afterwards the complex impedance is calculated. Alternatively, the second version is called Galvanostat EIS, where the sample is stimulated with a sine-wave current, and the voltage drop across the specimen is measured, then impedance is computed. PalmSens (2019) stated that the current and voltage waves are of the same frequency given that one wave produces the other, and there exists a constant time shift between the waves known as the phase shift, which is illustrated in Figure 24.

The equations governing those calculations are as follows:

$$V(t) = \bar{V} + \hat{V} \cdot \sin(\omega t) \tag{12}$$

Where $V(t)$ is sine-wave voltage
$\bar{V}$ is the direct current value of voltage
$\hat{V}$ is the voltage amplitude
ω is the angular frequency
t is the time

$$I(t) = \bar{I} + \hat{I} \cdot \sin(\omega t + \varphi) \tag{13}$$

Where $I(t)$ is the induced current
$\bar{I}$ is the direct current value
$\hat{I}$ is the current amplitude
φ is the time phase difference between voltage and current

$$Z(j\omega) = \frac{V(j\omega)}{I(j\omega)} = \frac{\hat{V}}{\hat{I}} \cdot e^{j.Arg(Z)} = Re(Z) + j \cdot Im(Z) \tag{14}$$

Where $Z(j\omega)$ is the complex impedance
$V(j\omega)$ is the Steinmetz transform of $V(t)$
$I(j\omega)$ is the Steinmetz transform of $I(t)$
$Re(Z)$ is the real part of impedance (resistance)
$Im(Z)$ is the imaginary part of impedance (reactance)

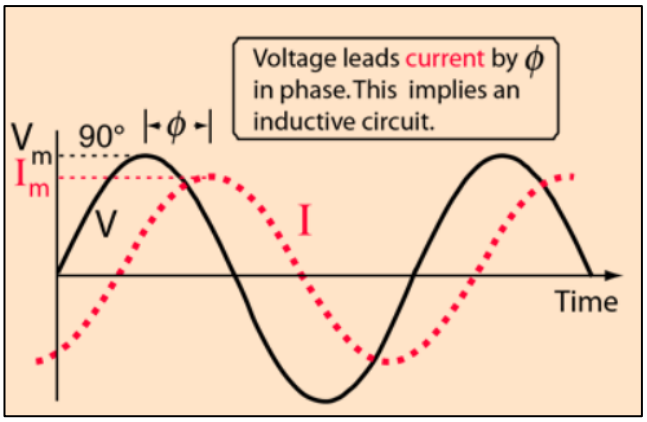

Figure 24. Schematic visualization of the phase shift in the case of voltage leading current (Nave, 2000).

According to PalmSens (2019) one of two plots is used to visualize the impedance spectra; Bode plot and Nyquist plot (Figure 25), where Nyquist plots are more popular to use due to their high sensitivity to changes, and the relative ease to directly read common electrical parameters for different circuits using them. In the case of Bode plots, they stated that their abscissa is the logarithmic scale of the frequency, with the two other ordinates being the logarithmic scale of the impedance and the phase shift. On the other hand, Nyquist's plots draw the relationship between the negative imaginary impedance on the vertical axis and the positive real part of impedance on the horizontal axis (PalmSens, 2019).

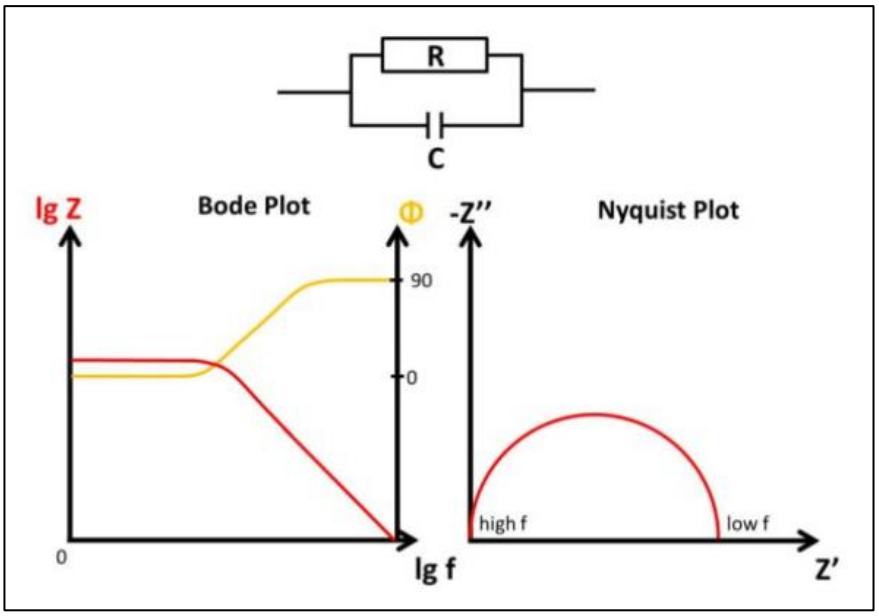

Figure 25. Schematic Bode and Nyquist plots for a parallel resistor and capacitor (PalmSens, 2019).

Practically, during EIS the current response of the tested sample is measured, using a frequency response analyser and a setup of electrodes that subject the specimen to a low amplitude alternating current over a certain range of frequencies (Grossi & Riccò, 2017). There are various setups for electrodes that can be used during EIS measurements as shown by Grossi & Riccò (2017), which commonly include the two-, three-, and four-electrode implementation. The first one, is the simplest, where the working electrode (WE) and counter electrode (CE) both measure the impedance including the influence from the sample interface on each of them. They showed that in order to decrease that effect, a third electrode, named reference electrode (RE), can be added. Given that the signal in this case is exchanged between WE and RE, the effect of the interface is only counted at the CE (Grossi & Riccò, 2017). Lastly, they found that an addition of a fourth electrode is possible, in which case the test current is sent between WE and CE, and the voltage is measured between the extra added electrode and RE, providing a measurement free of the influence of the sample interface. Generally, the use of more electrodes leads to a more complicated yet more accurate measurements.

2.3.2 Electrical Properties of Fresh Concrete

McCarter (1994) stated that concrete is composed by mixing cement, aggregates, and water together, where the cement reacts with the mixing water providing hydration products. This process of cement hydration consists of a series of chemical reactions that lead to the setting and then hardening of the paste. He showed that throughout hydration, the paste becomes saturated with calcium and hydroxide ions, accompanied by other ions, such as sodium, potassium, and sulphate, which makes it much less resistive compared with aggregates.

Table 3 shows the values of conductivity and resistivity for different aggregates and concrete types. It is apparent that the resistivity of aggregates is significantly higher in value than concrete, making them non-conductive. Therefore, as Whittington (1981) pointed out, the conductive behaviour of fresh concrete is mainly controlled by the hydrated cement paste and the water-filled capillary pores. Additionally, the difference of W/C ratio and chemical composition of the hydrated cement paste leads to the observed variance in values of concrete conductivity in each environment (Whittington, et al., 1981).

Table 3. Typical resistivities and conductivities for concrete in different environments at 20° C and different aggregates (Karhunen, 2013).

Material	Environment	Resistivity (Ωm)	Conductivity (mS/cm)
Concrete	Wet	15-200	0.05-0.67
	Outdoors (exposed)	100-400	0.025-0.1
	Outdoors (sheltered)	200-500	0.02-0.05
	Indoors (50% RH)	>3000	$<3*10^{-3}$
Aggregate	Quartz	$4*10^{4}$-$1*10^{12}$	$1*10^{-11}$-$2.5*10^{-4}$
	Granite	5000-$1*10^{6}$	$1*10^{-5}$-$2*10^{-3}$
	Sandstone	180-4000	$2.5*10^{-3}$-0.056
	Limestone	300-1500	0.007-0.033

J. McCarter, as cited in Karhunen (2013), suggested that ionic conduction in the evaporable water of plastic concrete is the main mechanism through which the current is conducted. In contrast, conduction through cement compounds plays a smaller role in the overall conductivity of concrete. Yet, separating these two mechanisms is not possible, since electric conduction in concrete is dependent on the concentration of the evaporable water, which is linked to the structure of the solid phase composed of cement compounds.

From an electrical point of view, the concrete mixture can be divided into a resistive part and a conductive part, with the first being the aggregates and air bubbles, while the latter is the cement paste and the water-filled capillary pores (Karhunen, 2013). The possible paths through which electrical charges move within concrete were postulated by Song (2000) to be of three different types: a continuously conducting path (CCP), a discontinuously conducting path (DCP), and an insulator conductive path (ICP). The CCP is comprised of a series of micro-pores connected together, providing the least resistance. While DCPs are a connection of micro cavities that is blocked by cement paste layers, and ICPs are paths through the solid part of the cement paste or aggregates (Figure 26).

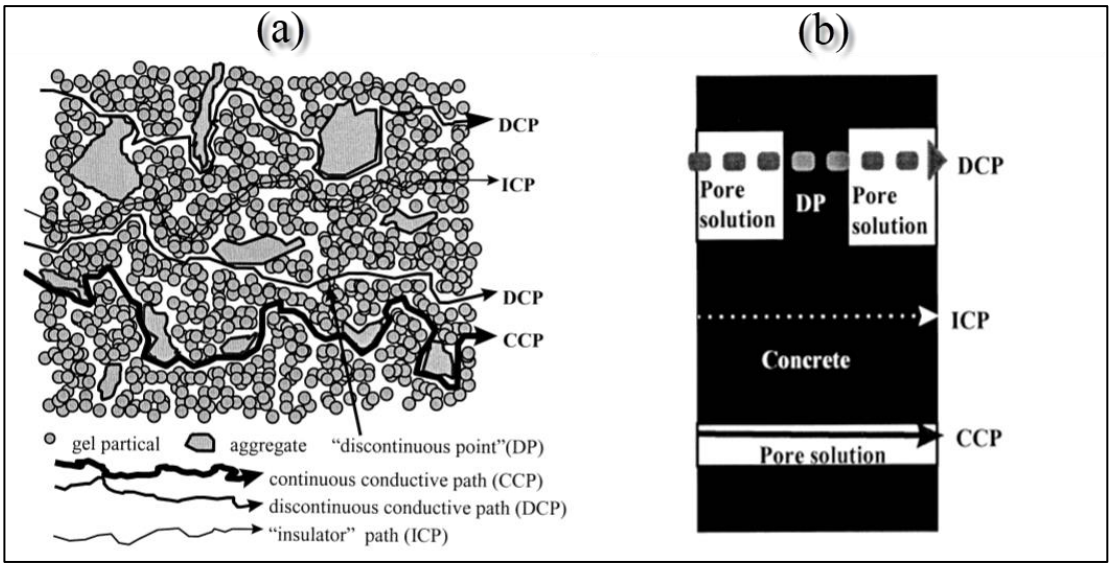

Figure 26. (a) schematic illustration of the microstructure of concrete with the possible conduction paths displayed, (b) a simplification of the conduction paths inside concrete (Song, 2000).

The impedance response of cement pastes, mortars, and concretes in the fresh state displays a capacitive behaviour, which has been reported by McCarter et al. (2004), Loche et al. (2004) and Woo et al. (2006). Namely, their Nyquist plots (Figure 27) are shown by Karhunen (2013) to be comprised of two distinctive areas: the electrode response and the bulk response. He showed that the bulk arc typically forms at around frequencies higher than 1 kHz and its formation is a result of ions accumulating in the blocked parts of the DCP and pore necks, which causes a capacitive response. On the other hands, for frequencies lower than about 1 kHz, the measuring electrodes and concrete's interface become polarized creating the electrode response part of the plot. The lowest point at which the electrode arc connects with the bulk arc, noted R, represents the bulk resistance of the tested specimen (Karhunen, 2013).

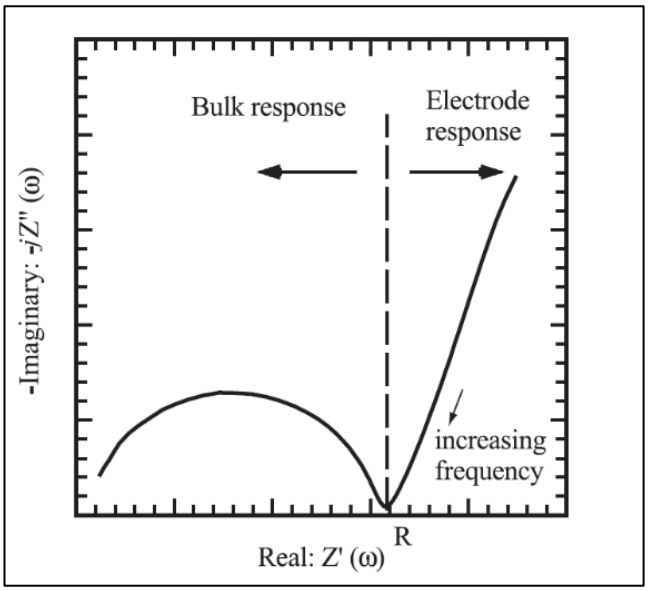

Figure 27. Nyquist plot of ordinary Portland cement paste (McCarter, et al., 2004).

2.3.3 Previous studies of EIS for Fresh Concrete and Cementitious Mixtures

McCarter (1996) studied the influence of water content, cement type and mineral admixtures on the EIS analysis of fresh concrete, over a frequency range of 100 Hz —10 MHz. All measurements were taken from a plastic cell with dimensions of 15 cm x 15 cm x 15 cm and fitted with two 15 cm x 15 cm stainless steel electrodes facing each other. Firstly, to study the water content effect, he tested 4 Ordinary Portland Cement (OPC) concrete mixes with W/C ratios varying from 0.38 to 0.56. Drawing the Nyquist plots for each mixture, he found that that the increase of water content leads to a significant decrease in the bulk resistance of the mix. As shown in (Figure 28), raising the water content by 30 kg/m^3 from Mix 2 to Mix 3, resulted in a decrease of bulk resistance of around 20 ohms. This confirms that water plays a major role in conducting electrical current in fresh concrete (McCarter, 1996).

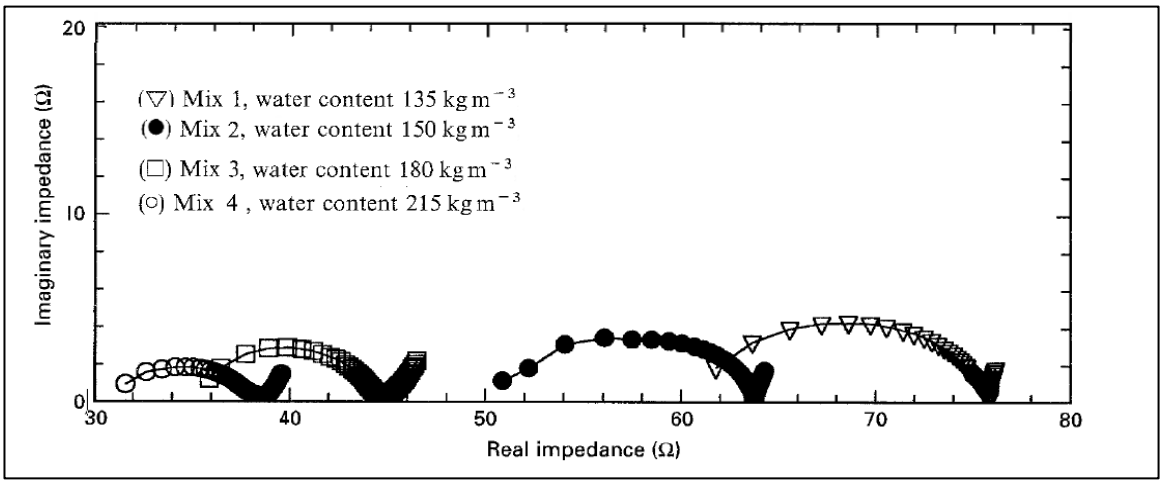

Figure 28. Nyquist plots for OPC concrete mixes with varying water content (McCarter, 1996).

In the second part of the experiment, McCarter (1996) analysed the impedance spectra of 3 other mixes with the same W/C ratio of 0.44. However, Mix 1 and 2 were made using Sulphate-Resistant Portland Cement (SRPC) with the second one having Ground-Granulated Blast-Furnace Slag (GGBS) replacement of 50%, and the third mixture was made with OPC but also GGBS replaced 50% of the binder. He found that the Nyquist plots of the three mixes displayed in (Figure 29) show the prominent effect of the cementitious binder used on the impedance behaviour of the mix.

Observing the plot of Mix 2 with SRPC, it is clear that the bulk resistance is much higher than that of any mix made with OPC. McCarter (1996) linked this to the fact that SRPC has a low tricalcium aluminate (C_3A) content, which is known for its rapid breakdown as a result of reacting with water. Consequently, he found the decrease in C_3A in SRPC causes a lower ionic concentration in the mix, hence a more resistive behaviour. Additionally, he noted that the overall impedance of Mix 3 is higher than of that of the OPC mixtures of the first experiment with the similar water content, which is a result of GGBS having a much slower reaction with water than that of OPC, making it almost temporarily chemically inactive which decreases the overall ionic concentration of the mixture. Finally, the researcher showed that the inert effect of GGBS accompanied by the decrease in ions caused by lower C_3A is apparent in Mix 1, which has the highest bulk resistance of all the tested specimens.

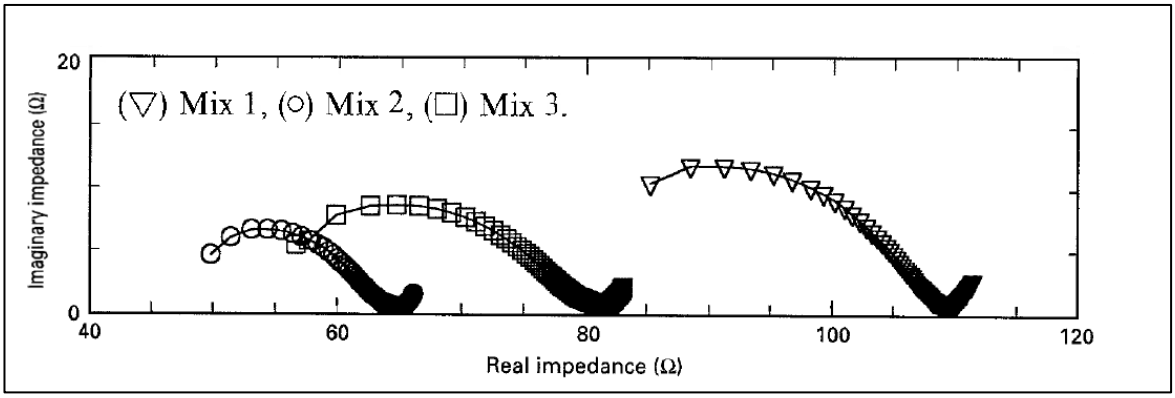

Figure 29. Nyquist plots for: Mix (1) Sulphate Resistant Portland Cement concrete with 50% GGBS, Mix (2) SRPC concrete, Mix (3) OPC concrete with 50% GGBS (McCarter, 1996).

In addition, the nature of the impedance spectra when cement is partially replaced with fly ash (FA) was studied by McCarter (1996), where he showed the response to consist of three distinctive parts: a high-frequency (> 150 kHz) bulk arc connected by a plateau region (1—150 kHz) to a low-frequency (< 1 kHz) spur, see (Figure 30c). Three years later, McCarter et al. (1999) published a study about the effect of FA content in cementitious mixtures on the impedance spectra, in order to devise a practical quality control method for quantifying the amount of FA in fresh concrete. In the study they tested 4 different samples of both concrete (C1—C4) and cement mortar (M1—M4), where the replacement percentage was 0%, 10%, 25%, and 40%, respectively.

Having analysed the measurements, McCarter et al. (1999) found out that there's a dependency of the FA amount on the frequency range of the plateau region, where the more FA content, the wider the plateau region was (Figure 30a, b). Moreover, it was shown that the resistivity of the mortars was proportional to the amount of FA added, as can be seen from the value of the bulk resistance in (Figure 30a, b).

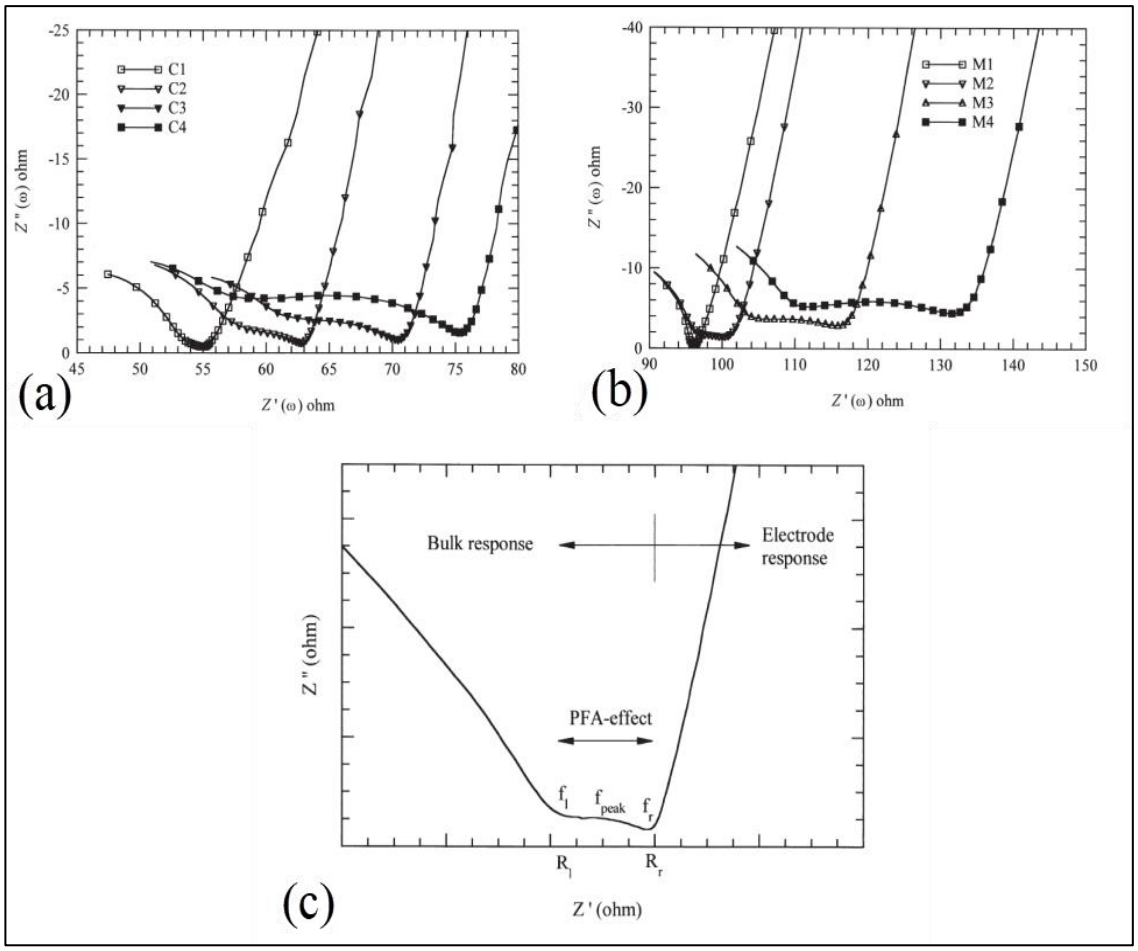

Figure 30. Complex Impedance response of (a) Concretes; (b) Mortars, both with varying FA replacement. (c) Schematic drawing of cementitious mixes with FA replacement under EIS (McCarter, et al., 1999).

McCarter et al. (1999) associated the formation of the plateau region to the double-layer polarization effect resulted from the spherical nature of FA particles compared with the more angular cement particles. Since this shape gives the ability for electrostatic charges to oscillate much easier over the surface, they found that it results in an easier polarization and the emergence of the plateau part.

However, McCarter et al. (2004) found out a stronger relationship between the unburnt carbon content of FA, measured by loss of ignition (LOI), and the development of the plateau part of the curve; suggesting a double layer polarization taking place on the carbon's surface. They achieved this by analysing the impedance spectra for a mixture of FA with sand, before and after its carbon content was removed by burning, and then adding some graphite powder to the same mix to reintroduce the extracted carbon. Consequently, they found that the plateau region disappeared from the first mix with no carbon left, and by re-adding the carbon the plateau region reappeared similar to the original mix.

3 Experimental Investigation

This chapter presents the materials and equipment used in the thesis, and the methodology with which the EIS measurements were obtained. In this chapter, Section 3.1 shows the properties and proportions of materials used in the preliminary testing and the concrete mix design. The equipment used in the EIS investigation along with the process of building the electrode panel and the testing mould are presented in Section 3.2. Section 3.3 introduces the preliminary testing phase and the assessment of measurements acquired from the fabricated mould. Finally, Section 3.4 presents the EIS investigation procedure for different vibration times.

All the experiments were carried out in the concrete laboratory of the Department of Civil Engineering at Aalto University. The testing mould was also developed in the same laboratory. However, the electrode panel was initially designed and built in the University of Eastern Finland with some enhancements later done at Aalto University.

3.1 Materials and Mix Design

During the preliminary testing phase, tap water and water with different salt concentrations were used to evaluate how responsive the developed electrode panel is to the changes in conductivity caused by increasing the content of NaCl in the water. In addition, the watertightness is evaluated to ensure no leakage when performing concrete tests. Tap water is used, which is distributed by the municipality of Espoo, at a temperature of around +20°C. Ordinary table salt was used with NaCl concentration of 98%. Five different saltwater mixtures were made by adding to 9.9 litres of tap water resulting in the following concentrations of salt: 0.1%, 0.2%, 0.3%, 0.4%, and 0.5% by weight. The investigated saltwater samples are codenamed by using "SW-" followed by a number that represents the salt concentration as shown in Table 4.

Table 4. Codenames and salt concentrations for each tested saltwater sample.

Codename	Salt (NaCl 98%) Concentration
SW-0	0%
SW-1	0.1%
SW-2	0.2%
SW-3	0.3%
SW-4	0.4%
SW-5	0.5%

The main testing procedure was carried out on seven concrete mixes, all of which followed one recipe. As shown in Table 5, each mix consisted of coarse and fine aggregates, sulphate resistant (SR) cement, water, air-entraining agent (AEA), and superplasticizer (SP). The specified amounts are for 1 m^3 of concrete, while each batch yielded 30 litres of concrete. This provided enough concrete to perform the required fresh concrete tests before investigating the impedance spectra of the mix.

Table 5. Concrete mix ingredients for a 1-m^3 concrete batch.

Concrete Ingredient	Amount (kg)
SR Cement	425
Water	152
Aggregates	1751
AEA	2
SP	6

The following discusses the properties of each component used, followed by the mixing procedure. Firstly, the SR cement used is a Finnish Portland cement manufactured at the plants of Finnsementti. It is distributed under the name of SR-sementti CEM I 42.5 N, where CEM I denotes that it is a Portland cement, 42.5 refers to the minimum characteristic strength at 28 days expressed in MPa, and N means it provides a normal early strength unlike rapid binders (Ruokonen, 2018). According to (Finnsementti, 2012), this type of cement is produced using a special clinker that contains lower than 3% of tricalcium aluminate (C_3A). The chemical composition, strength, and properties of that cement are shown in Table 6. The water used was from the same source as that used in the preliminary test, but with an amount that provided a W/C ratio of 0.43.

Table 6. (a) Properties of SR-Cement manufactured by Finnsementti, and (b) its chemical composition as adapted from (Finnsementti, 2012).

(a)

Properties	Values
1-Day Strength	13…16 MPa
2-Day Strength	28…32 MPa
7-Day Strength	43…48 MPa
28-Day Strength	51…57 MPa
Initial Setting Time	160…200 min
Soundness	0…3.5 mm
Fineness	310…390 m^2/kg

(b)

Chemical Composition	Percentage
CaO	64…66%
SiO_2	20…22%
Al_2O_3	3.1…3.7%
Fe_2O_3	3.9…4.2%
MgO	2.7…3.5%
Limestone	≤ 5%

Secondly, the aggregates used had a maximum size of 16 mm. In total, seven different fraction sizes were used to produce each mix, which were previously sieved. The particle size distributions of the aggregates is shown in Table 7, followed by the grading curve in Figure 31. The absorbed moisture in aggregates was assumed to be 0.8% in weight. Based on that value the adjustments were carried out on the weights of mixing water and aggregates.

Table 7. Particle size distribution of combined aggregates used in concrete mix.

Aggregate Type	Fraction	Portion (%)	Sieve Size (mm)									
			0,125	0,25	0,5	1	2	4	8	16	32	64
Filler	Filler 96	8	42.1	80.7	92.9	96.6	98.2	100	100	100	100	100
Fine Aggregates (FA)	R 0,1 - 0,6	12	2.7	21	76	100	100	100	100	100	100	100
	R 0,5 - 1,2	12	0	2	6	70	100	100	100	100	100	100
	R 1,0 - 2,0	15	0	1	2	7	79	100	100	100	100	100
	R 2,0 - 5,0	15	0	0	1	1	1	47	100	100	100	100
Coarse Aggregates (CA)	R 5,0 - 10,0	18	0	0	0	0	0	3	82	100	100	100
	R 8,0 - 16,0	20	0	0	0	0	0	0	5	99	100	100
	Total (%)	100										
	Combined Aggregates (%)		4	9	18	29	44	55	78	100	100	100

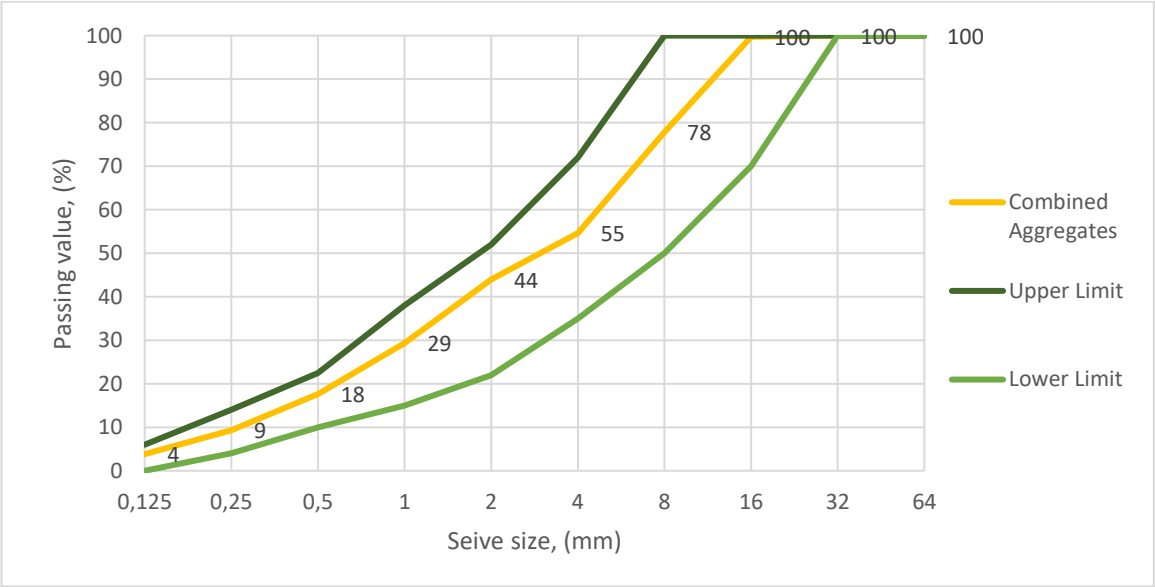

Figure 31. Grading curve of the combined aggregates.

Finally, the admixtures used were produced by BASF Oy. They were a polycarboxylate ether-based superplasticizer (MasterGlenium SKY 600) and an air-entraining agent (MasterAir 100), which are both suitable for use with SR-cement. For each mix the dosage per binder used was 0.9% for the SP, and 0.35% for the AEA.

The concrete mixes were produced using a pan-type mixer. In the beginning, the inner surface of the pan was wetted with a wet sponge, then the dry ingredients were added in the order shown in Figure 32. The mixing procedure consisted of five steps lasting for three and a half minutes as follows:

1. Dry mixing for 30 seconds
2. Adding 80% of the water then mixing for another 30 seconds
3. Adding the AEA with 10% of the water while mixing for 30 second
4. Adding the remaining 10% of the water and mixing for 30 seconds.
5. Adding the SP and mixing for 90 seconds

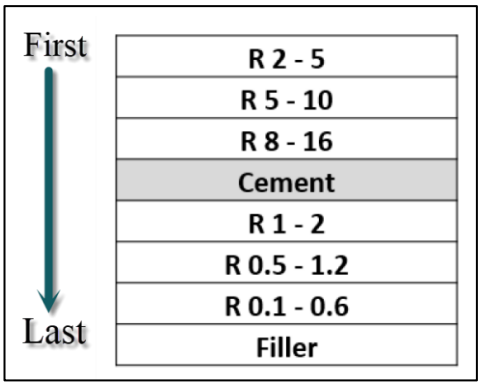

Figure 32. Illustration of the order in which aggregates and cement were poured into the mixing pan.

3.2 Equipment Used in EIS Investigation of Compaction

The equipment used during the process of compaction monitoring were: a specifically fabricated electrode panel fitted inside a uniquely designed plexiglass mould, an impedance analyser, a laptop with the measuring software installed, and a vibrating table. The fabrication process as well as the set-up of the mould and the panel are discussed below, followed by the description along with the use of the remaining devices.

Firstly, the electrode panel consists of electrodes and banana plug sockets fixed on a plate. The plate is 510 mm x 150 mm x 10 mm and was made of Polyvinyl Chloride (PVC), since it is a non-conducting material and will only allow the current to flow through the electrodes. While electrodes were made of thin copper sheets, given that copper is a highly conductive material. Electrodes were glued on the PVC plate using an epoxy adhesive and then fixed using bolts and nuts. Two types of electrodes were used: measuring and grounding electrodes.

Figure 33 shows that the front side of the plate is fitted with six Measuring Electrodes (ME) and 4 Grounding Electrodes (GE), whereas the back side (Figure 34) is covered with one large grounding electrode. The electrodes were connected to seven banana plug sockets using wires fitted under the nuts holding the bolts. The sockets where classified as one for grounding and 6 for measuring electrodes. The grounding electrodes were connected to the middle socket, where the top measuring electrodes were connected to the outer sockets, the middle electrodes to the middle sockets, and the bottom electrodes to the inner sockets.

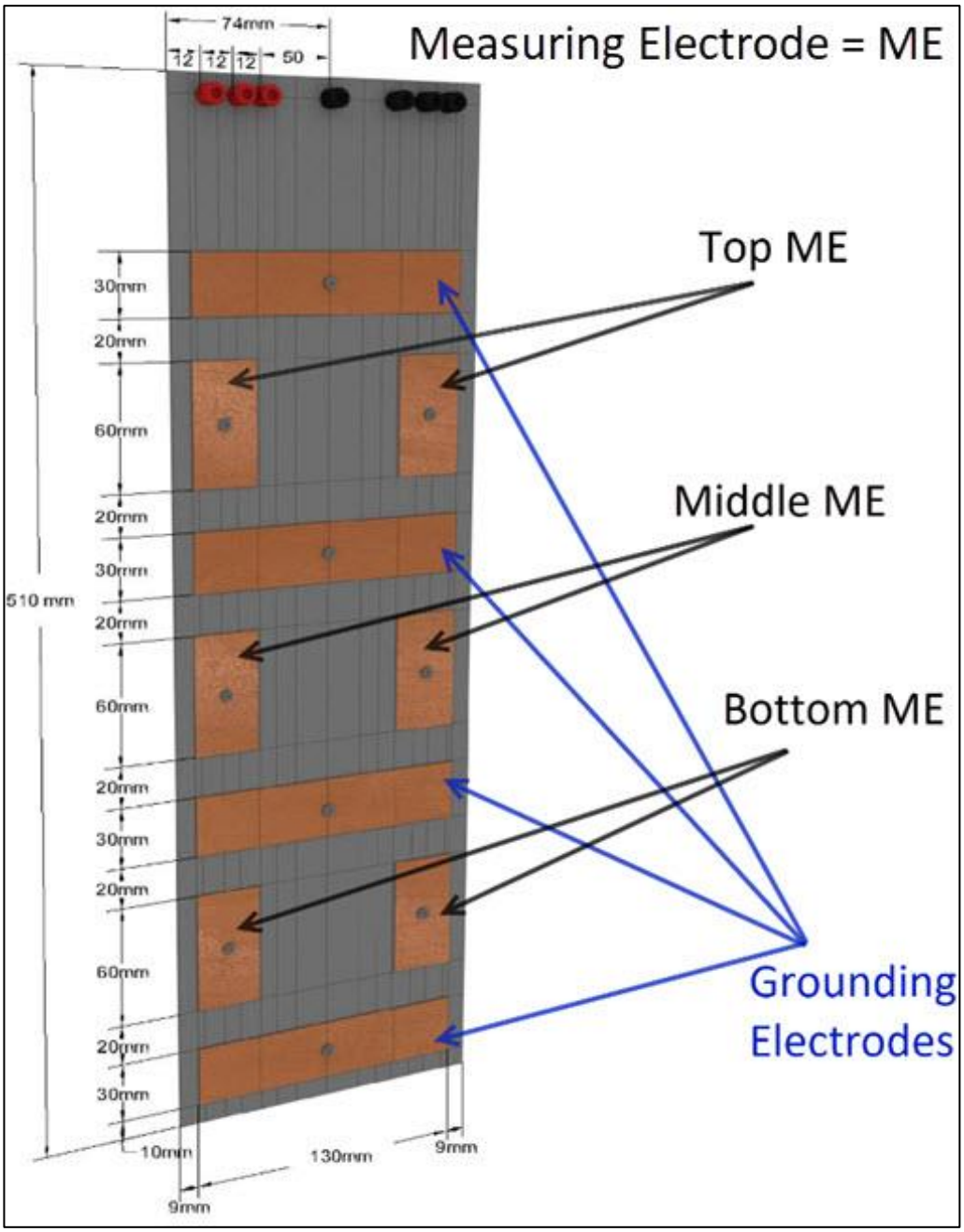

Figure 33. Model of the front side of the electrode panel showing dimensions and lay out of the electrodes used.

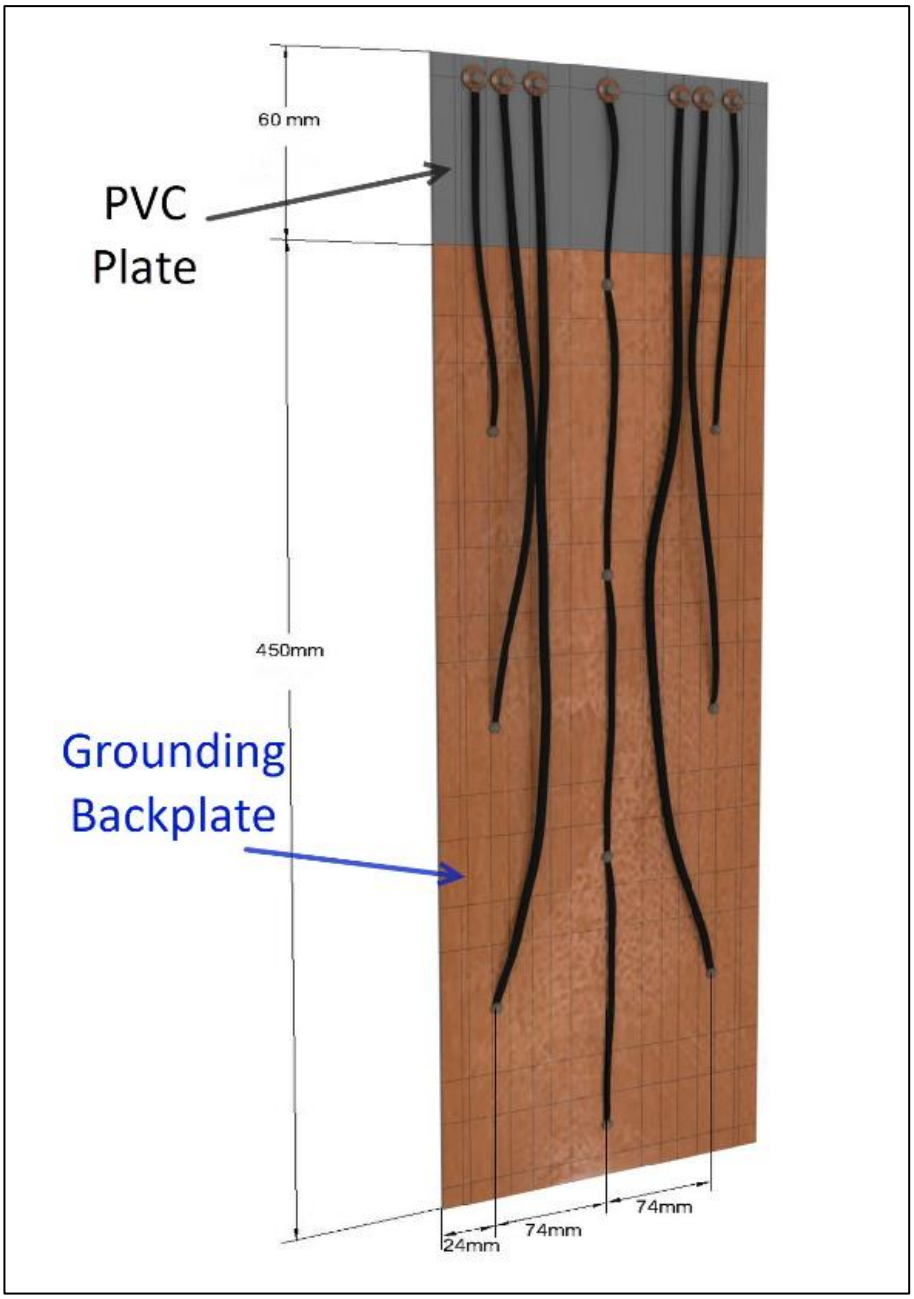

Figure 34. Model of the back side of the electrode panel showing the layout of the wires and grounding backplate.

This electrode-setup was chosen because the quality of compaction will be assessed based on segregation. Consequently, it was important to divide the measured parts of the fresh concrete into different layers: top, middle, and bottom, which can be later investigated in the hardened concrete. Each layer had a thickness of 100 mm and was denoted by the part into which the measuring electrodes conduct the current. The current flow in fresh concrete is demonstrated in Figure 35.

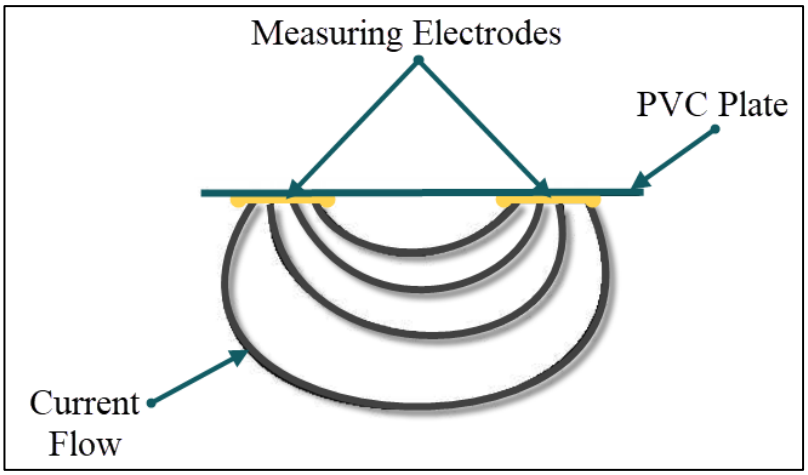

Figure 35. Schematic illustration of the top view of the current flow between the two measuring electrodes during EIS investigation.

The measuring electrodes were placed as far as possible from each other, in order to avoid the concentration of the current flow in a certain part, which might have led to an incorrect representation of the concrete mixture. Since if they were placed closer to each other, the current would have flown more strongly between their edges, and in the case of an aggregate being randomly located in the vicinity, the readings would have represented the aggregate only instead of concrete as a whole. However, it was also important to use large electrodes so that the current can flow through the whole layer and avoid partial narrow flow, which measurements would not represent the whole layer, but only part of it. Accordingly, the measuring electrodes were chosen to be 60 mm x 30 mm, with a distance of 70 mm between their inner edges.

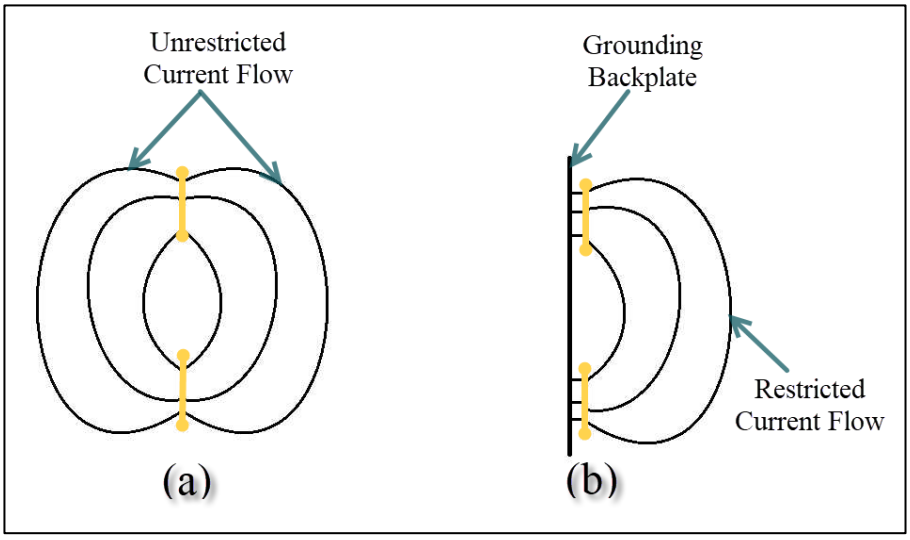

Figure 36. Schematic representation of the current flow during EIS investigation in case of: (a) not using and (b) using the grounding backplate.

Grounding electrodes were fitted both on the front and the backside of the plate. The function of grounding electrodes is to control the path of the current. In the case of frontal electrodes, they were 30 mm x 130 mm and were used to ensure the current does not overflow from one layer to another. Hence, two grounding electrodes were placed above and below each pair of measuring electrodes to limit the current flow to the layer thickness.

Furthermore, the lowest and highest grounding electrodes prevent altering the measurements by inhibiting the current from extending outside of the concrete mixture. In addition, the back side was equipped with a 440 mm x 150 mm thin copper electrode, which limits transmitting the current into air behind the plate. Since at higher frequencies, the current might favour flowing into air instead of concrete as shown in Figure 36a, but this was prevented using the grounded backside electrode with the full length of the tested specimen (Figure 36b).

Secondly, the electrode panel was fixed inside a specially developed orthotopic plexiglass mould with a height of 450 mm and inner area of 150 mm x 150 mm. Plexiglass was chosen due to its very high resistance to electricity conduction, which ensures that the current will flow into concrete and not into the mould. Additionally, plexiglass is very durable, hence the mould was reusable for various castings. Furthermore, plexiglass is a lightweight material, which made the mould easy to move, demould, and reconstruct.

Figure 37. Front and back view of the plexiglass mould.

As shown in Figure 37, the mould consists of five plexiglass plates: four vertical plates with the dimensions of 180 mm x 450 mm x 15 mm and a horizontal 230 mm x 230 mm x 10 mm bottom plate. The two vertical plates on the side of the mould were connected to the front and back plates using 40 plastic bolts: 20 in the front and 20 in the back. While the bottom plate was connected to the vertical plates using 6 plastic bolts: 2 bolts per plate. The bolts were 8 mm in diameter and 30 mm in length. In order to ensure the watertightness of the mould, the edges were sealed using a plastic padding gasket from the inside, and a steam sealing tape from the outside. This method of sealing provided sufficient tightness during all tests.

Thirdly, the impedance analyser used was “Hioki 3532-50 LCR HiTester”. This analyser can measure the current, voltage, phase angle, and the real as well as the imaginary part of the impedance over different frequencies ranging from 42 Hz to 5 MHz. The connection between the analyser and the electrode panel is achieved by two coaxial cables, with banana plugs fitted on the end connected to the panel, and coaxial radio frequency connectors on the end linked to the analyser.

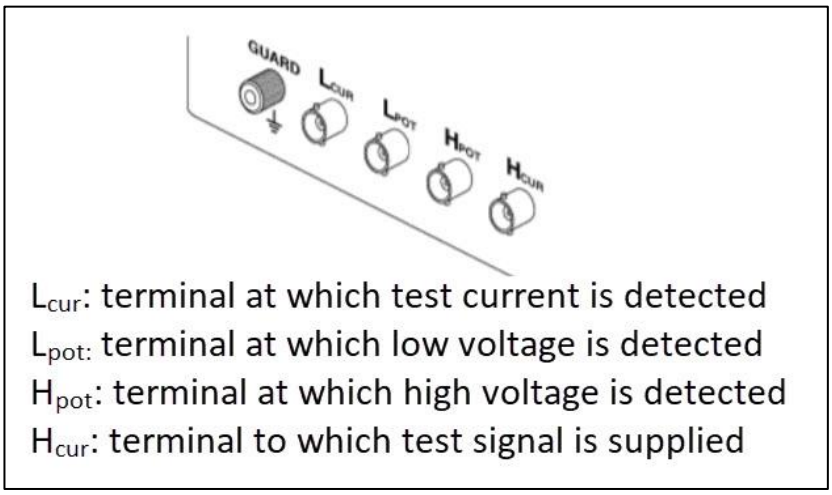

Figure 38. Illustration of the test terminals of the impedance analyser.

The setup of the cables connected on the analyser end was fixed for all different measurements. Each cable had 2 branches, which were connected to the terminals shown in Figure 38. Two branches of a cable were connected to the L_{CUR} and the L_{POT}, while the other cable branches were connected to H_{POT} and H_{CUR}. The first cable connected to the L terminals had two branches on the end linked to the electrode panel, one of which was the grounding plug and the other was the measuring plug, while the cable connected to the H terminals had a measuring end-plug only.

The fourth device used is a laptop that is connected to the analyser. Using the software installed on the laptop gives a full control over the functions of the analyser. Through the software it is possible to enter the desired range of frequencies for EIS investigation and save the acquired data in the form of a comma-separated list, which in turn is easy to be analysed using Microsoft Excel. Additionally, the software has a built in Data Viewer, which offers a graphical representation of the acquired data during testing.

Finally, a high-frequency vibrating table with a timer switch is used to compact the fresh concrete. The table comes with a 9000 RPM motor, and a power knob that can be adjusted to different vibrating frequencies. Additionally, the timer switch can be set to any desired time, with a minimum setting of one second.

3.3 Initial Device Setup

The same device setup was used in all the experiments, and the electrodes were carefully cleaned off of any remaining concrete or water from previous tests. Additionally, the electrodes were washed with water and then wiped dry to ensure the cleanliness of the electrode surface and full contact with the tested concrete.

Additionally, some steps were carried out before every EIS investigation. The purpose of these initial setup steps to calibrate the impedance analyser to avoid the effects of non-ideal short or open circuit impedance of the measurement setup. The steps for the short circuit calibration are as follows:

1. Turn on the analyser at least 30 minutes before testing to warm up.
2. Arrange the configuration of the measuring ends of the cables to be as close as possible by holding them together using a bolt and nuts.
3. Choose "SHORT" from the menu of the analyser, then "RUN" for "ALL" frequencies.
4. Wait until the screen shows that it was "COMPLETED NORMALLY

In the case of open circuit calibration, the configuration of the measuring ends in "step 2" is changed to be as far as possible from each other, and in that case the option "OPEN" is chosen from the menu in "step 3".

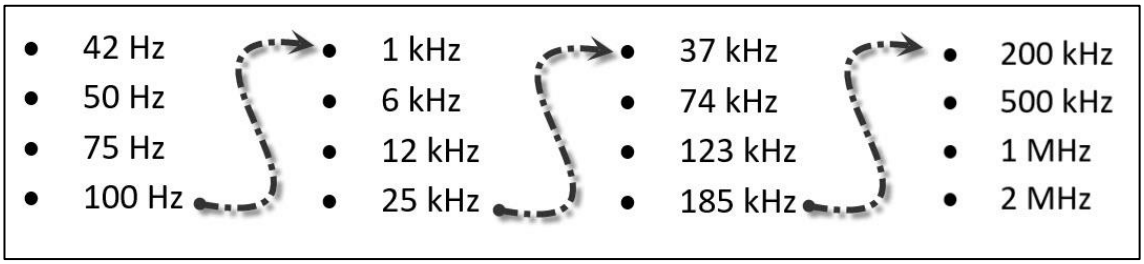

Figure 39. Sequence of the frequencies using during EIS investigation of compaction.

After calibrating the analyser, the mould was filled with the testing sample, and the desired frequency range was entered into the software on the laptop. The frequencies used are presented in.

Following that, the banana plugs on the measuring ends of the cables were inserted into the sockets, and in all cases the grounding cable end was inserted into the middle socket. The arrangements of the banana plugs are divided into three positionings: one for the top layer, the second is for the middle layer and the third is for the bottom layer. As illustrated in Figure 40 during the EIS investigation of the top layer the banana plugs are connected to sockets (1) and (7), while for the middle layer the banana plugs are inserted into sockets (2) and (6), lastly for the bottom layer the plugs are plugged into sockets (3) and (5).

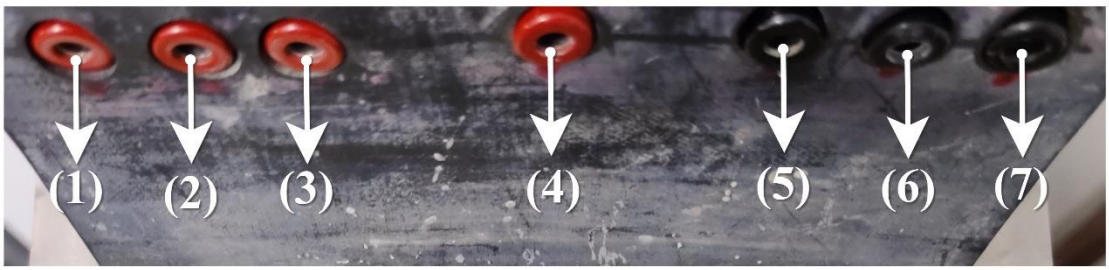

(1) and (7): Sockets connected to left and right top ME, respectively
(2) and (6): Sockets connected to left and right middle ME, respectively
(3) and (7): Sockets connected to left and right bottom ME, respectively
(4): Socket connected to all GE

Figure 40. Illustration of electrode panel sockets arrangement and their connection to measuring and grounding electrodes.

3.4 Preliminary Tests

This chapter discusses the different initial testing done before taking the EIS measurements for the vibrated concrete. The tests are grouped into 3 sections: Section 3.4.1 presents results of air content and slump tests for EIS investigated concrete. Section 3.4.2 discusses the first test used to assess the data acquired from the device, using varying salt concentrations of salt water. Lastly, Section 3.4.3 shows the behaviour of measurements when concrete is left in the mould without vibration.

3.4.1 Fresh Concrete Tests Prior to Compaction

Two fresh concrete tests were carried out after mixing each batch: the slump test and the air content test. Given that the EIS measurements are very sensitive to small changes in concrete properties, the selected batches were almost identical in measured slump and air content.

Immediately after mixing, the workability of the mixture was evaluated using the slump test based on the standard "SFS-EN 12350-2 – Testing fresh concrete. Part 2: Slump test". The target slump is chosen as 25 cm with a tolerance of ±0.5 cm. This slump value provides a more fluid concrete, thereby a better connection between the fresh concrete and the electrodes. In addition, compaction quality will be evaluated based on segregation, and highly flowable concretes have a high tendency to segregate.

After confirming that the slump was within the acceptable range, the pressure method was used to determine the air content of the mixes. The procedure of measuring air content of the fresh concrete was done in accordance with the standard "SFS-EN 12350-7 – Testing fresh concrete. Part 7: Air content. Pressure methods". The target air content was set to be 6% with a tolerance of ±0.7%, which falls within the range of air content for freeze-thaw resistant concrete.

The concrete tested for slump and air content was discarded after the tests, since the first was manually compacted, and the latter had water introduced into it. Hence, the fresh concrete EIS measurements were carried out on the concrete remaining in the pan.

3.4.2 Sensitivity of EIS measurements to The Conductivity Degree

After carrying out the initial device set up steps, and in order to evaluate the measurements obtained by the device, the previously mentioned water samples with different salt concentrations (Table 4) were tested separately. Measurements were taken for each layer; top, middle, and bottom.

Nyquist plots were drawn for the obtained measurements. Layer resistances were acquired from these plots at the lowest point connecting the bulk part with the electrode curve. Additionally, the relative resistance was calculated for each layer through dividing the value of the resistance of that layer by the layer resistance value of SW-0. The obtained relative resistances are shown in Table 8.

Table 8. Relative resistance values for top, middle and bottom layers of saltwater samples.

Salt Concentration (%)	Relative Resistance		
	Top	Middle	Bottom
0.0	1.00	1.00	1.00
0.1	0.0741	0.0728	0.0732
0.2	0.0394	0.0382	0.0385
0.3	0.0258	0.0261	0.0265
0.4	0.0196	0.0200	0.0204
0.5	0.0171	0.0162	0.0165

Afterwards, for each layer the relationship between the increase in salt concentration and the calculated relative resistance was graphically represented as shown in Figure 41. It is apparent that the relative resistance decreased dramatically when 0.1% of salt was added to the water. This is observed in the three layers, as the value drops down from 1 to around an average of 0.07, losing about 93% of the resistance. This is expected due to the nature of salt water being much more conductive than tap water. The higher conductivity is caused by the existence of more ions in salt water, where the higher salt concentration, the more conductive the liquid (David, 2017). Additionally, it is evident that as salt concentration increases from SW-1 to SW-5, the relative resistance follows a gradual decrease.

The above-mentioned observations confirm that the measurement acquired from the device are reliable to be used to draw Nyquist plots. Since the results proved the ability of the device to detect the increase in ions, which is reflected as a decrease in the obtained resistance from the plots.

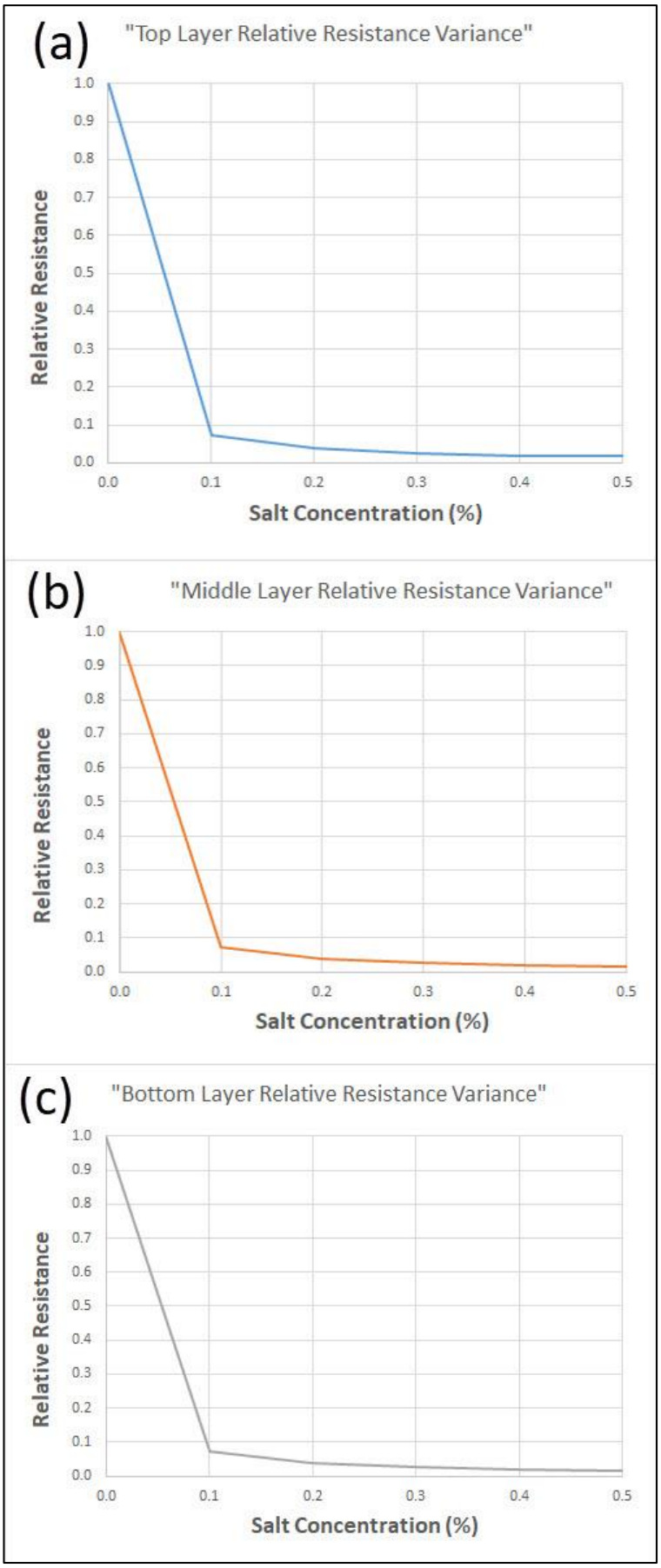

Figure 41. Relative resistance variance for: (a) Top, (b) Middle, and (c) Bottom layers as salt concentration increases.

3.4.3 Sensitivity of EIS measurements to Change Over Time

To investigate the effect of time on the acquired EIS measurements for concrete samples, a concrete mix was tested without any vibration. Firstly, the initial device setup steps were done. Secondly, the mould was filled with water, and measurements were taken to be used for calculating the relative concrete resistance. Finally, concrete was poured into the mould and measurements were obtained right after pouring, denoting time 0, followingly measurements were taken at 5 mins, 10 mins and 20 minutes (Table 9).

Table 9. Relative resistance values for un-vibrated concrete over time.

Time (min)	Relative Resistance		
	Top	Middle	Bottom
0	0.0602	0.0618	0.0652
5	0.0596	0.0620	0.0652
10	0.0594	0.0641	0.0651
20	0.0608	0.0644	0.0650

Similar to the saltwater samples, Nyquist plots were drawn using the values of reactance and resistance acquired from each layer. The concrete resistances acquired from Nyquist plots were then were divided by water resistance values and converted into relative resistances. Figure 42 shows the change in relative resistance for each layer over the time period previously specified.

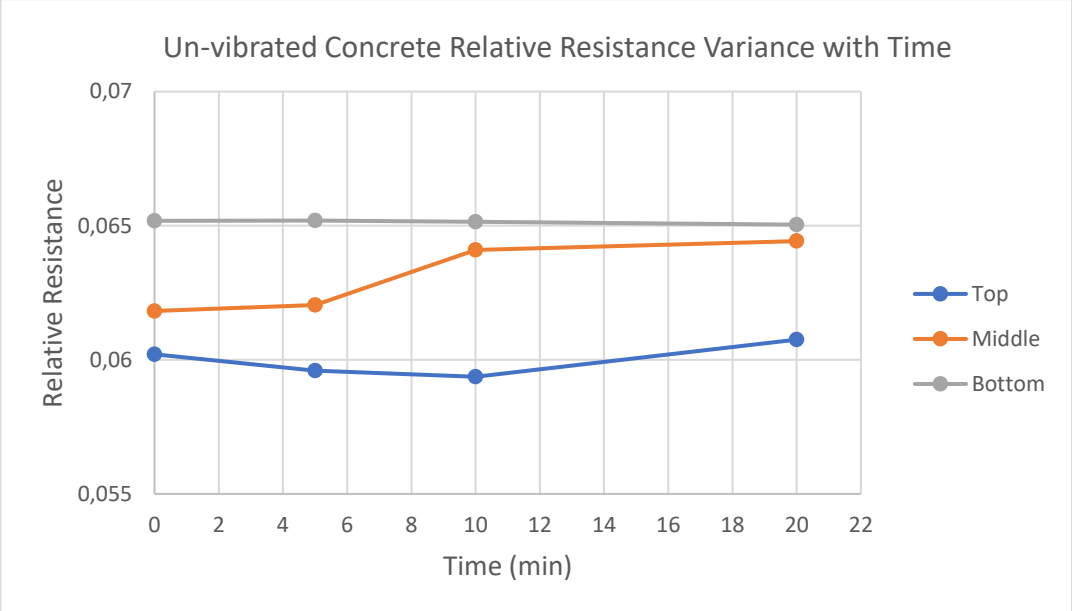

Figure 42. Relative resistance variance for un-vibrated concrete over time.

It can be noted that for the top layer, there is a very slight change in relative resistance values over time. The values gently drop from time 0 s to 10 s, then start a marginal increase towards 20 s. In the case of the bottom layer the values are quite similar, where they are presented with an almost horizontal line. However, the middle layer displays a marginal shift in the relative resistance values. Nevertheless, this change is negligible since the maximum difference between the obtained values is only 0.0026. In addition, the standard deviation of the different acquired values for the middle layer is 0.0012, which is almost close to zero denoting that the values are acceptably close to each other.

The aforementioned observations and findings prove that the EIS measurements obtained, specifically those used in Nyquist plots, remain nearly unchanged through a period of 20 minutes of no vibration. This suggests that any monitored changes through measuring different concrete samples will be mainly affected by the vibration of concrete, and that the measuring time does not play any major role in altering those measurements.

3.5 EIS Investigation Plan for Concrete During Compaction

Given that there were no reference studies of EIS investigation during concrete vibration, two preparatory tests on vibrated concrete are carried out to understand the behaviour of each layer during vibration. These test were named: Test-1 and Test-2. The vibration duration for these tests is divided into smaller time steps, after each step the EIS measurements are recorded. The time steps used, and the frequencies of the vibrating table are shown in Table 10.

Table 10. Time steps and frequencies for the preparatory concrete vibration test.

Time (s)	Frequency (Hz)
0	86
10	
20	
30	
40	
50	
70	129
90	
130	

The measured slump values for Test-1 and Test-2 are 24.5 cm and 24.6 cm, respectively. These values fall within the specified acceptable tolerance range. Additionally, the measured air content for these tests were 6% and 6.6% respectively, which is also within the allowable limits of air entrainment.

Having carried out the initial device setup steps, a water sample was tested to be used as the reference for calculating the relative resistance of different concrete layers. The use of this reference measurement minimizes the differences resulting from random changes between different tests. Afterwards, the EIS investigation of concrete was done, where the sample was intentionally over-vibrated until a foamy layer of cement paste appeared on the surface indicating the occurrence of segregation, which happened at 130 s.

Figure 43 presents a comparison between the surface of the concrete sample at time 0 and at time 130 s. Appendix 1 contains figures of the surface taken at each vibration time step, along with written observations of the state of the surface during vibration. Afterwards, the concrete sample was left in the mould to harden for 24 hrs before demoulding.

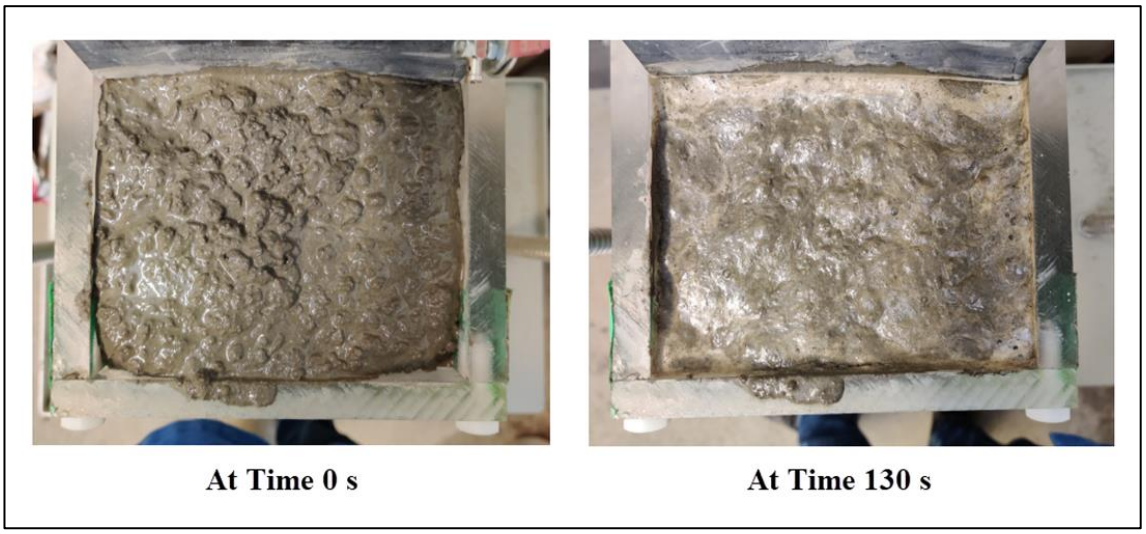

Figure 43. Difference in concrete surface before vibration and after 130 s of vibration.

Figure 44 illustrates the obtainment of concrete bulk resistance for the different layers. The figure shows Nyquist plots for Test-1 at time of 130 s, where the resistance is acquired at the lowest point connecting the electrode part of the curve with the bulk reaction part separated by the dotted line. Consequently, the results acquired from both tests were as shown in Table 11.

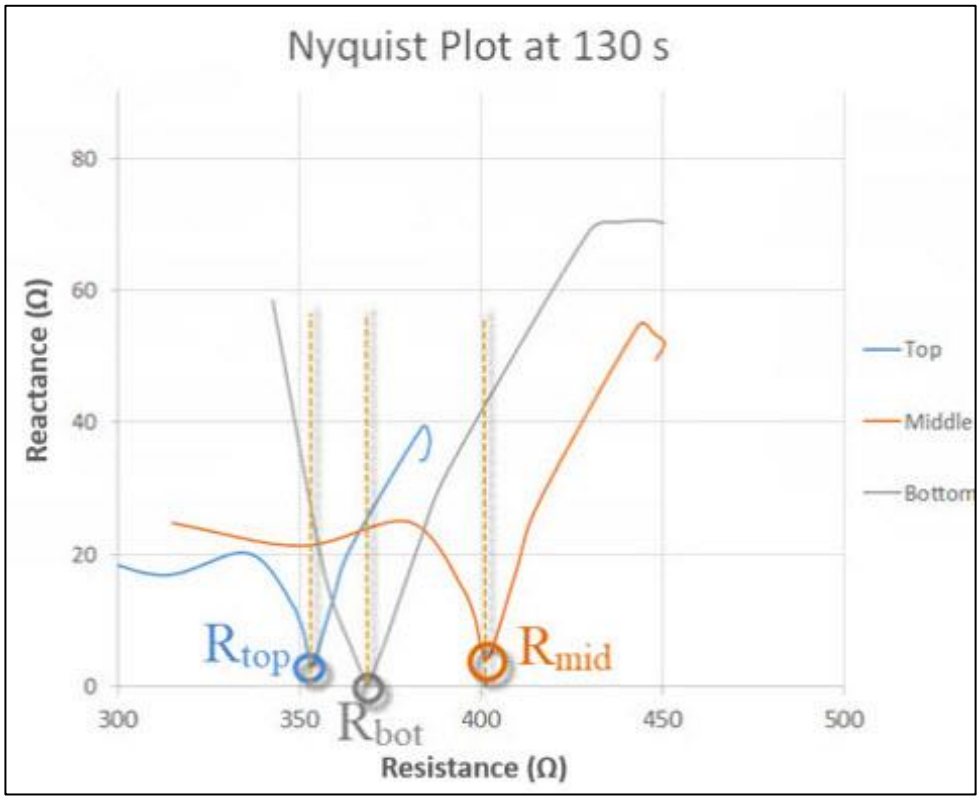

Figure 44. Nyquist plot for top, middle, and bottom layers of Test-1 at time 130 s and the illustration of the electrode response and bulk response.

Table 11. Relative resistance values for top, middle and bottom layers of the first two EIS investigated concrete samples.

Time (s)	Test-1 Relative Resistance			Test-2 Relative Resistance		
	Top	Middle	Bottom	Top	Middle	Bottom
0	0.0602	0.0618	0.0652	0.0674	0.0677	0.0684
10	0.0653	0.0644	0.0664	0.0708	0.0692	0.0689
20	0.0673	0.0634	0.0660	0.0711	0.0680	0.0684
30	0.0677	0.0650	0.0650	0.0715	0.0675	0.0691
40	0.0702	0.0646	0.0651	0.0710	0.0691	0.0692
50	0.0683	0.0640	0.0649	0.0732	0.0713	0.0694
70	0.0746	0.0671	0.0631	0.0768	0.0738	0.0662
90	0.0791	0.0642	0.0655	0.0791	0.0692	0.0652
130	0.0672	0.0612	0.0741	0.0716	0.0678	0.0687

The graphical representation of the relative resistance variance during vibration is shown in Figure 45. Studying the behaviour of the top layer in Test-1 and Test-2, it could be seen that there is a steady rise of in the relative resistance from time 0 until time 90 s, amounting to 0.02 and 0.01 for the two tests, respectively. This increase is followed by considerable plummeting towards time 130 s of around 0.01 for both tests . On the other hand, the bottom layer has slight changes over the period 0—90 s, with an increase in value after time 90 s. Lastly, the middle layer follows a similar trend of the top layer, with a slightly less pronounced changes over the mentioned time periods. The main difference between Test-1 and Test-2 graphical representation is that the previously mentioned changes are more pronounced in the first test. It is apparent that the drop in the top and middle resistance values steeper in the case of the first test compared with that of the second. The same applies for the bottom layer, which shows a stronger increase in Test-1 than that in Test-2.

Generally, the increase in relative resistance could denote the existence of air and or aggregates in the measured layer hindering the movement of electricity. While, the decrease in the relative resistance suggests an increase in cement paste providing better electrical conduction. Based on the behaviour of the top layer, it could be suggested that at time 90 s, the layer was comprised of more cement paste and less aggregates, providing a decrease in relative resistance. Additionally, a similar situation could have happened in the middle layer, but with more aggregates still remaining inside, causing a slighter decrease in relative resistance after 90 s. Conversely, the bottom layer could have had an increase in sunken aggregates after 90 s that caused a rise in the relative resistance. Finally, the steeper behaviour of change observed in Test-1 might indicate larger differences in the number of aggregates and or air voids at different time steps, which leads to higher resistance difference when these aggregates sink down, or air bubbles leave the layers.

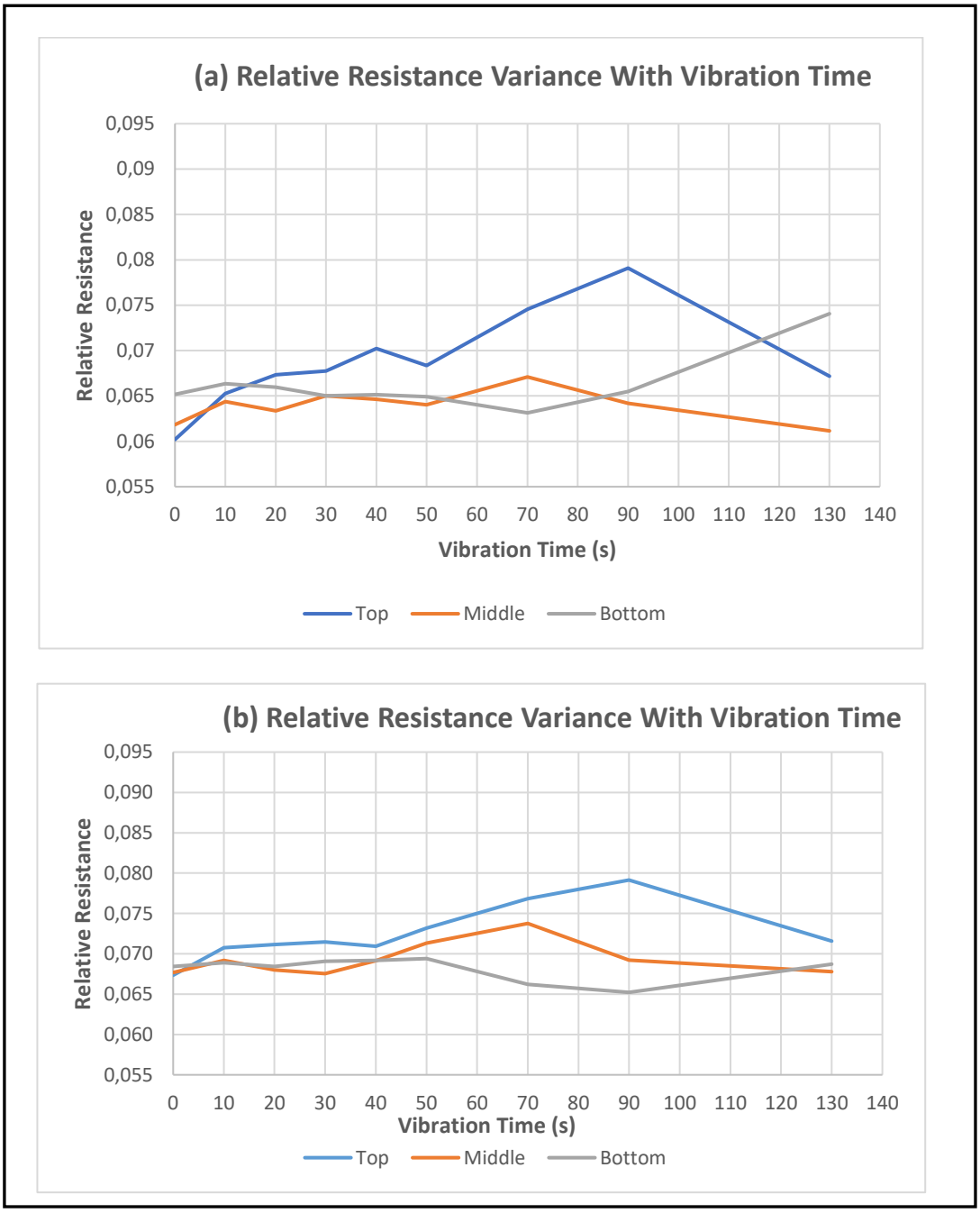

Figure 45. Relative resistance variance for EIS investigated concrete: (a) Test-1 and (b) Test-2 over the vibration duration.

The process of demoulding is carried out in two steps as shown in Figure 46. The first step was to unscrew the 20 plastic bolts connecting the front plexiglass plate to the side plates. Secondly, the rectangular concrete prism was easily taken out of the mould. It should be noted that during demoulding of all tested samples, the concrete prisms came out in one piece without any significant breakage.

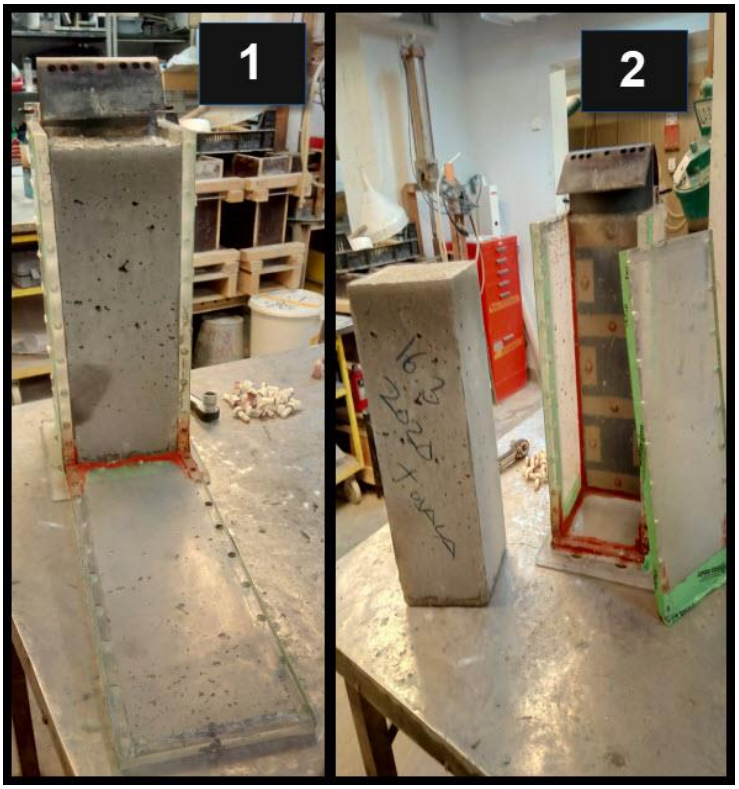

Figure 46. Demoulding steps of a hardened EIS investigated concrete sample.

Following demoulding, the mould was put back together using the plastic bolts, then re-sealed by the plastic padding gasket from the inside and the steam sealing tape from the outside to ensure watertightness for future tests. While the demoulded concrete was put in a climate room of 95% relative humidity and a 20 ºC temperature.

In order to be able to better interpret the previous observations, segregation analysis was carried out using two methods: comparing the densities of drilled cores representing each layer, and visual inspection of vertically cut sections in the concrete sample. Firstly, three cores were drilled each representing a layer: top, middle, and bottom. The diameter of each core was 75 mm. Cores were cut with their axis parallel to the two measuring electrodes and a full sample width of 150 mm. Secondly, segments of width 20 mm were vertically cut from both the electrode side and the front side of the concrete prism. The dimensions and layout of the cores and sections are shown in Figure 47.

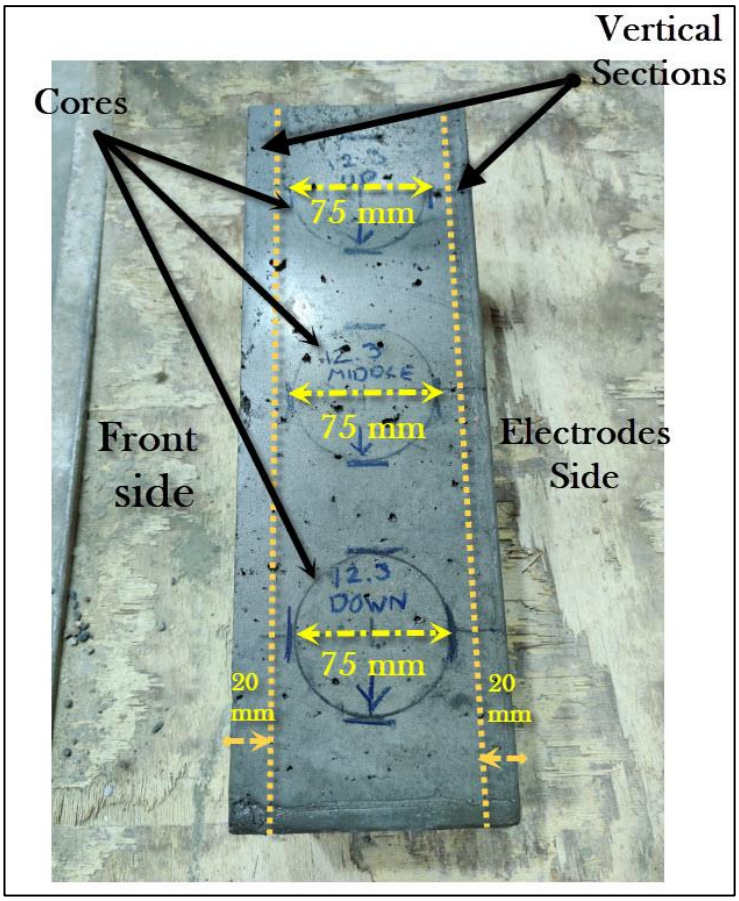

Figure 47. Dimensions and layout of the drilled cores and the vertical cut sections on a hardened concrete sample.

The drilled cores were weighed, and their densities were calculated from the predetermined core volumes based on the standards "SFS-EN 12390-1 – Testing Hardened Concrete. Part 1: Shape, Dimensions and Other Requirements For Specimens and Mould" and "SFS-EN 12390-7 – Testing Hardened Concrete. Part 7: Density of hardened concrete".

Table 12. Density values of the drilled cores from Test-1 and Test-2.

Core Position	Density (kg/m^3)	
	Test-1	Test-2
Top	2280	2373
Middle	2357	2412
Bottom	2441	2447

The density values of the drilled cores for the first and second tested samples were as presented in Table 12. Four statistical parameters were calculated to measure the spread in the calculated densities: range, mean, standard deviation, and Coefficient of Variation (CV). Where the range represents the difference between the minimum and maximum densities, the mean is the arithmetic average of the values, the standard deviation measures the dispersion in values, and lastly CV provides an indication of how high the standard deviation is through dividing the mean by the standard deviation. These values along with the theoretical mix density are shown in Table 13.

Table 13. Calculated statistical parameters for the core densities of Test-1 and Test-2.

Statistical Parameter	Test-1	Test-2
Range (kg/m^3)	161	74
Standard Deviation(kg/m^3)	65.8	30.2
Mean (kg/m^3)	2359	2411
Theoritical Density (kg/m^3)	2338	2338
Coefficient of Variation	0.028	0.013

In the case of a perfectly vibrated and cast concrete, the CV should be as close to zero as possible, since the densities of the top, bottom and middle layer will have a very low value of standard deviation, whereas it is apparent that for both samples the values were higher than zero.

To further investigate the phenomena of segregation in the hardened concrete, the two cut sections were visually inspected for segregation signs, such as the accumulation of aggregates or cement paste in certain parts. The sections from both samples showed different signs of segregation as discussed in the following.

Firstly, the electrode side segment for Test-1 was investigated. The upper part of this segment has about 15 mm of cement paste only, followed by around 45 mm of concrete with no aggregate larger than 10 mm. Afterwards, aggregates larger than 10 mm are more present, with the highest concentration of these aggregates at the last 100 mm of this section (Figure 48a). The same is observed for the front side segment of Test-1, except for the cement paste comprising 5 mm only of the top part (Figure 48b).

Secondly, the electrode side section for Test-2 had about 10 mm of cement paste accumulated on the upper side. The first aggregate with a size larger than 10 mm was spotted after 50 mm of the cement paste layer. Similar to Test-1, the aggregates larger than 10 mm are more frequently present in the middle part, and the last 100 mm have a much higher concentration of these larger aggregates (Figure 49a). The front side section has quite a similar distribution of aggregates and cement paste as shown in (Figure 49b).

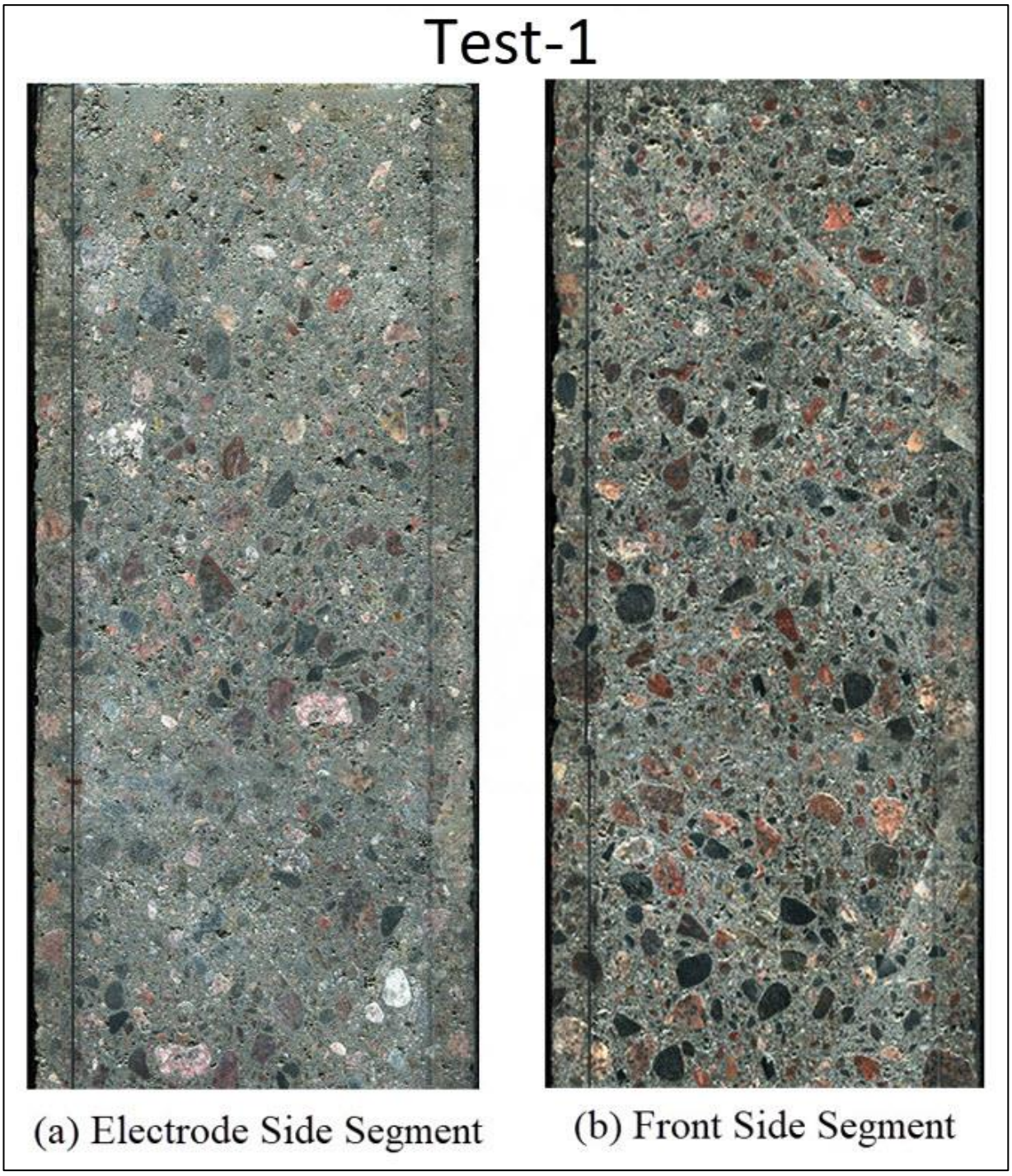

Figure 48. Vertical cut concrete segments of Test-1 from the: (a) Electrode Side and (b) Front Side.

Figure 49. Vertical cut concrete segments of Test-2 from the: (a) Electrode Side and (b) Front Side.

In conclusion, the statistical analysis of the acquired densities paired with the visual inspection of cut segments indicate that Test-1 and Test-2 were segregated. Consequently, a testing plan was put in place to further investigate the ability of EIS for monitoring compaction. Previously, it was suggested, based on the charts in Figure 45, that at around time 90 s segregation begins to take place, since the top and middle layers start to lose resistance, and the bottom layer shows an increase in resistance. Hence, the devised testing plan was as shown in Table 14.

Table 14. Groups of EIS investigated concrete, number of tested samples, vibration time and codenames.

	Over-vibrated	**Normally vibrated**	**Under-vibrated**
Vibration Time (s)	130	90	50
Number of Samples	4	2	1
Codename of Tests	OVER-1, OVER-2, OVER-3 and OVER-4	NORM-1 and NORM-2	UNDER-1

For the over-vibrated group, the already tested samples were named OVER-1 and OVER-2. Additionally, in order to have a better understanding of the relative resistance behaviour around time 90 s, two more samples, OVER-2, and OVER-3, were over-vibrated with extra time steps 80 s as well as 100 s added to the vibration time plan. In the normally vibrated group, two samples were vibrated until time 90 s: NORM-1 and NORM-2. Finally, the under-vibrated group consisted of 1 tested sample: UNDER-1 which vibration stopped early at 50 s. The time steps and the frequency of the vibration table used for each step are shown in Table 15. The results of these tests are presented and analysed in the following chapter.

Table 15. Time steps and vibration frequencies for the EIS investigated samples.

	OVER-1 & OVER-2	**OVER-3 & OVER-4**	**NORM-1 & NORM-2**	**UNDER-1**
Time Steps (s) at 86 Hz	10, 20, 30, 40 and 50	10, 20, 30, 40 and 50	10, 20, 30, 40 and 50	10, 20, 30, 40 and 50
Time Steps (s) at 129 Hz	70, 90 and 130	70, 80, 90, 100 and 130	70, 80 and 90	-

4 Results and Analysis

This chapter presents the EIS vibration investigation and segregation results as well as analysis for the tested concrete samples. It is divided into 5 chapters as follows. The first chapter shows the measured values of slump and air content for all tests. The testing results and analysis for over-vibrated, well-vibrated, and under-vibrated concrete are presented in chapters 4.1, 4.2 and 4.3, respectively. The results presented in each chapter include the relative resistance variance charts, the statistical analysis of core densities, and the visual observations of segregation in vertically cut sections. Finally, chapter 4.4 provides an overall analysis of the acquired results from the seven tested concrete mixtures.

4.1 Fresh Concrete Test Results

The values of measured slump and air content are shown in Table 16 for all the tested concretes. Firstly, the mean value of measured slump is 25 cm with a standard deviation of 0.40 cm. Secondly, the mean value of the measured air contents is 6.3% with a standard deviation of 0.3%. This analysis shows that the tested concretes show high similarity in properties, where all the measurements are all within the specified tolerable limits.

Table 16. Measured slump and air content values for EIS investigated concretes.

Tested Sample	Measured Slump (cm)	Measured Air content
OVER-1	24.5	6.0%
OVER-2	24.6	6.6%
OVER-3	25.5	6.7%
OVER-4	25.4	6.3%
NORM-1	25.0	5.9%
NORM-2	25.0	6.2%
UNDER-1	25.0	6.2%
Mean Value	25.0	6.3%
Standard Deviation	0.40	0.3%

4.2 Over-vibrated Concrete

Chapter 3.5 presented the results of the first two vibrated concretes OVER-1 and OVER-2. It was found that both tests showed a behaviour of resistance loss in the top and middle layer and increase in the bottom layer, which occurred within the vicinity of time 90 s. This change in resistance was then correlated with the occurrence of segregation confirmed by the variance in density between drilled cores as well as the accumulation of larger aggregates in the bottom parts of the cut segments. Further inspection was done for over-vibrated concrete by performing OVER-3 and OVER-4 tests. These tests had two added time steps: 80 s and 100 s and provided relative resistance values as shown in Table 17.

Table 17. Relative resistance values of top, middle, and bottom layers for OVER-3 and OVER-4 samples.

Time	OVER-3			OVER-4		
	Top	Middle	Bottom	Top	Middle	Bottom
0	0.0668	0.0636	0.0671	0.0667	0.0671	0.0676
10	0.0648	0.0635	0.0660	0.0679	0.0696	0.0684
20	0.0636	0.0639	0.0654	0.0692	0.0786	0.0700
30	0.0653	0.0628	0.0661	0.0659	0.0773	0.0703
40	0.0633	0.0623	0.0652	0.0645	0.0731	0.0686
50	0.0620	0.0614	0.0672	0.0641	0.0733	0.0692
70	0.0615	0.0630	0.0665	0.0648	0.0685	0.0718
80	0.0631	0.0619	0.0672	0.0645	0.0667	0.0803
90	0.0609	0.0627	0.0690	0.0631	0.0691	0.0854
100	0.0605	0.0618	0.0731	0.0617	0.0681	0.0881
130	0.0582	0.0604	0.0754	0.0591	0.0687	0.0932

Graphically representing these values over the vibration time is shown in Figure 50. It is apparent that middle and top layers have quite a similar overall behaviour during the vibration time in both tests. Both layers have a fluctuation in values at the start of vibration, followed by a dip towards the final vibration time. Additionally, the bottom layers in OVER-3 and OVER-4 display variance in values at the beginning of vibration, then resistance starts to noticeably increase towards the end. These behaviours suggest that segregation occurred, given that the decrease in resistance for both top and middle layer could be linked to having less aggregates than the bottom layer which resistance significantly increased.

The inclusion of the two new time steps 80 s and 100 s provided an inconsistent behaviour among different layers at these times. Figure 50 shows that the decrease in top layer values took place at time 80 s, while the gradual decrease in middle layer resistance for both tests starts occurring at time 90 s, and for the bottom layer the values start to steadily increase at time 70 s. Given that change instability, it is evident that one time cannot be chosen as the critical vibration time for all layers.

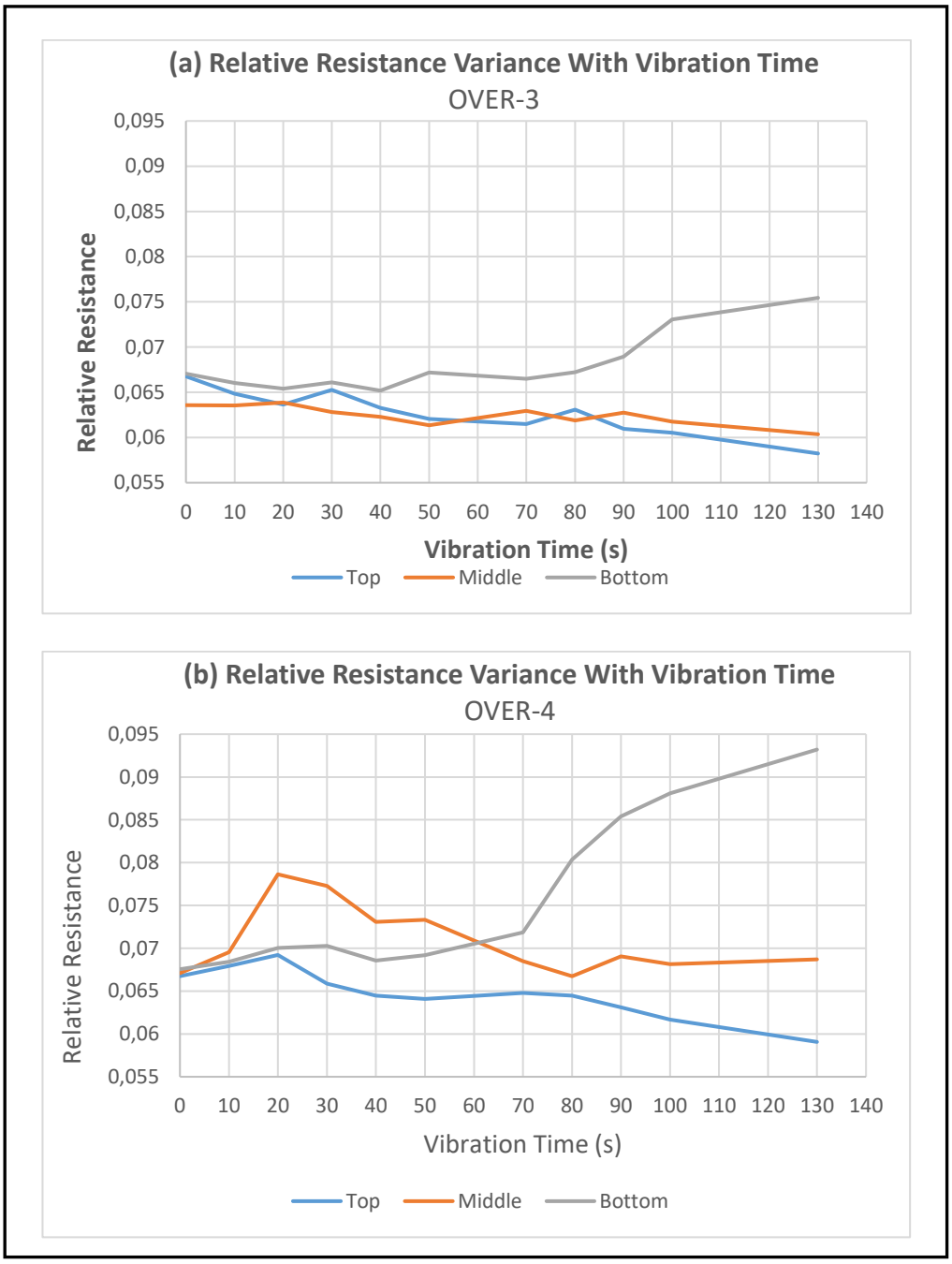

Figure 50. Relative resistance variance for EIS investigated concrete: (a) OVER-3 and (b) OVER-4 over the vibration duration.

The density values of the drilled cores for OVER-3 and OVER-4 tests along with the statistical parameters are presented in Table 18. It is evident that there is a large difference between density values in both tests. For cores drilled from OVER-3, and OVER-4 hardened sample, the standard deviation in density values for cores from both tests were 58.6 and 64.4 kg/m^3, respectively. Based on results from Good Vibration project, the limit for standard deviation in densities in one concrete element is 50 kg/m^3, since these values are above 50 kg/m^3 for both samples, it denotes segregation has taken place.

Table 18. Core densities and statistical parameters for OVER-3 and OVER-4 tests.

	Density (kg/m^3)			Statistical Parameters				
	Top	Middle	Bottom	Mean (kg/m^3)	Theoretical Density (kg/m^3)	Standard Deviation (kg/m^3)	Range (kg/m^3)	CV
OVER-3	2361	2423	2504	2429	2338	58.6	143	0.024
OVER-4	2349	2421	2507	2426	2338	64.4	158	0.027

Segregation was confirmed through the visual inspection of the electrode and front side sections for OVER-3 and OVER-4 tested concrete. Firstly, It is shown in the electrode segment (Figure 51a) that the first 10 mm contain no aggregates, while the following 80 mm lack any aggregates larger than 10 mm in size. Afterwards, the number of aggregates larger than 10 mm start to gradually increase towards the bottom of the section, where most larger aggregates are accumulated at the last 100 mm. The case is similar for the backside, with some minor differences in dimensions of aggregate concentration areas, as shown in (Figure 51b).

Secondly, Figure 52a presents the electrode segment of OVER-4 hardened concrete, where the first 10 mm are almost pure cement paste. The 70 mm following the cement paste layer are free of any aggregates larger than 10 mm, which concentration increases the lower it is in the section. The case is almost similar in Figure 52b for the front side section, except that the thickness of the cement paste layer is almost 15 mm, followed by 45 mm without any aggregates larger than 10 mm, then the larger aggregates increase in number towards the bottom of the section.

In conclusion, the segregation resulted from over-vibrating the concrete samples can be linked to the EIS investigated change in the relative resistance for all layers. Where the top and middle layer show a decrease in their final values over time, which denotes the lack of aggregates. On the other hand, the bottom layer displays a steady increase in the last calculated relative resistances, which represents the accumulation of larger aggregates in that layer.

Figure 51. Vertical cut concrete segments of OVER-3 sample from the: (a) Electrode Side and (b) Front Side.

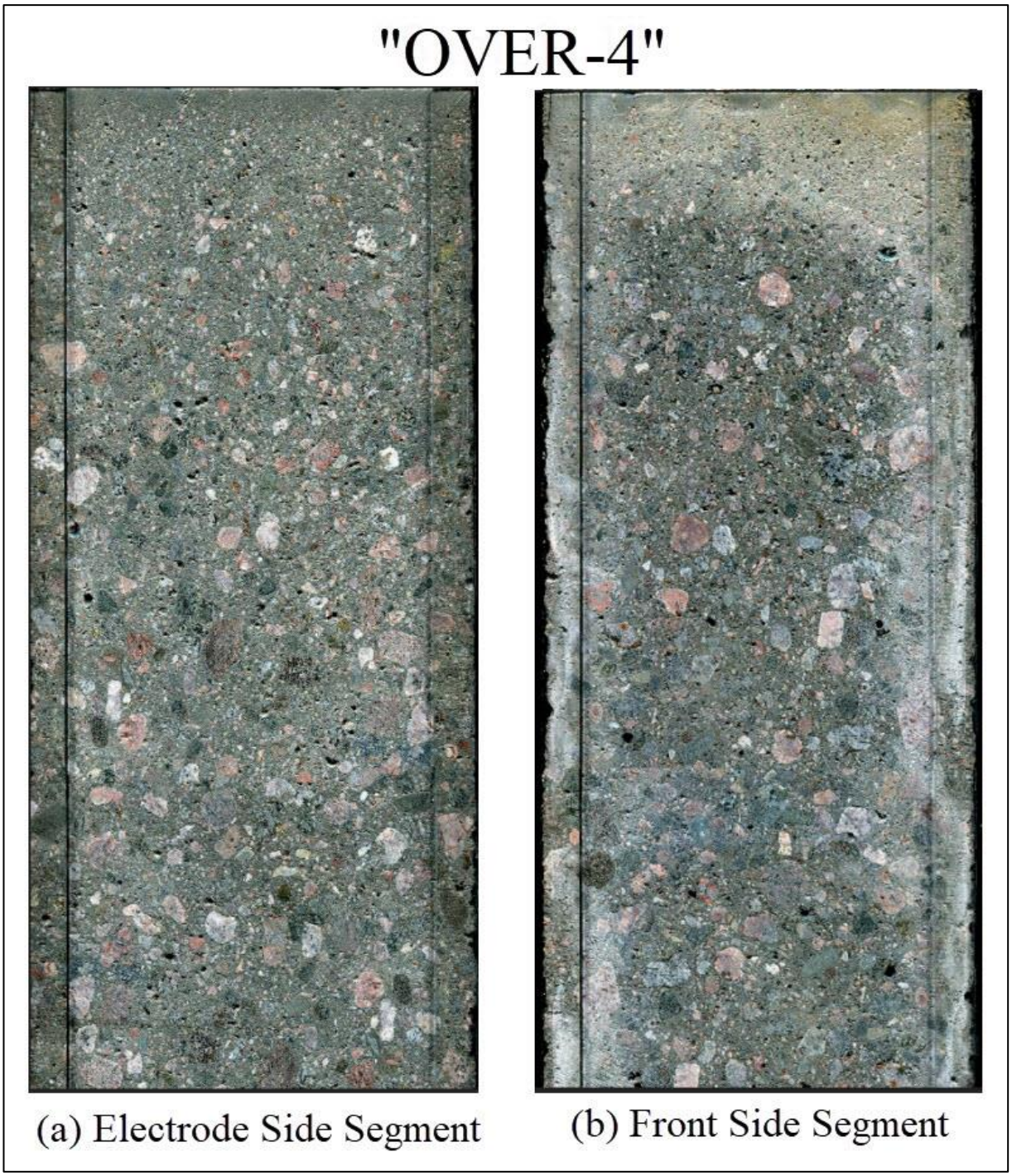

Figure 52. Vertical cut concrete segments of OVER-4 sample from the: (a) Electrode Side and (b) Front Side.

4.2 Normally vibrated concrete

The relative resistance values acquired from analysing Nyquist plots for NORM-1 and NORM-2 samples are presented in Table 19, below which the graphical representation of these values is provided in Figure 53.

Table 19. Relative resistance values of top, middle, and bottom layers for NORM-1 and NORM-2 samples.

Time	NORM-1			NORM-2		
	Top	Middle	Bottom	Top	Middle	Bottom
0	0.0613	0.0647	0.0607	0.0714	0.0702	0.0673
10	0.0635	0.0672	0.0619	0.0731	0.0747	0.0675
20	0.0631	0.0662	0.0592	0.0675	0.0721	0.0664
30	0.0635	0.0670	0.0591	0.0655	0.0741	0.0670
40	0.0633	0.0647	0.0587	0.0665	0.0730	0.0663
50	0.0620	0.0645	0.0590	0.0661	0.0748	0.0650
70	0.0622	0.0591	0.0637	0.0621	0.0699	0.0732
80	0.0656	0.0616	0.0667	0.0602	0.0661	0.0787
90	0.0651	0.0601	0.0690	0.0557	0.0662	0.0804

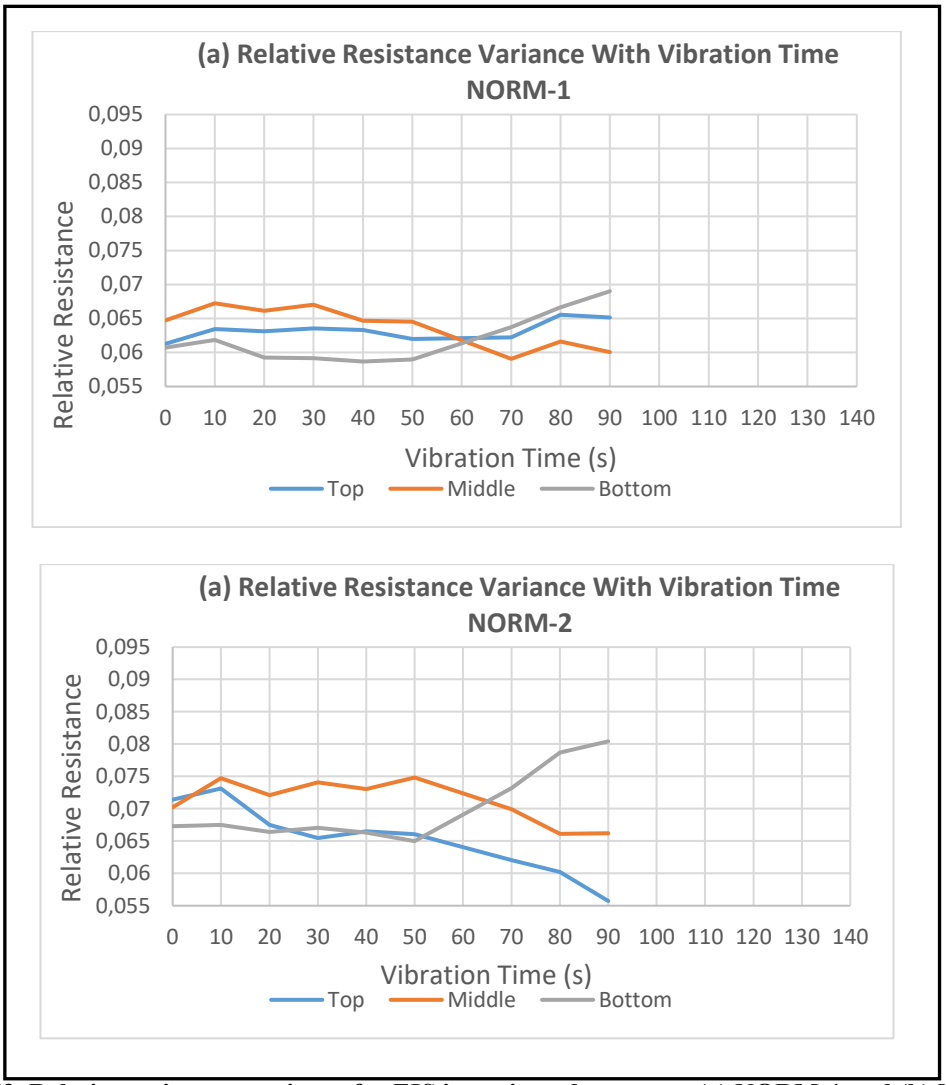

Figure 53. Relative resistance variance for EIS investigated concrete: (a) NORM-1 and (b) NORM-2 over the vibration duration.

There is a clear difference in behaviour of the three layers for the two tested concretes. Although vibration was stopped in both cases at 90 s, Figure 53a shows that the values for the top, middle and bottom layers were relatively closer to each other compared with those in Figure 53b.

Firstly, NORM-1 sample top layer displays some fluctuation in values without any significant decrease towards the end. On the other hand, the middle layer presents variance in relative resistance until the time 50 s, after which the values start to slightly decrease. While the bottom layer presents some variance until time 50 s, followed by a gentle increase towards the final time of vibration. These observations suggest that this sample was not segregated, given that no significant variance in resistances was noted, which could be the result of an almost even distribution of aggregates and air bubbles in the hardened concrete.

Secondly, NORM-2 shows a fluctuation in the top layer resistance values until time 50 s, after which starts a significant decrease in values. Similarly, the middle layer follows a behaviour of variance until time 50 s, then values start to plummet towards the end. In contrast, the bottom layer displays a simple fluctuation in values at the beginning of vibration, followed by a significant rise after time 50 s towards time 90 s. These three layers follow a pattern that suggests segregation took place in the hardened sample, due to the large gap in resistance between those layers, which was probably caused by uneven distribution of aggregates and air bubbles in concrete.

Investigation of the hardened concrete samples for NORM-1 and NORM-2 provided the densities and statistical parameters shown in Table 20. It can be seen that densities of cores for NORM-1 are not as spread as those of NORM-2. NORM-1 cores had a relatively lower standard deviation than that of NORM-2, where the first was less than 50 kg/m^3, and the latter was 54.1 kg/m^3, suggesting that unlike NORM-2, the first test of this group did not segregate. Additionally, the standard deviation of NORM-1 is less than half of NORM-2 standard deviation, which stresses that the first was unsegregated.

Table 20. Core densities and statistical parameters for NORM-1 and NORM-2 tests.

	Density (kg/m^3)			Statistical Parameters				
	Top	Middle	Bottom	Mean (kg/m^3)	Theoretical Density (kg/m^3)	Standard Deviation (kg/m^3)	Range (kg/m^3)	CV
NORM-1	2362	2407	2406	2392	2338	21.2	45	0.009
NORM-2	2356	2397	2485	2413	2338	54.1	129	0.022

Confirmation of segregation was carried out through visually inspecting the cut segments for both tests. Firstly, NORM-1 electrode side segment (Figure 54a) shows around 4 mm at the top free of any aggregates, followed by around 60 mm where no aggregates larger than 10 mm were present. However, the rest of the section shows an almost even distribution of aggregates until the bottom of the section. The front side section (Figure 54b) for the same test also shows around 4 mm of cement paste at the top, while it is only 35 mm until 10-mm-aggregates start to show up. Similar to the electrode side segment, there was no apparent inconsistent distribution of aggregates throughout the rest of the section. These observations establish that NORM-1 concrete did not fully segregate.

Secondly, NORM-2 electrode side segment (Figure 55a) showed around 5 mm at the top with cement paste only, followed by 60 mm until the first 10-mm-aggregate was spotted. Followingly, the larger aggregates start increasing in number in the lower part of the section, with the last 100 mm having the highest concentration of aggregates. The front side segment (Figure 55b) of test NORM-2 almost exactly follows the same aggregates distribution of the electrode side segment. The examination of NORM-2 cut sections confirms that the sample was segregated, given the uneven distribution of aggregates throughout the cut sections.

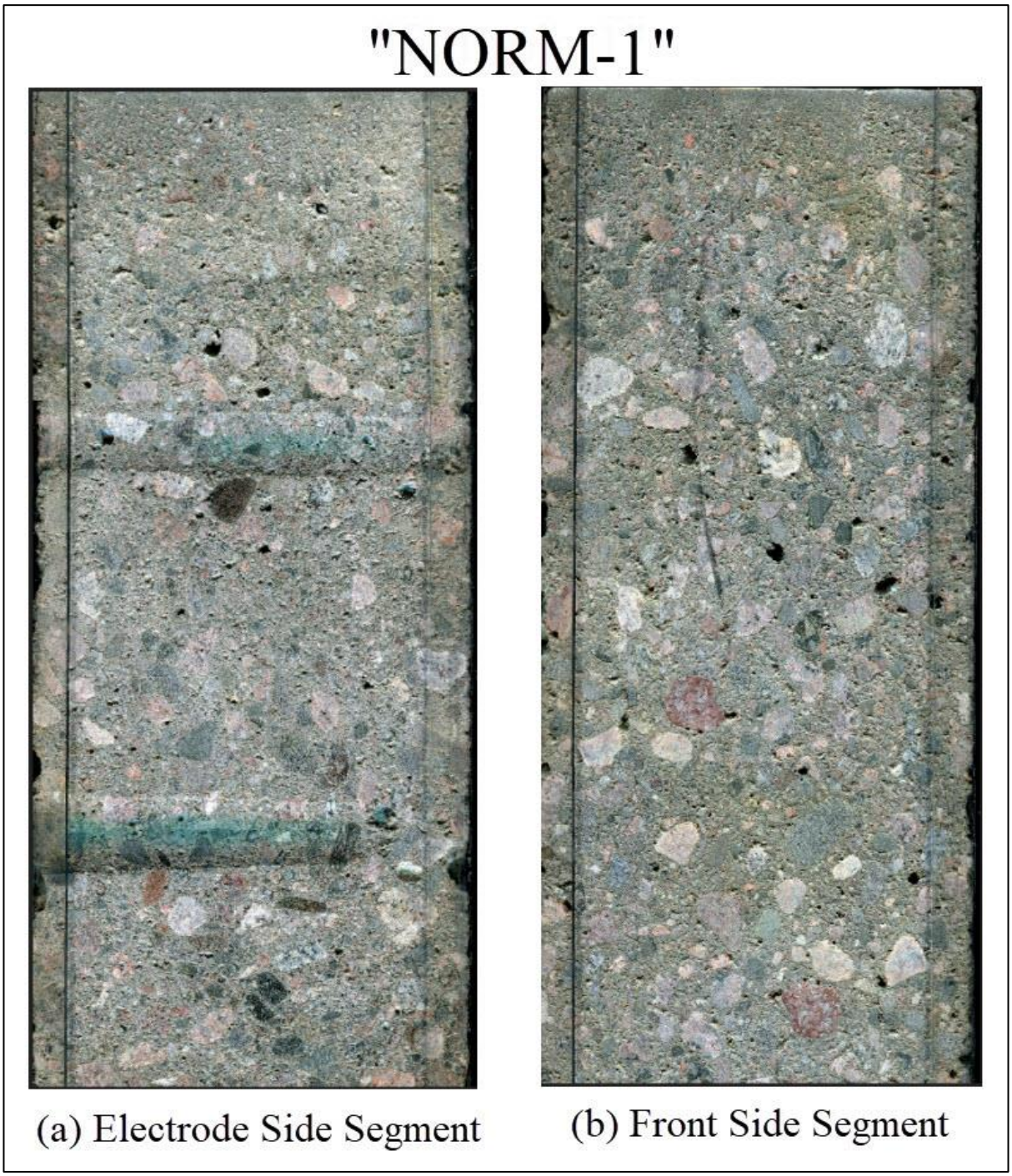

Figure 54. Vertical cut concrete segments of NORM-1 sample from the: (a) Electrode Side and (b) Front Side

Figure 55. Vertical cut concrete segments of NORM-2 sample from the: (a) Electrode Side and (b) Front Side

4.3 Under-vibrated Concrete

The relative resistance values obtained from the EIS investigation of test UNDER-1 are displayed in Table 21 followed by the graphical representation (Figure 56) of these values over the period of vibration.

Table 21. Relative resistance values of top, middle, and bottom layers for UNDER-1 test.

Time	UNDER-1		
	Top	Middle	Bottom
0	0.0609	0.0604	0.0598
10	0.0614	0.0615	0.0605
20	0.0594	0.0600	0.0575
30	0.0563	0.0553	0.0583
40	0.0542	0.0560	0.0584
50	0.0550	0.0576	0.0603

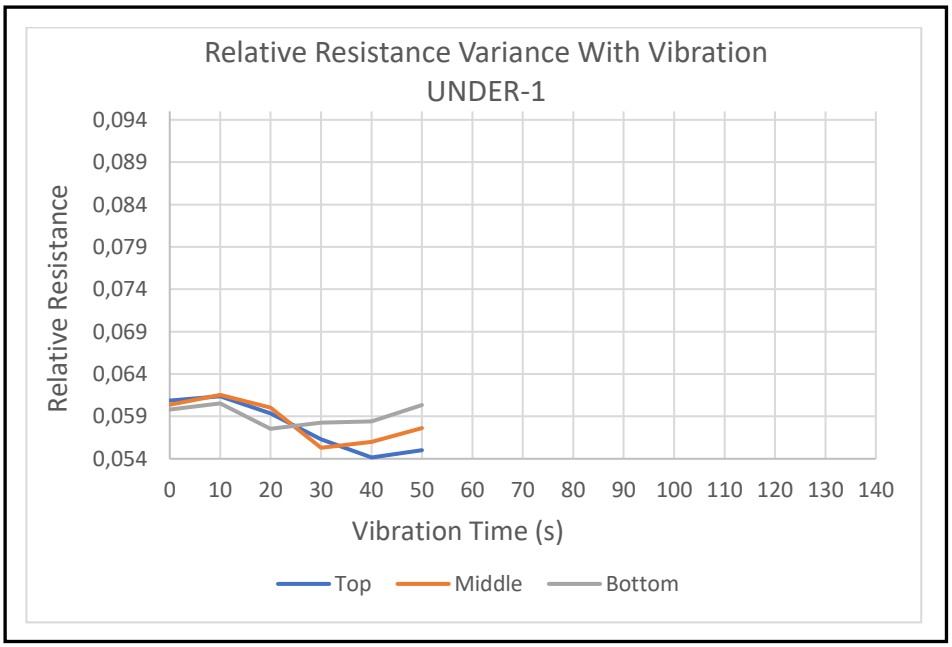

Figure 56. Relative resistance variance for EIS investigated concrete of test UNDER-1

It is apparent in Figure 56 that the three layers had quite a similar behaviour, where the relative resistance values were in a close proximity. Firstly, the top layer shows a decrease in values up to time 40 s, followed by a slight increase toward 50 s. Secondly, the middle layer has a small variance in values until time 20 s, followed by plummeting towards 30 s, then a slight increase until 50 s. Lastly, the values of the bottom layer keep fluctuating, with a minor rise at time 40 s towards 50 s. The interpretation of these values implies that the distribution of aggregates was quite similar in the three layers.

In order to check the occurrence of segregation in the sample, the values of densities for the drilled cores were statistically analysed and presented in Table 22.

Table 22. Core densities and statistical parameters for UNDER-1 test.

Density (kg/m³)			Statistical Parameters				
Top	Middle	Bottom	Mean (kg/m³)	Mix Theoritical Density (kg/m³)	Standard Deviation (kg/m³)	Range (kg/m³)	CV
2348	2372	2433	2384	2338	35.7	85	0.015

Although the standard deviation is lower than 50 kg/m^3, the range and CV values are quite close to those of the previously segregated samples, which suggests segregation has happened. In order to further confirm the occurrence segregation, the cut samples from both the electrode and front side of the sample (Figure 57) were visually inspected as follows.

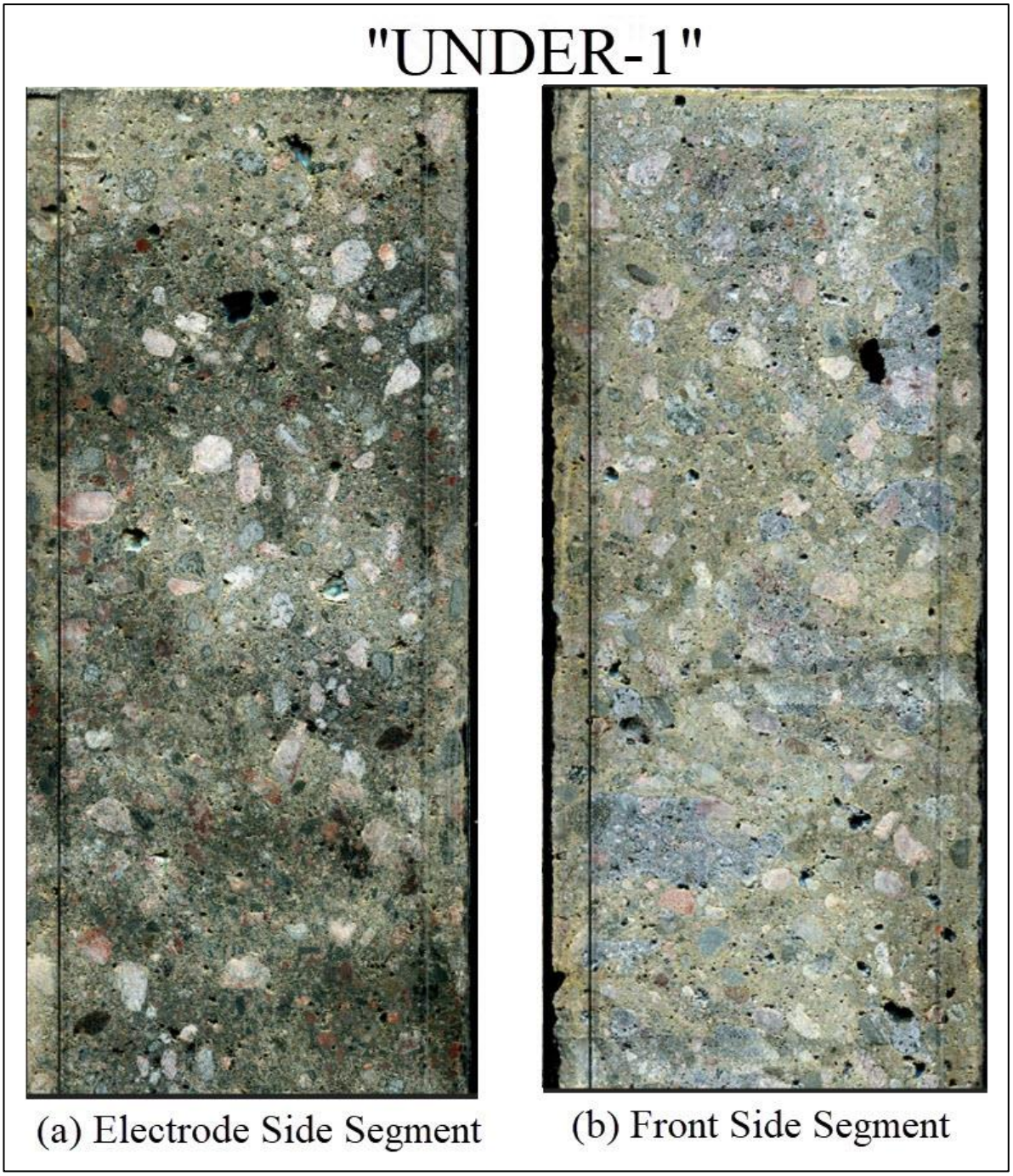

Figure 57. Vertical cut concrete segments of UNDER-1 sample from the: (a) Electrode Side and (b) Front Side

It can be seen in Figure 57a that the electrode side segment of UNDER-1 has no layer of cement paste on top, with aggregates larger than 10 mm already spotted after less than 10 mm from the top. Additionally, several air voids larger than 1 mm and up to 6 mm in size could be spotted throughout the section, which decrease in number towards the bottom. Similarly, the front side segment (Figure 57b) shows a dense distribution of these large air voids. However, these voids still show in a similar concentration at the bottom of the sample. These observations show that the duration of vibration was not sufficient to expel the larger air voids from the concrete, hence causing difference in densities due to uneven air distribution through the sample. This means that the sample was under-compacted leading to a larger difference in densities caused by unreleased entrapped air. The EIS results do not distinguish between an increase in resistance caused by the air voids or the aggregates, which leads to similar readings of the unsegregated concrete.

4.4 Test Results Combined Analysis

The original testing plan aimed towards achieving five segregated and two unsegregated samples, where the first five included four over-vibrated and one under-vibrated concrete sample. However, it was shown in the previous analysis subsections that six of the tested samples showed signs of segregation.

Table 23. Values of range, Coefficient of Variation (CV), and segregation state for the EIS investigated samples.

Test	Range (kg/m^3)	CV	Segregation State	Compaction State
OVER-1	161	0.028	Segregated	Over-compacted
OVER-2	74	0.013	Segregated	Over-compacted
OVER-3	143	0.024	Segregated	Over-compacted
OVER-4	158	0.027	Segregated	Over-compacted
NORM-1	45	0.009	Unsegregated	Well-compacted
NORM-2	129	0.022	Segregated	Over-compacted
UNDER-1	85	0.015	Segregated	Under-compacted

Through analysing the densities of the drilled cores from each tested sample, different statistical parameters were obtained, including the range and Coefficient of Variation. These values as well as the segregation state of the samples are shown in Table 23. It can be seen that for the one unsegregated sample, the value of range was 45 kg/m^3, while the rest have values higher than higher than that, to the point of being more than 3 times higher. In addition, the CV values for all the segregated samples were above 0.01, while NORM-1 test CV value was only 0.009. This shows that the CV and range could be used to distinguish segregated from unsegregated samples. Since the sole dependence on standard deviation would show that OVER-2 sample and UNDER-1 sample were both unsegregated, given that their standard deviation was lower than 50 kg/m^3, which was not the case.

Segregation was additionally inspected by visually observing the cut hardened segments from different tests. It should be noted that air bubbles movement played an important role in affecting the measurements of both the top and middle layer. Given that as aggregates start sinking down, air bubbles simultaneously rise up. This means that these layers experience much less change in resistance compared with the bottom layer, since the drop caused by losing aggregates is almost recovered by resistive air bubbles rising upwards. In contrast, the bottom layer resistance is more controlled, since air bubbles escape upwards lessening the resistance, while aggregates keep accumulating downwards gradually increasing that resistance. This holds true for over-vibrated concretes, since the long duration of vibration ensures that the bottom layer has no entrapped air inside. This could be observed in all cut segments of OVER-1…4 tests, and it shows that during the visual inspection changes in the lower part of the sample give better estimates of the segregation state of the concrete.

Further analysis was carried out on the relative resistance values obtained from the EIS investigation, where the difference between relative resistance of the top and bottom layers was calculated for each different test. These values are presented in Table 24. It can be seen that for all the segregated samples that reached over-vibration, this difference rose to a value higher than 0.01 at some point during vibration. These values are yellow highlighted in Table 24, and they are located in the range of 70—100 s. On the other hand, NORM-1, which did not segregate, along with the under-vibrated segregated UNDER-1, both did not have a value higher than 0.01.

Table 24. Change in relative resistance values for top and bottom layers over the duration of vibration for different EIS investigated concretes.

Time Step	Relative Resistance Change Between Top and Bottom						
	OVER-1	OVER-2	OVER-3	OVER-4	NORM-1	NORM-2	UNDER-1
0	0.005	0.001	0.000	0.001	0.001	0.004	0.001
10	0.001	0.002	0.001	0.001	0.002	0.006	0.001
20	0.001	0.003	0.002	0.001	0.004	0.001	0.002
30	0.003	0.002	0.001	0.004	0.004	0.002	0.002
40	0.005	0.002	0.002	0.004	0.005	0.000	0.004
50	0.003	0.004	0.005	0.005	0.003	0.001	0.005
70	-	-	0.005	0.007	0.002	0.011	-
80	0.011	0.011	0.004	0.016	0.001	0.018	-
90	-	-	0.008	0.022	0.004	0.025	-
100	0.014	0.014	0.013	0.026	-	-	-
130	0.007	0.003	0.017	0.034	-	-	-

It was previously shown in the cut segment figures for the tests: OVER-1, OVER-2, OVER-3, OVER-4, and NORM-2 that larger aggregates sunk down to the bottom layer, leaving the top layer with a much lower amount of aggregates. The abundance in aggregates at the bottom results in higher resistance compared with that of the top layer which has more cement paste and much less aggregates, providing much lower resistance values.

However, in the normally vibrated and unsegregated sample, NORM-1, the aggregates distribution as well as the air voids distribution in the top and bottom layers were quite

similar, hence the relatively small change in resistance. Lastly, the under-vibrated segregated sample, UNDER-1, showed no higher change than 0.01, which could be explained by the existence of larger air voids in the upper part of the sample, compared with the lower number of voids towards the bottom. In addition to the fact that less amount of larger aggregates sunk to the bottom in comparison with the over-vibrated samples, which along with the high air void existence in top, led to a similar resistance among all layers.

The difference in relative resistance between the top and bottom layers over time for 3 tests is represented in Figure 58. These tests are NORM-1, UNDER-1, and OVER-3 representing unsegregated and two segregated samples, respectively. It is apparent that the overall behaviour of the change is to fluctuate a bit at the beginning followed by an increase, then if vibration continues, this difference drops down, and finally segregation shows by an increase in that difference.

This behaviour was shown by the one unsegregated sample, where the change increases up to 0.005 at 40 s, then steadily decreases towards 80 s to 0.001, after which an increase to 0.004 is achieved at the final vibration time. Similarly, for the over-vibrated segregated sample, OVER-3, the change rises to 0.005 at time 50 s, then gently decreases to 0.004, followed by a surge to 0.017 at time 130s. Finally, the under-vibrated sample showed the first part only of that behaviour, where the change grew to 0.005 at 50 s.

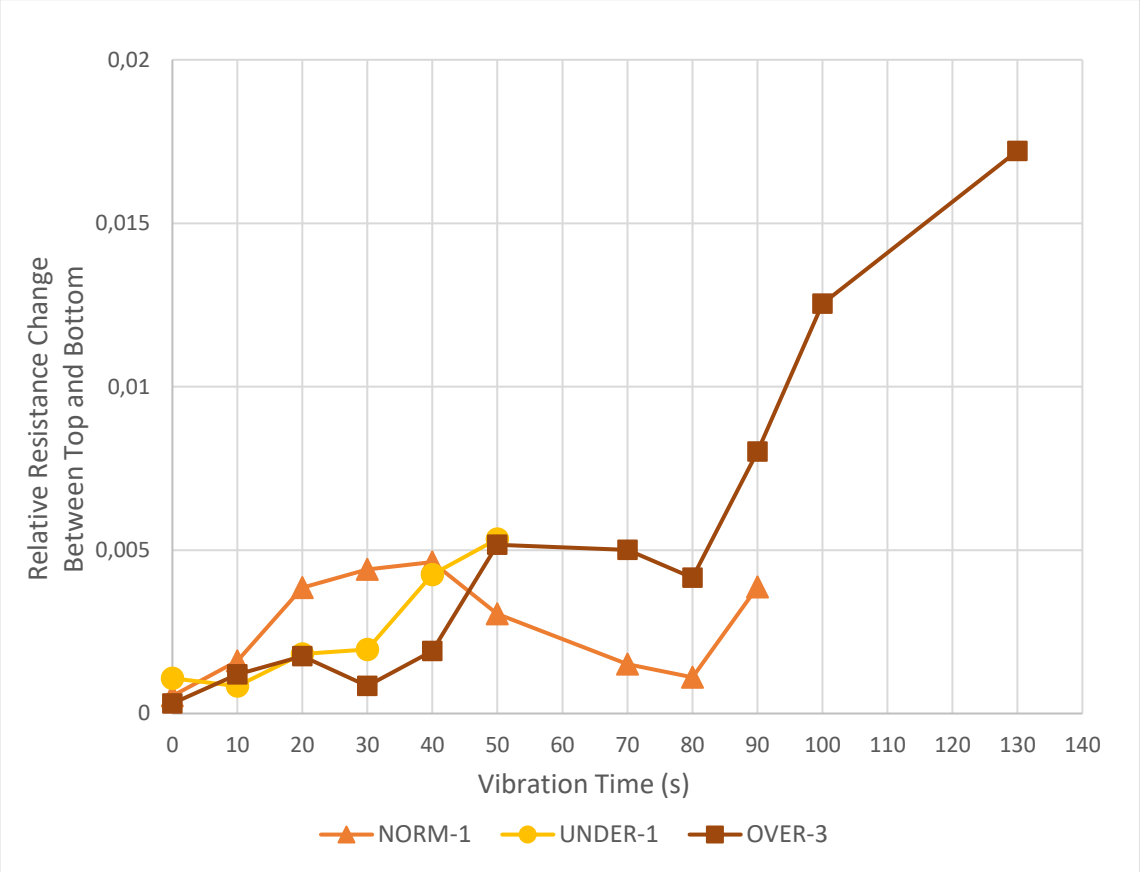

Figure 58. Variance over time of relative resistance change between Top and Bottom layers of NORM-1, UNDER-1, and OVER-3 tests.

On the other hand, graphical representation of the relative resistance change in the other 3 over-vibrated samples provided two different patterns, where the middle part, at which values decrease, does not exist. Firstly, OVER-4 sample showed that values follow a slight increase to 0.007 at 70 s, then change surges to 0.034 at 130 s. Secondly, for both OVER-1 and OVER-2, the values fluctuate at the beginning then increase to around 0.011 at 80 s, after which the values plummet to 0.007 and 0.003 for OVER-1 and OVER-2, respectively. This finding shows that although all segregated samples reached changes of 0.01 or higher during vibration, the pattern through which they got to that change was not constant amongst different samples.

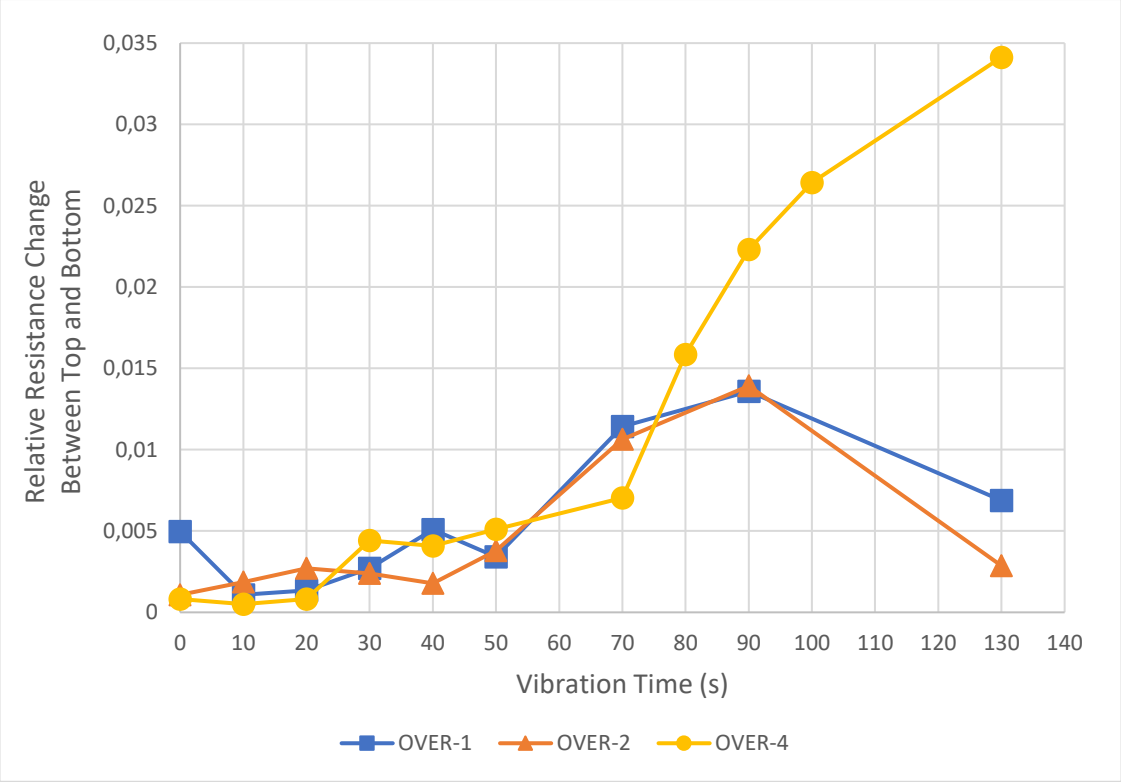

Figure 59. Variance over time of relative resistance change between Top and Bottom layers of OVER-1 ,OVER-2, and OVER-4 tests

5 Discussion and Future Research

The thesis main objective was to test the ability of the designed electrode panel to detect concrete quality of compaction during vibration using EIS investigation. A relationship between the acquired resistances over vibration times could be established to distinguish between segregated and unsegregated concrete samples.

Originally, the vibration times chosen were meant to have four over-vibrated samples, two normally vibrated and one under-vibrated. However, given the known inconsistent behaviour of concrete, the second normally vibrated sample was segregated, nevertheless the measurement could detect that segregation.

Segregation was detected through the overall behaviour of the layers relative resistance variance over vibration time, where after some fluctuation in values, top and middle layer displayed a steady decrease, with a simultaneous increase in the bottom layer resistance. This behaviour was expected due to the electrical properties of concrete ingredients, where aggregates have much higher resistance to electrical conduction than cement paste. It was shown in segregated concretes that the bottom layer had a much higher concentration of aggregates compared with the top and middle layers. This was visually clear in the cut hardened concrete segments. Additionally, segregation was confirmed through the densities comparison of the drilled concrete cores.

This difference in value between the relative resistance of top and bottom layer was found to reach 0.01 or higher, in case of over-vibration. On the other hand, the change stopped at a maximum value of 0.05 for unsegregated concrete. However, the under-vibrated sample, although segregated, did not reach the 0.01 mark. This shows that the ability of the devised method to detect segregation was only limited to over-vibrated samples solely based on the value of that difference. Nevertheless, studying this change between layers for under-vibrated and normally vibrated concrete showed that they both followed a similar pattern. This suggests that if the vibration of the under-vibrated sample were continued, it could have followed the same arrangement, and then the point at which vibration should be stopped could have been specified.

The early distribution of entrapped air in the sample could be one reasoning for the relative resistance values of all three layers fluctuating in the same range around the first 50 seconds, since it was shown in UNDER-1 sample that the top and middle part had an increased number of large air voids compared with the bottom part. When air rises from the bottom, the resistance decreases, yet aggregates start to sink down, which might nullify this decrease and result in a similar value of resistance for all layers. This shows the insufficiency for solely using the value of change without observing the overall behaviour over time, which was shown in Figure 58.

The outcome of this thesis along with the faced limitations opens a chance for different future research approaches to better develop this method. Some of these suggestions are mentioned below:

1. Investigating a larger a number of the same concrete mixture, in order to better understand the behaviour of change between top and bottom layer. Given that this thesis provided only one unsegregated sample, which limits the view of a well-vibrated concrete to only one sample.

2. Experimenting with different concrete mixes. This could be achieved by investigating a less flowable concrete, in order to be closer to the limit used in actual construction sites. Additionally, different type of cement could be used to understand the behaviour of change for other cement types. Lastly, different W/C ratios will provide different values for resistance, which might affect the relationship of change between the layers and provide new limits for over-vibration.

3. The addition of rebars to the sample to experiment with reinforced concrete, which is more commonly used on site. Given that steel is highly conductive, it will change the overall resistance of the sample, added to that some local changes in resistance that will affect the behaviour of change between layers.

4. Devising a different set up for electrodes. Since the middle layer almost always followed the same behaviour as the top layer, a simpler set up consisting of a top and bottom electrode could be used. This will cut down the duration of testing and make analysis more focused on that change.

5. The device could be used for monitoring the dynamic stability of concrete. Given that it can assess the stability of concrete against segregation during compaction.

6 Conclusions

Compaction of concrete through vibration is a very complicated process. Although vibration has been used for almost a century, there are no approved methods for monitoring its quality. Previous suggested methods relied on statistical data to assess concrete compaction, which proved to be inaccurate given the several factors that affect vibration. Therefore, this thesis studied the use of EIS investigation for online evaluation of vibration quality for a certain concrete mixture. The concluded results from this thesis can only be associated with the specified concrete mix tested, since results would be different in case of different concrete mixes. The following conclusions can be drawn based on the analysis of the data acquired in this thesis:

1. Quality of compaction for a certain concrete mixture cannot be solely determined based on vibration time. Given that for two batches of the same concrete mixture both with almost identical measured slump and air content, the vibration time of 90 s using one vibrating table with the same frequencies, resulted into segregation of one sample, while the other remained unsegregated. This shows the importance of having an online measuring system to assess vibration quality at certain points during casting.

2. EIS monitoring of compaction can detect the occurrence of segregation through the change in relative resistance for different layers. This detection is based on the decrease of relative resistance in top and middle layers, where cement paste rises, and aggregates sink down providing better conductivity. Contrarily, the relative resistance values of the bottom layer increases as more aggregates sink down and obstruct the movement of current.

3. The segregation limit was specified to be a 0.01 or higher change in relative resistance values between top and bottom layers.

4. Inspection of segregation in hardened concrete samples can be carried out by calculating the range and coefficient of variation for density values of these drilled cores. It was found that for segregated samples, the coefficient of variation was always greater than 0.01, while the range was always higher than 50 kg/m^3.

References

ACI 309.1R-08, 2008. *Report on Fresh Concrete Behavior During Vibration,* Farmington Hills: American Concrete Institute.

Arslan, M. E., Yozgat, E., Pul, S. & Husem, M., 2011. *Effects of Vibration time on Strength of Ordinary and High Performance Concrete.* s.l., s.n., pp. 270-274.

Banfill, P. F. G., Yongmo, X. & Domone, P. L. J., 1999. Relationship between the rheology of unvibrated fresh concrete and its flow under vibration in a vertical pipe apparatus. *Magazine of Concrete Research*, 3 June, pp. 181-190.

Banfill, P., Teixeira, M. & Craik, R., 2011. Rheology and vibration of fresh concrete: Predicting the radius of action of poker vibrators from wave propagation. *Cement and Concrete Research,* pp. 932-941.

Beris, A. N., Tsamopoulos, J. A., Armstrong, R. C. & Brown, R. A., 1985. Creeping Motion of a Sphere Through a Bingham Plastic. *Journal of Fluid Mechanics,* Volume 158, pp. 219-244.

Bhattacharjee, B., 2007. *Construction Practices,* s.l.: s.n.

Blekhman I., I. et al., 2014. *Vibrational segregation – simulation, experiment and application to create new classifying machines.* St. Petersburg, s.n.

Burlingame, S. E., 2004. *Application of Infrared Imaging to Fresh Concrete: Monitoring Internal Vibration.* [Online]
Available at:
http://www.concretepipe.org/secure/newscast/0608nc/0608nc.php#application_of_infrared_imaging

Cement Concrete & Aggregates Australia, 2006. *Compaction of Concrete,* s.l.: s.n.
Claude Goguen, P. L. A., 2012. *National Precast Concrete Association.* [Online]
Available at: https://precast.org/2012/12/air-entrainment-versus-air-entrapment/

David, I., 2017. *Sciencing.* [Online]
Available at: https://sciencing.com/salt-water-can-conduct-electricity-5245694.html
[Accessed 16 April 2020].

de Larrard, F. & Roussel, N., 2011. Flow Simulation of Fresh Concrete Under a Slipform Machine. July.

Eurokomax, n.d. *CONSTRUCTION AND AGRICULTURAL EQUIPMENT.* [Online]
Available at: http://eurokomax.com/concrete-vibrator/

Finnsementti, 2012. *Suomalainen sementti,* s.l.: Finnsementti Oy.

Ghadban, A. A., 2016. *Effect of Vibration on Freeze-Thaw Resistance of Concrete,* Manhattan: Kansas State University.

Golovanevskiy, V. A. et al., 2011. Vibration-induced phenomena in bulk granular materials. *International Journal of Mineral Processing,* pp. 79-85.

Gong, J., Yu, Y., Krishnamoorthy, R. & Roda, A., 2015. Real-time tracking of concrete vibration effort for intelligent concrete consolidation. *Automation in Construction,* pp. 12-24.

Gopi, S., 2010. *Basic Civil Engineering.* New Delhi: Dorling Kindersley (India) Pvt. Ltd.

Grossi, M., 2017. *Theory and Applications of Electrical Impedance Spectroscopy (EIS): a Review,* s.l.: s.n.

Grossi, M. & Riccò, B., 2017. Electrical impedance spectroscopy (EIS) for biological analysis and food characterization: a review. *Journal of Sensors and Sensor Systems,* pp. 303-325.

Hackley, V. A. & Chiara, F. F., 2001. *Guide to Rheological Nomenclature: Measurements in Ceramic Particulate Systems,* s.l.: National Institute of Standards and Technology.
Hover, K. C., 2001. *Concrete Construction.* [Online]
Available at: https://www.concreteconstruction.net/how-to/construction/entrained-air-in-concrete_o

Karhunen, K., 2013. *Electrical resistance tomography imaging of concrete,* Kuopio: University of Eastern Finland Dissertations in Forestry and Natural Sciences.

Koch, J. A., Castenda, D. I., Ewoldt, R. H. & Lange, D. A., 2019. Vibration of fresh concrete understood through the paradigm of granular physics. *Cement and Concrete Research,* pp. 31-42.

Lange, D. et al., 2016. *Control of Entrained Air and Vibration of Concrete for Production of Crossties.* s.l., s.n.

Loche, J. M., Ammar, A. & Dumargue, P., 2004. Influence of the migration of chloride ions on the electrochemical impedance spectroscopy of mortar paste. *Cement and Concrete Research,* Volume 35, pp. 1797-1803.

Lopez, M. & Navarrete, I., 2016. Estimating the segregation of concrete based on mixture design and vibration energy. *Construction and Building Materials,* Volume 122, pp. 384-390.

Mahajan, D., 2008. *Encyclopedia Britannica.* [Online]
Available at: https://www.britannica.com/science/electrical-impedance
[Accessed 30 March 2020].

Mata, R., Pitroda, J. & Bhavsar, J. J., 2014. *MECHANICAL COMPACTION OF CONCRETE: A GOVERENING FACTOR FOR DURABILITY AND SERVICEABILITY OF THE CONCRETE.* s.l., s.n.

McCarter, W. J., 1994. A PARAMETRIC STUDY OF THE IMPEDANCE CHARACTERISTICS OF CEMENT-AGGREGATE SYSTEMS DURING EARLY HYDRATION. *Cement And Concrete Research,* 24(6), pp. 1097-1110.

McCarter, W. J., 1996. The a.c. impedance response of concrete during early hydration. *Journal of Materials Science,* Volume 31, pp. 6285-6292.

McCarter, W. J., Starrs, G. & Chrisp, T., 2004. The complex impedance response of fly-ash cements revisited. *Cement and Concrete Research,* Volume 34, pp. 1837-1843.

McCarter, W. J., Starrs, G. & Chrisp, T. M., 1999. Immittance spectra for Portland cement/fly ash-based binders during early hydration. *Cement and Concrete Research,* Volume 29, pp. 377-387.

McCarter, W. J., Starrs, G. & Chrisp, T. M., 2004. The complex impedance response of fly-ash cements revisited. *Cement and Concrete Research,* Volume 34, pp. 1837-1843.

McCarter, W., Starrs, G. & Chrisp, T., 2004. The complex impedance response of fly-ash cements revisited. *Cement and concrete research.*

Nave, R., n.d. *HyperPhysics.* [Online]
Available at: http://hyperphysics.phy-astr.gsu.edu/hbase/electric/phase.html
[Accessed 30 March 2020].

Ojala, T., Al-Neshawy, F. & Punkki, J., 2019. *Betonin koostumuksen vaikutus sen tiivistettävyyteen - Raportti tilaustutkimusprojektista [The effect of concrete composition on its compactibility],* Espoo: Aalto Yliopisto.

PalmSens, 2019. *PalmSens Compact Electrochemical Interfaces.* [Online]
Available at: https://www.palmsens.com/electrochemical-impedance-spectroscopy-eis/#
[Accessed 30 March 2020].

Patel, R., 2019. *Methods of Concrete Compaction and Types of Vibrators.* [Online]
Available at: https://gharpedia.com/blog/concrete-compaction-and-vibrators/

Petrou, M. F. et al., 2000. Influence of Mortar Rheology on Aggregate Settlement. *ACI Materials Journal,* 97(4), pp. 479-485.

Polder, R., 2001. Test methods for on site measurement of resistivity of concrete–a RILEM TC-154 technical recommendation. *Construction and Building Materials,* Volume 15, pp. 125-130.

Popovics, S., 1973. A review of the concrete consolidation by vibration. pp. 454-455.

Punkki, J. et al., 2019. Ohjeistus betonin tiivistämiseksi tärysauvalla. *Betoni*, pp. 104-107.

Rosato, A. D., Blackmore, D. L., Zhang, N. & Yidan, L., 2002. A PERSPECTIVE ON VIBRATION-INDUCED SIZE SEGREGATION OF GRANULAR MATERIALS. *Chemical Engineering Science,* pp. 265-275.

Ruokonen, S., 2018. *Sideaineet eri käyttökohteisiin,* s.l.: betoniyhdistys.

Shraddhu, S., 2017. *Compaction of Concrete: Voids and Methods | Concrete Technology.* [Online]
Available at: http://www.engineeringenotes.com/concrete-technology/compaction/compaction-of-concrete-voids-and-methods-concrete-technology/31401

Song, G., 2000. Equivalent circuit model for AC electrochemical impedance spectroscopy of concrete. *Cement and Concrete Research,* Volume 30, pp. 1723-1730.

Suprenant, B. A., 1988. *Concrete Vibration: The why and how of consolidating concrete.* Florida: The Aberdeen Group.

Suryakanta, 2014. *What Are The Methods For Compacting Concrete In The Field.* [Online]
Available at: https://civilblog.org/2014/05/08/what-are-the-methods-for-compacting-concrete-in-the-field/

Tattersall, G., 2003. *Workability and Quality Control of Concrete.* s.l.:s.n.

Tian, Z. & Bian, C., 2014. Visual Monitoring Method on Fresh Concrete Vibration. *KSCE Journal of Civil Engineering,* pp. 398-408.

Tian, Z. et al., 2019. Development of real-time visual monitoring system for vibration effects on fresh concrete. *Automation in Construction,* pp. 61-71.

Tuncan, M. et al., 2007. EFFECT OF COMPACTION ON ASSESSED CONCRETE STRENGTH. *seres'07,* pp. 847-853.

Walker, H. N., Lane, D. S. & Stutzman, P. E., 2006. *Petrographic Methods of Examining Hardened Concrete: A Petrographic Manual,* Charlottesville: Federal Highway Administration Research and Technology.

Whittington, H. W., McCarter, J. & Forde, M. C., 1981. The conduction of electricity through concrete. *Magazine of Concrete Research*, March, pp. 48-60.

Woo, L. Y., Kidner, N. J., Wansom, S. & Mason, T. O., 2006. Combined time domain reflectometry and AC-impedance spectroscopy of fiber-reinforced fresh-cement composites. *Cement and Concrete Research,* Volume 37, pp. 89-95.

European Standards Referred

EN 12350, Testing fresh concrete:

- Part 2: Slump test.
- Part 7: Air content – pressure methods.

EN 12390, Testing hardened concrete:

- Part 1: Shape, Dimensions and Other Requirements For Specimens and Moulds.
- Part 7: Density of hardened concrete.

Appendices

Appendix 1. Surface Observations of Test-1 During Vibration. 2 pages.
Appendix 2. Values of Actual Resistance for all EIS Tested Concretes. 2 pages.

Appendix 1

This appendix shows the changes observed in the surface of Test-1 concrete at the different vibration time steps. Figure 60 shows the captured photo of the surface at the end of the vibration time. The observed changes were recorded during the time of vibration and were as follows:

- **From 0 s to 10 s:** Aggregates started to sink down, while there were hardly any air bubbles rising.
- **From 10 s to 20 s:** Aggregates continued sinking down, while the amount of air bubbles rising increased significantly.
- **From 20 s to 30 s:** The rate of aggregates sinking and air rising up was almost similar to the previous step.
- **From 30 s to 40 s:** Cement paste started showing up on the surface, but lesser amount of air bubbles rose to the top.
- **From 40 s to 50 s:** Cement paste continued to rise, while air bubbles were rising in a rate similar to that of the previous step.
- **From 50 s to 70 s:** Cement paste rose in a rapid manner, while the rising air bubbles increased in size and frequency of showing on the surface.
- **From 70 s to 90 s:** No significant change in cement paste on the surface, while air bubbles rising became less in both size and frequency of rising.
- **From 90 s to 130 s:** Much more cement paste rising to the top and a foamy layer was formed, where hardly any bubbles could be spotted rising to the surface.

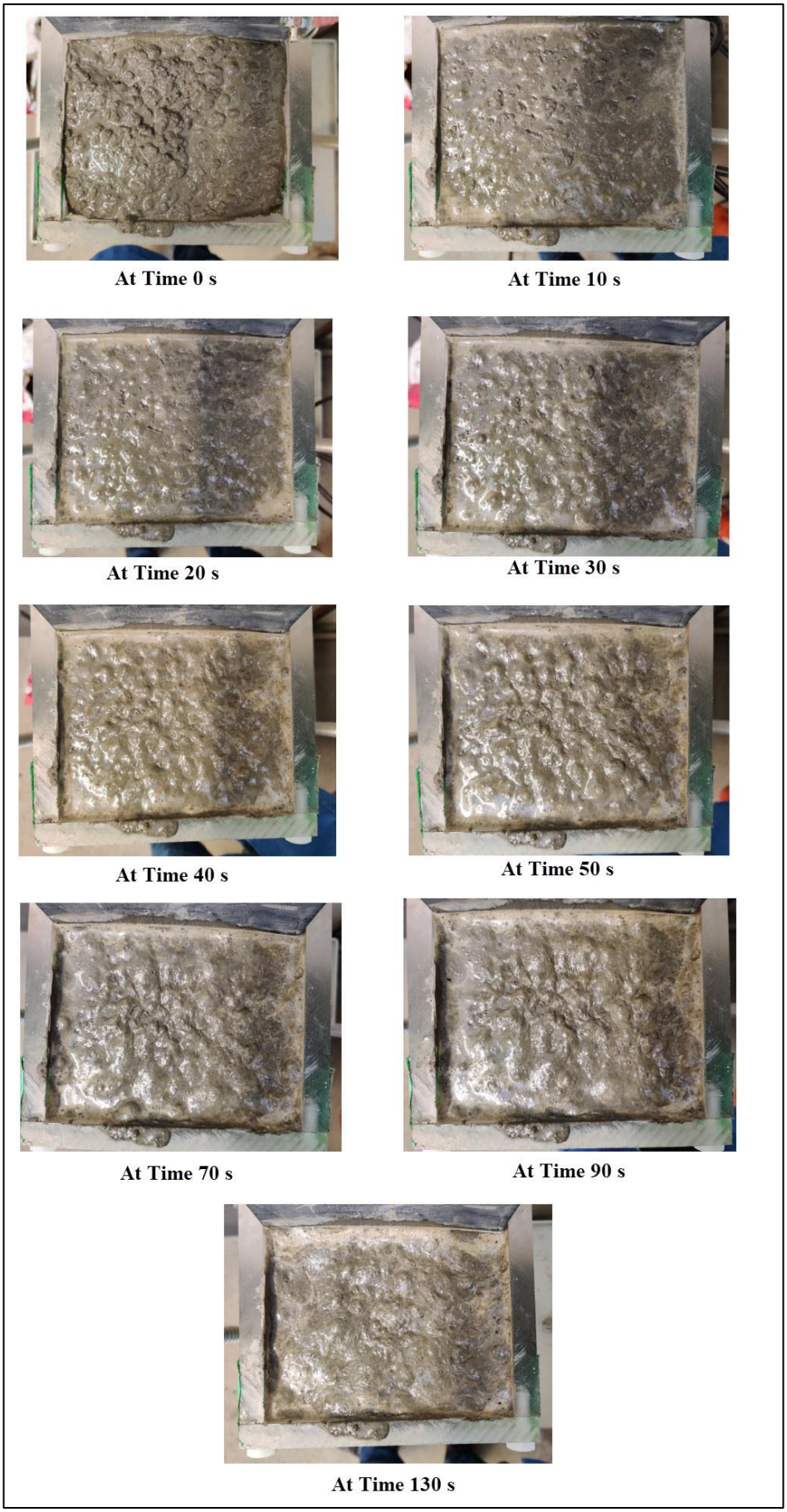

Figure 60. Changes in Test-1 concrete surface at different time steps during the process of vibration.

Appendix 2

Table 25 presents the actual resistance values of the three layers: top, middle, and bottom for the seven EIS investigated concrete samples. The resistances are those obtained from Nyquist plots after each vibration time step.

Table 25. Actual resistance values for EIS investigated concretes at different vibration times.

		Resistance (Ω)		
	Time (s)	Top	Middle	Bottom
OVER-1	0	317	380	368
	10	344	395	374
	20	355	389	372
	30	357	399	367
	40	370	397	367
	50	360	393	366
	70	393	412	356
	90	417	394	369
	130	354	376	418
OVER-2	0	332	400	367
	10	349	409	369
	20	351	402	367
	30	352	400	370
	40	350	409	371
	50	361	422	372
	70	379	436	355
	90	390	409	350
	130	353	401	368
OVER-3	0	364	394	378
	10	354	394	372
	20	347	396	368
	30	356	389	372
	40	345	386	367
	50	339	380	378
	70	336	390	374
	80	344	383	379
	90	333	389	388
	100	330	382	411
	130	318	374	425
OVER-4	0	347	386	357
	10	354	401	361
	20	360	453	370
	30	343	445	371
	40	336	421	362
	50	334	422	365
	70	337	395	379
	80	336	384	424
	90	329	398	451

	100	321	392	465
	130	308	396	492
NORM-1	0	337	414	357
	10	349	430	363
	20	347	423	348
	30	349	429	347
	40	348	414	345
	50	341	413	346
	70	342	378	374
	80	360	394	391
	90	358	384	405
NORM-2	0	375	412	354
	10	384	439	355
	20	354	423	350
	30	344	435	353
	40	349	429	349
	50	347	439	342
	70	326	411	386
	80	316	388	414
	90	292	389	423
UNDER-1	0	319	352	312
	10	321	359	316
	20	311	350	300
	30	295	323	304
	40	283	327	305
	50	288	336	315